UNIVERSITÀ DEGLI STUDI DI CATANIA
Dipartimento di Ingegneria Elettrica, Elettronica e Informatica

Dottorato di Ricerca in Ingegneria Elettronica, Automatica e del Controllo di Sistemi Complessi
XXV CICLO

Tesi di Dottorato

ANTONIO PISTORIO

Experimental and Computational Approaches to Enhance the Gravimetric Monitoring of Volcanic Areas

Tutors: Prof. Eng. Luigi Fortuna
Dr. Ciro Del Negro
Dr. Filippo Greco

Coordinator: Prof. Eng. Luigi Fortuna

to my family

Acknowledgements

A sincere thank goes to my tutor and Ph.D. school coordinator Prof. Luigi Fortuna who, first, gave me the opportunity to participate to a Ph.D. course. He represent for me a precious sample of scientific rigor and devotion.

I would like to express my gratitude to my tutors Dr. Ciro Del Negro and Dr. Filippo Greco for introducing me to the interesting area of Volcano Geophysics and for giving me continuous and endless chances to learn from their experience.

I am indebted to "Unità Funzionale Gravimetria e Magnetismo (UFGM)" of the "Istituto Nazionale di Geofisica e Vulcanologia (INGV) - Sezione di Catania - Osservatorio Etneo" for providing generous financial support throughout the Ph.D. I wish also to thank Eni S.p.A., Exploration & Production Division for providing the FG5#238 absolute gravimeter and Scintrex CG5#08064041 relative gravimeter and sponsoring my Ph.D.

I am immensely grateful also with Dr. Rosalba Napoli, Eng. Gilda Currenti and Antonino Sicali of the UFGM research group, for their innumerable hours that they have spent for me.

Last but not least, I deeply thank my family to be always ready to encourage me, giving me the certainty to have always someone behind me.

Index

Introduction

Gravity measurements are a crucial component for any volcano monitoring strategy since they are essential for detecting underground mass movements due to the volcanic activity, which could trigger a pre-eruptive state [Williams-Jones and Rymer, 2002; Battaglia et al., 2003; Carbone et al., 2003; Greco et al., 2010; Bonaccorso et al., 2011a]. The local gravity field in volcanic areas related to sub-surface mass/volume/density redistributions or to elevation changes can vary significantly in both space (wavelengths ranging from hundreds of meters to tens of kilometers) and time (periods ranging from minutes to years) according to the size, depth and rate of evolution of perturbing sources [Greco et al., 2007].

The gravimetric monitoring of a volcano consists both in discrete and continuous gravity acquisitions near the active areas. If discrete measurements (typically performed with relative and/or absolute gravimeters) are taken into account for their high spatial resolution at the expense of a low temporal resolution, vice versa continuous

gravity recordings (usually performed only with relative gravimeters) are prized for the high temporal resolution at the expense of a low spatial resolution. Discrete measurements are useful to highlight long-period volcanic processes. For the high frequency information that continuous measurements provide, they are a good means of investigations in order to recognize forerunners to paroxysmal volcanic events.

A relative gravimeter measures the gravity difference, Δg, between two points while an absolute gravimeter measures the value of the acceleration of gravity, g, in a specific point. Modern spring relative gravimeters and absolute gravimeters are particularly suitable for high-precision gravity measurements in volcanic areas because they are capable of sensing changes of a few part per billion of the Earth's gravity field.

The aim of this thesis is to improve the techniques of the gravimetric method, by enhancing the quality of discrete gravity measurements and a better understanding of the gravity signals provided by the gravimeters in continuous recording during paroxysmal events, for increase the knowledge of the dynamics of active volcanoes through an accurate determination of the position and shape of the volcanic sources. The preferred scenario for this study is Mt Etna not only because it is the most intensively monitored volcano in the world but also because there was the possibility to perform directly in the field gravity measurements, both discrete and continuous, with the instruments owned by the "Istituto Nazionale di Geofisica e Vulcanologia (INGV) - Sezione di Catania - Osservatorio Etneo".

Chapter 1 gives a technical background to gravimetric monitoring of active volcanoes in terms of measurements techniques with spring

relative and absolute gravimeters. It also discusses on the complexity of the gravity signal and on different gravity contributions that must be quantified in volcanic areas. Finally it presents the existing gravity monitoring network of Mt Etna.

It is well-known that the uncertainty of spring relative gravimeters is largely limited by the instrumental drift; this instrumental effect, together with the influences due to temperature and pressure variations, prevents the detection of small gravity anomalies. Using an absolute gravimeter, the measurement's uncertainty of the free-fall acceleration is very high compared to the final uncertainty of the gravity measurements achieved with relative gravimeters. Then, in *Chapter 2*, are shown the results of measurements conducted using two ballistic absolute gravimeters in two different conditions: in dedicated gravity laboratories and in a place used for geophysical studies (volcano monitoring) which present unfavourable environmental conditions (temperature, humidity, vibration, etc.). The chosen instruments represent the steady advance in ballistic gravimeter technology: the FG5#238, a commercial instrument produced by the U.S.A. Micro-g LaCoste Inc. and the IMGC-02, developed in Italy by the Istituto Nazionale di Ricerca Metrologica (INRiM) (prototype). Besides, the IMGC-02 is recognized as national standards instrument in Italy [D'Agostino et al., 2008] and generally the FG5 (family) is more commonly employed for the absolute gravity studies while, specifically, the FG5#238 gravimeter is normally used for different applications from volcano monitoring to the study of gas storage areas [Greco et al., 2011].

With the aim of improving the quality of discrete gravity measurements, to achieve a balance between uncertainty and efficiency in gravity measurements, in *Chapter 3* was investigated the applicability of combined measurements of absolute and relative gravity as a hybrid method for volcano monitoring. Between 2007 and 2009, three hybrid gravity surveys were conducted at Mt Etna volcano, in June 2007, July 2008, and July 2009. The use of absolute gravimeters in a field survey of the summit area of Mt Etna is unprecedented. The annual changes of the gravity measured over 2007-2008 and 2008-2009 provide unequivocal evidence that during the 2007-2009 period, two main phenomena of subsurface mass redistribution occurred in distinct sectors of the volcano, accompanying different eruptive episodes. From 2007 to 2008, a gravity change of −60 μGal was concentrated around the North-East Rift. This coincided with a zone affected by strong extensional tectonics, and hence might have been related to the opening of new voids. Between 2008 and 2009, a North-South elongate feature with a maximum gravity change of +80 μGal was identified in the summit craters area. This is interpreted to indicate recharge of a deep-intermediate magma storage zone, which could have occurred when the 2008-2009 eruption was still ongoing.

Even if the gravimetric monitoring of volcanic areas is traditionally performed by mean of discrete measurements, in the recent years, on Etna volcano, it was also supported by continuous measurements through the installations of gravity stations in continuous recording. Observations with spring relative gravity meters on the Etna volcano during lava fountains show great variations in the gravity signals amplitude, both in the average value than in the background noise,

coinciding with increasing of the inertial acceleration components recorded by the seismic stations, making the detection of the gravity field component more difficult. Then, in *Chapter 4*, to evaluate the coupling degree between inertial acceleration components and the gravity signal provided by these instruments, the results of a laboratory tests on a Scintrex CG-3M and a LaCoste & Romberg model D gravimeters using a vibrating platform to excite them along the *x*, *y* and *z* axes will be explained. Vibrating platforms for testing the dynamic behavior of mechanical components or instruments are widely used. They represent an ideal tool to perform, in general, experiments in the field of seismic engineering. The experimental analysis with a vibrating platform consists in detecting the response of a component or instrument when at the platform is applied a controlled harmonic acceleration. The sinusoidal test type, is a good means to investigate the dynamic properties of the instruments, at specific frequencies. In addition, with this test it can be determined the critical resonance frequencies to which the coupling is bigger. For this purpose, to extract the parameters with which to excite the vibration platform, the seismic signals recorded at two different stations during the 10 April 2011 lava fountain, one of the strongest paroxysmal episode in 2011 eruptive events, were analyzed. Finally, to separate the signal from the gravimeter into gravity field contribute due to the subsurface mass or density variations and the inertial acceleration components due to the ground oscillation, a mathematical approach based on the neural network was also proposed.

Chapter 1

Gravimetric Monitoring of Active Volcanoes

Gravimetry is that branch of applied geophysics which deals with the study and measurement of the mass distribution within the Earth. Gravity surveys make use of the fact that different geological structures have different densities, ρ, the basic physical parameter of the gravimetric method. The fundamental physical law behind this method is that of Newton, defining the force of attraction and therefore the acceleration between two masses within a certain distance. This acceleration is directly proportional to the masses itself and therefore to the densities of the two bodies. In a more formalized

way these basic physical rules can be expressed by the *law of gravitation* as formulated by Newton in 1687:

$$F = G\frac{m_1 \cdot m_2}{r^2}$$

where r is the distance and F the mutual force of attraction along r between the masses m_1 and m_2; G is the gravitational constant ($6.673 \cdot 10^{-11}$ $m^3 kg^{-1} s^{-2}$).

Applied gravimetry allows measuring the acceleration between a probe mass and masses in the subsurface. From the result an idea about the density distribution can be derived, although the observation in the field is affected not only by one mass but the sum of all masses. This integral effect in gravimetry is one reason for a certain ambiguity that can be reduced by taking into consideration some known constraints.

From imaging the structure of the Earth to research on geodynamical processes like mass transport phenomena or deformation processes to near surface, gravity field data contribute to a wide range of geo-scientific research. Among the different possible applications, very accurate gravity measurements are used to detect underground cavities [Elawadi et al., 2001; Mochales et al., 2008], to estimate groundwater-storage change [Pool, 2008; Pool and Eychaner 1995], in oil and gas exploration [Nabighian et al., 2005], for geological-geodynamic studies [Mishra, 2011]. They also play an important role in fundamental metrology, like in the most recent advancements in the Watt-balance experiments for the redefinition of the mass standard, the kilogram [Quinn, 1991; Merlet et al., 2010; Genevès et al., 2010].

For volcano monitoring, the gravimetric method serves two key functions: it provides basic scientific data to develop our understanding of the structure and dynamics of volcanoes and is crucial for hazard assessment, eruption prediction and risk mitigation at times of volcanic unrest. A huge array of monitoring techniques has been tested on several volcanoes: methods that have proved successful in monitoring and sometimes in predicting eruptions include observations of seismicity, ground deformation and microgravity [Rymer et al., 1998]. These, together with magnetic, gas geochemistry and various remote sensing techniques have also provided key information on the volcanic plumbing system and the eruption process.

The study of volcanic related gravity variations can address the solution of ambiguous source problems when density is a key variable to discriminate between different processes leading to the same ground deformation pattern. As an example, both the intrusion of new magma and exolution of gas within a reservoir may cause the volume of the chamber to increase and can lead to the same pattern of ground deformation, but the gravity changes observed at the surface will be very different in the two cases. Also the same pattern of subsidence can result either from magma drainage or contraction due to magma solidification. In this case to the gravitational effect of these processes is different. Microgravity studies can even be the only tool allowing certain internal processes to be detected. For example drainage of radial dyke and a passive intrusion within an open fracture, both leading to negligible elevation changes and no seismicity, could be detected by microgravity observations. Also

changes in magma level in the conduits feeding summit craters could be detected through analysis of gravity variations.

New developments in technology and methodology have allowed several microgravity studies to be accomplished successfully at active and quiescent volcanoes all over the world during the last few decades. Through interpretation of temporal variations of the gravity field and simultaneous temporal elevation changes these studies have provided insights into dynamical changes within the feeding system of various volcanoes. Observed gravity changes and the associated elevation changes have allowed inflation-deflation sequences of shallow magma chambers to be recognized and the magma transfer processes responsible for them to be interpreted.

At some volcanoes gravity decreases associated with minor inflation during times of higher activity and gravity increases associated with subsidence during times of declining eruptive activity have been noted. A possible explanation of such pattern of changes could be given by the displacement of high-density degassed magma by low-density vesiculated magma leading to gravity decrease and weak inflation followed by loss of gases by fumarole activity leading to density decrease and a reduction in volume of the magma body involved and thus deflection at the surface.

One of the main drawbacks of the gravimetric monitoring is the lack of information on the rate at which the volcanic processes occur since only the change of the subsurface mass distribution between the times when two successive surveys have been performed can be assessed and therefore there remains some ambiguity as to the nature of the processes themselves. Also a common problem on active volcanoes is snow coverage which makes gravity changes on the

summit zone not identifiable on a timescale of less than six months during the winter time. Coupled with the desire to reduce the exposure of personnel in active areas, there is a need to develop gravity techniques that

(i) produces a continuous picture of the gravity signal with time (and therefore the processes occurring inside the volcano) and

(ii) operate automatically in remote regions for several months at a time.

Microgravity studies have also given a significant contribution to the understanding of the internal plumbing system of Mt Etna. They have represented the only geophysical tools able to detect in a completely non-invasive way the intrusion of magma inside open fractures/conduits and solve ambiguous source problems when different phenomena lead to the same deformation pattern.

1.1 Units of Acceleration of Gravity *g*

Any mass on the Earth's surface is affected both by the mass attraction of the Earth and other celestial bodies and by the centrifugal acceleration. The resultant, called gravity acceleration, *g*, hence depends on the arrangement of the terrestrial and extraterrestrial masses, as well as on the Earth's rotation. The study of the changes of the *g* average value ($\approx$9.81 ms^{-2}), called microgravity changes, given their amplitude, which reflect the temporal variations of the Earth's body, are of particular interest at tectonically active areas and active volcanoes.

Different units for the gravity acceleration are in use. In the SI system the basic unit is ms^{-2}. Because the gravity variations seen in geophysical surveying are always small as compared to the average value, other units are commonly used. Examples from the SI system are $\mu ms^{-2} = 10^3$ nms^{-2}. Frequently used in gravity surveys, as is the case of this thesis, is the "Gal" (which owes its name to Galileo Galilei) where 1 $\mu Gal = 10^{-8}$ ms^{-2}. Finally, often it is also expressed in "g" where 1 g = 9.81 ms^{-2}; this value, coincident with that of the gravity acceleration *g*, allows to measure the acceleration proportional to it.

1.2 Discrete Measurements with Relative Gravity Meters

Basically, with relative gravimeters, discrete gravity measurements are obtained by the gravity differences, Δg, measured between a couple of adjacent stations and according to work objectives and field conditions the "step method", "star method" and/or "profile method" can be accomplished. To measure the gravity network of Mt Etna, the "step method" is mainly used. Following the multiple occupation sequence in the various stations, as required by the method (A-B B-A A-B B-C …), starting from a primary reference point, each station is occupied at least three times. In this way the final Δg values between pairs of adjacent stations can be obtained from the mean of the three Δg calculated.

Systematic investigation of discrete gravity measurement has been continued at Mt Etna since 1986 [Budetta and Carbone, 1998]. Since then the most effective geometry for an extended array for studying

volcano dynamics and for forecasting eruptions has been sought. The network covers now an area of about 400 km^2 with stations 0.5÷3 km apart. It allows mass redistributions occurring at depths between about 8 km b.s.l. and a few hundred meters below the surface (magma level changes within the shallower parts of the feeding conduits) to be detected [Budetta and Carbone, 1998].
Generally, considering all relative gravity stations as part of a loop, to evaluate the gravity acceleration, *g*, at each station with the associated total uncertainty, is applied a strict compensation procedure. Starting from a reference station, in which the *g* value is well known, this procedure is based, for example, on the least squares adjustment method by solving a linear system consisting by observation equations.

1.3 Discrete Measurements with Absolute Gravity Meters

Transportable absolute gravimeters must be used to obtain precise in situ gravity acceleration, *g*, measurements. For this work, are used two absolute gravimeters, which represent the state of the art in recent advances in ballistic gravimeter technology: (1) the commercial instrument Micro-g LaCoste FG5#238 and (2) the prototype instrument IMGC-02 built by the "Istituto Nazionale di Ricerca Metrologica (INRiM)". The instruments are high precision absolute gravimeters with a standard uncertainty of 2.3 μGal (FG5) and 3.8 μGal (IMGC-02) for laboratory use [Vitushkin et al., 2010]. Considering the site-dependent contribution to the uncertainty, the

minimum achievable expanded uncertainties, as when they are used in the international comparisons, are 5.2 and 8.6 μGal, for FG5 and IMGC-02, respectively [Jiang et al., 2011]. Because of these low uncertainties in measurements, FG5 is widely used for the absolute gravity studies and IMGC-02 is recognized as a national standards instrument in Italy [D'Agostino et al., 2008].

1.4 Continuous Measurements with Relative Gravity Meters

Continuous microgravity studies at active volcanoes have been scarcely made in the past because of the logistic difficulties of running them in places where the conditions are far from the clean, ideal laboratory and so it is quite difficult to attain the required precision in the data. Most of the few studies available deal with continuous measurements acquired at sites remote from the summit craters to either obtain precise tidal gravity factors of the area where the volcano lies or to determine correction algorithms for the main external perturbations to each instrument employed. Jousset et al. (2000) have found a correlation between the residual drift of a LaCoste & Romberg D meter which recorded continuously between 1993 and 1995 at a site 4 km away from the summit of Merapi volcano (Indonesia) and seismic and volcanic activity. In addiction they found shifts in the ratio between the records and the theoretical response of the Earth (tides) also correlated with the volcanic activity.

Discrete micro-gravity measurements usually provide excellent spatial coverage of the area of interest (in this case, usually the

summit region of an active volcano), but the temporal resolution is only as good as the repeat frequency of the observations. Tidal gravity observations provide excellent temporal resolution, with measurements collected every second if desired, but the spatial resolution is limited by the number of instruments available. Thus it is necessary to place the instrument in a position where there is the greatest chance of detecting meaningful gravity changes - this may be close to an active crater. The conditions at such a station are far from the clean, ideal laboratory and so on it is quite difficult to attain the required precision in the data. Because of this, continuous gravity observation at active volcanoes have not developed as quickly as other geophysical techniques. However, technological improvements in recent years have overcome most of this difficulties.
Measurements are routinely performed every second with spring relative gravimeters, then data are decimated to one minute through a CR10X data logger by Campbell Scientific Ltd. Other useful parameters, such as temperature, pressure, humidity and tilt are recorded at the same time.

1.5 Complexity of the Gravity Signal

Gravity measurements are affected by the simultaneous action of several physical parameters which act both on the local gravity field and on the behavior of the gravimeter. In addition to geophysical effects, the instrumental effects act on the measurement system of the gravimeters causing apparent variations of the gravity field.

Instrumental Drift

Spring gravity meters exhibit a temporal variation in the display of the zero position, and this constitutes the instrumental drift. Usually the term "drift" implies the summation of two components [Torge, 1989]:

1) the stationary drift, presumed to be due to creep in the spring and lever system and exhibiting an overall linear behavior;
2) the transport drift which appears during field work, is mainly the effect of mechanical and thermal shocks and features a marked nonlinear behavior.

Continuously recording instruments are of course principally affected by the first component. The stated stationary drift on a gravimeter is about 30 μGal/day when the instrument is new and tends to decrease with instrument use to less than 10 μGal/day. If the stationary drift was perfectly linear, to correct continuous gravity records for would be easy. Unfortunately, nonlinearities over long periods (of the order of months) do arise and are due to external (long-wave temperature and pressure fluctuation) and instrumental (i.e. drift) effects. This superimposition of internal and meteoric effects makes correction formulae for the effect of long-term temperature and pressure changes via correlation analyses difficult to assess.

Effect of Meteorological Parameters

Meteorological parameters are expected to affect continuous recording spring gravity meters [Torge, 1989]. Apparent gravity changes have different character and magnitude, depending on the temporal development and magnitude of the meteorological change that caused them as well as on the insulation and compensation of the

gravity meter. Thus, the correction formulas are instrument-specific and must be established through case-by-case experimentally assessed transfer functions. Each continuously running gravity station of the Etna array has been equipped with temperature and pressure sensors. The thermometers used (LM35 by National Semiconductor) have an accuracy better than ±0.1 °C and work over a temperature range of 0÷100 °C. As for pressure changes, Honeywell 140PC absolute sensors have been used (range ≈0÷1034 mbar; repeatability ≈0.2 mbar). The main component of the temperature signal has a seasonal character and so a several-year long sequence should be used to perform an analysis. However, the relationship between gravity and meteorological signals has been investigated preliminarily over the data sequences available at the moment (about 1 year).

1.6 Gravity Variations in Volcanic Areas

When trying to investigate the applicability of precise in situ gravity measurements for providing effective volcano monitoring there are several challenges that need to be addressed. After correcting for tidal and instrumental effects, the observed gravity g_{obs} is the difference in gravity between benchmark and reference but to extract the gravity signal produced by a subsurface mass and/or density change, different contributions must be quantified.

The gravity anomaly, δg, related to the mass redistribution, can be calculated by solving the following Poisson's differential equation

for the gravitational potential ϕg using appropriate boundary conditions [Cai and Wang, 2005]:

$$\nabla^2 \phi_g = -4\pi G \Delta\rho(x, y, z) \quad (1.1)$$

where G denotes the universal gravitational constant and $\Delta\rho(x,y,z)$ is the change in the density distribution. Generally, the total gravity change at a benchmark on the ground surface associated with pressure source changes is given by:

$$\delta g(x, y, z) = -\frac{\partial \phi_g}{\partial z} + \delta g_0 \quad (1.2)$$

where δg_0 represents the "free-air" gravity change accompanying the uplift of the observation site. In fact, the deformation moves the point of measurement relative to the center of gravity of the Earth with a consequent change in gravity. The density variations related to the subsurface mass redistribution can be accounted for by three main terms:

$$\Delta\rho(x, y, z) = -\mathbf{u} \cdot \nabla\rho_0 + \delta\rho_1 - \rho_0 \nabla \cdot \mathbf{u} \quad (1.3)$$

where $\boldsymbol{u}$ is the displacement field, ρ_0 is the embedding medium density and $\delta\rho_1$ is the density change due to the new intrusive mass. The first term is due to the displacement of density boundaries in heterogeneous media. The second-term originates from the density change related to the introduction of the new mass into the pressurized volume, and the third term is the contribution due to the volume change arising from compressibility of the surrounding medium [Bonafede and Mazzanti, 1998].

Each term in the density variation contributes in the total gravity change observed at the ground surface. Therefore, the gravity

changes caused by pressure sources are made up by four different contributions:

$$\delta g = \delta g_0 + \delta g_1 + \delta g_2 + \delta g_3 \quad (1.4)$$

where δg_1 arises from the first term in Equation 1.3; δg_2 denotes the contribution of the inflation source (second term in Equation 1.3); and δg_3 is the gravity change produced by density variations in the surrounding medium (third term in Equation 1.3).

Free-air correction only adjusts for the elevation of the observation point that, in first approximation, is given by:

$$\delta g_0 = \gamma \cdot \delta h \quad (1.5)$$

where γ is the free-air gravity gradient (the value of the theoretical gradient is −308.6 μGal/m); δh is the elevation change (positive for relative uplift and negative for relative subsidence).

Usually, δg_1 is only accounted for the excess mass above the reference level corresponding to the upheaved portion of the free surface. A simple Bouguer correction is applied assuming the mass distributed as an infinite slab with thickness equal to the uplift.

Moreover, the δg_1 and δg_3 terms highlight that the computation of the displacement field at depth is required in order to evaluate these gravity contributions. It calls that changes in the gravity field cannot be interpreted only in term of additional mass input disregarding the deformations of the surrounding rocks [Charco et al., 2006].

The gravity changes δg_1, δg_2 and δg_3 caused by the expansion of a spherical source embedded in a homogeneous Poisson's medium ($\lambda = \mu$) are given by the following analytical expressions [Hagiwara, 1977]:

$$\delta g_1 = 2\pi G \rho_0 \delta h \quad (1.6)$$

$$\delta g_2 = G[(\rho' - \rho_0)\Delta V + (\rho' - \rho)V] \frac{z}{(z^2+r^2)^{3/2}} \quad (1.7)$$

$$\delta g_3 = -\frac{2}{3}\pi G \rho_0 \delta h \quad (1.8)$$

where $\rho(\rho')$ and V (V') are the average density and the volume of the source before (after) the inflation, $\Delta V = V' - V$ is the volume change, δh is the elevation change at the surface [Mogi, 1958], z is the depth to the source, and r is the surface distance out from the centre of the source. The δg_2 term takes into account: (i) the displacement of the source boundaries, which implies replacement of surrounding mass ($\delta g_{2\Delta V}$) and (ii) the input of new mass inside the source volume (δg_{2V}). Then the Equation 1.7 can be written as:

$$\delta g_2 = \delta g_{2\Delta V} + \delta g_{2V} \quad (1.9)$$

where (from Equation 1.7)

$$\delta g_{2\Delta V} = -G\rho_0 \Delta V \frac{z}{(z^2+r^2)^{3/2}} \quad (1.10)$$

$$\delta g_{2V} = G(\rho' V' - \rho V) \frac{z}{(z^2+r^2)^{3/2}} \quad (1.11)$$

Often, in Equation 1.11, the difference $\rho' V' - \rho V$ is expressed as ΔM_m to indicate the change in sub-surface magma mass.

It is worth to note that if the source inflates without addition of new mass ($\rho' V' = \rho V$), the δg_2 contribution becomes:

$$\delta g_{2(\rho' V' = \rho V)} = -G\rho_0 \Delta V \frac{z}{(z^2+r^2)^{3/2}} = -\frac{4}{3}\pi G \rho_0 \delta h = \delta g_{2\Delta V} \quad (1.12)$$

which is equivalent to the contribution of a volume ΔV that was initially filled with surrounding rock density material and become

empty after the expansion [Bonafede and Mazzanti, 1998]. In such a case the overall gravity change ($\delta g_1 + \delta g_{2\Delta V} + \delta g_3$) due to the deformation of a homogeneous half-space caused by a point source vanishes identically [Walsh and Rice, 1979].

In a more compact form, which takes into account also the change of the groundwater table level, the observed gravity change at each benchmark Δg_{obs} can be written as (Fig. 1.1):

$$\Delta g_{obs} = \gamma \cdot \delta h + \Delta g_W + \Delta g_D + \Delta g_R \qquad (1.13)$$

where Δ denotes a gravity difference over time at the site [e.g., $\Delta g_{obs} = g_{obs}(t_2) - g_{obs}(t_1)$]; Δg_w is the effect of groundwater table variation; Δg_D takes into account coupling effects between gravity and elastic deformation ($\delta g_1 + \delta g_{2\Delta V} + \delta g_3$); and Δg_R depends on the mass change accompanying the deformation (that is equal to δg_{2V}).

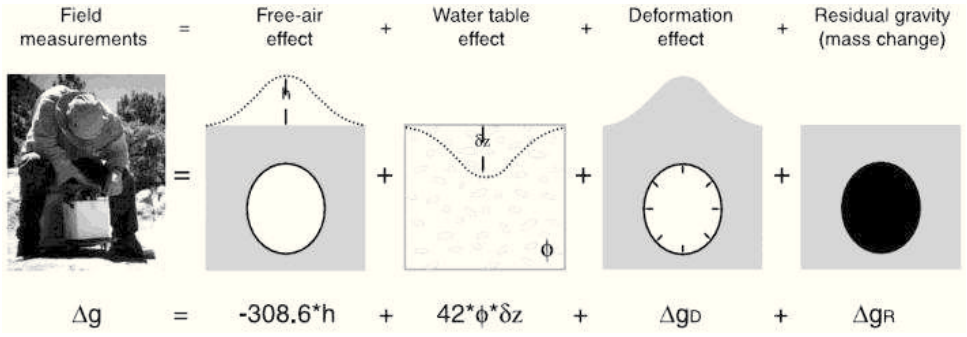

Figure 1.1 – The different effects that compose the observed gravity signal, $\Delta g \equiv \Delta g_{obs}$, measured in the field. All constants are in μGal/m, $h \equiv \delta h$ is the vertical displacement, ϕ the porosity and δz the water table change ($\Delta g_W = 42\phi\delta z$). The deformation effect Δg_D is zero for changes in gravity resulting from expansion of a isotropic source in a homogeneous elastic half-space [Walsh and Rice, 1979], [After Battaglia et al., 2003].

In this study, is used the local observed value of the free-air gradient (FAG) to compute the free-air gravity correction (reduction). The actual free-air gradient is determined from field measurements at each reference point of the Etna volcano gravity monitoring network, and significant variations with respect to the theoretical gradient are often observed (up to about 25%). Variations in the free-air gradient are mainly due to local topography and density anomalies (e.g., Kuo et al. 1969).

The water table correction ($\Delta g_w = 42\ \phi\ \delta z\ \mu Gal$) is proportional to the effective porosity ϕ and vertical water table change δz (in meters) of an unconfined aquifer. Since porosity and water level data are sparse or non-existent at gravity stations, a possible approach is to adopt survey strategies to minimize the water table correction. In particular, if all the surveys are conducted in the same season of the year, the water table effect can in most years be disregarded.

The deformation effect Δg_D is due both to the displacement of density boundaries in heterogeneous media and to the volume changes arising from compressibility of the medium surrounding the source (Bonafede and Mazzanti, 1998). The source's geometry significantly affects the Δg_D contribution. Δg_D is zero for changes in gravity resulting from an isotropic source in a homogenous elastic half-space (as stated before) [Walsh and Rice, 1979], is negligible for spheroidal sources, but may be significant for sill-like sources [Battaglia et al., 2006] and shallow magmatic intrusions [Currenti et al., 2011a].

The mass effect Δg_R originates from the gravity change related to the introduction of the new mass into the displaced volume [Currenti et al., 2007]. Then, when the water table effect and the deformation

correction are negligible, the residual gravity is computed by subtracting the free-air from the observed gravity changes. In such a case, Δg_R in Eq. 1.13 is the residual gravity. In this thesis, the studies will focus on the annual changes of the residual gravity measured at Etna.

1.7 Etna Volcano Gravity Monitoring Network

The INGV has been operating for the gravity monitoring of Mt Etna since 1986 [Budetta et al., 1989], see Figure 1.2 for locations of the gravity stations.

Relative Gravity Stations

The present relative network for discrete gravity measurements consists of 71 benchmarks, covering an area of about 400 km^2. The discrete gravity readings are usually related to several primary reference stations outside the area of interest (e.g., ADR station; 590 m a.s.l.; about 20 km South-West of the Summit Craters), which are the least likely sites to be affected by volcanically induced gravity changes. Most benchmarks are close to or coincident with GPS stations for monitoring height changes [Bonforte et al., 2007a], enabling corrections for any ground deformation. The whole gravity network is routinely occupied every summer (in the same season of the year to minimize seasonal variations). Since 1994, the annual gravity surveys have been carried out using the Scintrex CG-3M gravimeter. The average error attained for the relative gravity surveys is ±15 μGal [e.g., Pistorio et al., 2011], which allowed to detect some

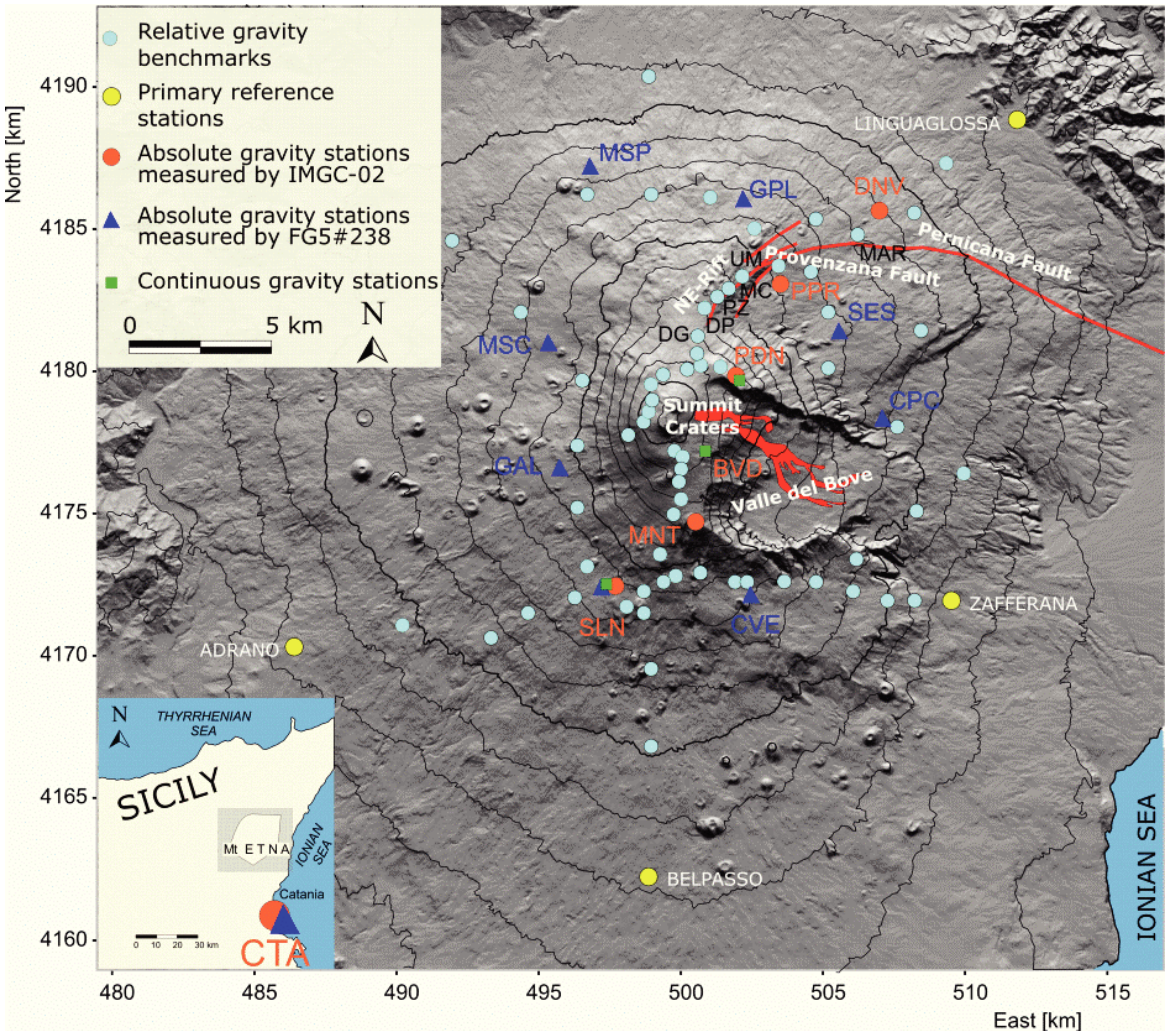

Figure 1.2 – Sketch map of Etna volcano showing the location of (1) the relative gravity benchmarks, for discrete and continuous measurements (cyan and yellow circles), (2) the absolute stations (orange circles and blue triangles) and (3) the continuous stations (green squares). The main structures (i.e., NE Rift, Provenzana, and Pernicana Faults) bordering the northeastern sector of the volcano (red lines) and the lava flow outpoured during the 2008-2009 flank eruption (red area) are drawn. Geographical coordinates are expressed in UTM projection, zone 33 N (WGS84 ellipsoid).

temporal gravity changes related to volcanic activity with amplitude more than 20-30 μGal [Carbone et al., 2003; Carbone and Greco, 2007; Bonforte et al., 2007a; Greco et al., 2010]. However, an uncertainty of 10 μGal or better is required in order to detect the different contributions of gravity changes related to volcanic sources from the unwanted components mainly due to instrumental, human, and seasonal effects [Currenti et al., 2007].

Absolute Gravity Stations

From 2007 to 2009, the Etna gravity network was expanded with several absolute stations. Due to the logistical difficulties on Mt Etna, the arrangement of the absolute stations mainly depends on the presence of buildings that can provide protection for the instrumentation. The first four stations for absolute measurements at Etna were installed in 2007 along a North-South profile crossing the summit craters at over 2850 m elevation. Another station was installed outside the volcanic edifice, inside the gravity laboratory of INGV-Catania (CTA) used as primary reference station. In 2009, was added other nine stations arranged as a ring around the volcano at elevations between 1500 and 2000 m a.s.l. Besides the CTA station, the present Etna gravity network includes 13 absolute stations distributed on the volcano edifice between 1500 and 2850 m a.s.l.

Continuous Gravity Stations

For continuous measurements, Etna gravity monitoring network is made up by three continuously running stations: SLN (Serra La Nave, 1740 m a.s.l.), 5 km distant from the North-East Crater; BVD (Belvedere, 2910 m a.s.l.), near to the south edge of Valle Del Bove,

about 1 km distant from the South-East Crater and about 900 m distant from the New South-East Crater; PDN (Pizzi Deneri, 2820 m a.s.l.), 2 km distant from the North-East Crater.

Chapter 2

Comparison between Two Ballistic Absolute Gravimeters

Measurements using two ballistic absolute gravimeters were conducted in two different conditions: in dedicated gravity laboratories and in a place used for geophysical studies (volcano monitoring) which present unfavourable environmental conditions (temperature, humidity, vibration, etc.). The chosen instruments represent the steady advance in ballistic gravimeter technology: the FG5#238, a commercial instrument produced by the U.S.A. Micro-g LaCoste Inc. and the IMGC-02, developed in Italy by the Istituto Nazionale di Ricerca Metrologica (INRiM) (prototype). Besides, the IMGC-02 is recognized as national standards instrument in Italy [D'Agostino et al., 2008] and generally the FG5 (family) is more

commonly employed for the absolute gravity studies while, specifically, the FG5#238 gravimeter is normally used for different applications from volcano monitoring to the study of gas storage areas [Greco et al., 2011].

The interest is to study the performances of two absolute gravimeters by operating *g* measurement at stations characterized by different logistics and environmental conditions. At the same time, was tested the behavior of the instruments and different measurement procedures performed by the operators.

To compare the performance of this two absolute gravimeters, were chosen three different sites: two of them are dedicated laboratory, the third one is a geophysical point of interest with particular conditions (Tab. 2.1).

1. *Gravity Laboratory of INGV at Catania (Italy)*. This site is normally used as reference for Etna volcano gravity network. Indeed, the gravity field here can be considered stable (not affected by volcano-induced gravity anomalies). Furthermore the FG5#238 is maintained and tested therein.
2. *Gravity Laboratory of INRiM at Turin (Italy)*. In this site normally the IMGC-02 is maintained, tested and improved.
3. *Mt Etna volcano (Italy)*. This site is one of the absolute monitoring station installed at Etna volcano and presents the difficulties normally encountered in a very hard environment such as those existing on an active volcano.

To validate the absolute measurements performed with the two instruments, was also included a link to the International and European Comparisons of Absolute Gravimeters (ICAG 2005 - 2009

and ECAG 2011), in which the two FG5#238 and IMGC-02 gravimeters have participated.

Station	Acronym	Latitude [deg]	Longitude [deg]	Elevation [m a.s.l.]
Catania	CTA	37.514	15.083	50
Turin	INRiM	45.017	7.642	236
Serra La Nave	SLN	37.694	14.973	1730
Sèvres	BIPM	48.829	2.219	56
Walferdange	WFG	49.665	6.153	295

Table 2.1 – Coordinates of the absolute gravity stations.

2.1 Two Transportable Absolute Gravimeters

Use of transportable absolute gravimeters is essential for the applicability of accurate in-situ gravity measurements. Both instruments employed in this study are very accurate absolute gravimeters with a standard uncertainty of 2.3 μGal (FG5 family) and 3.8 μGal (IMGC-02) for laboratory use [Vitushkin et al., 2010].

For both instruments, the measurement of the *g* value is obtained using the reconstructed trajectory of a corner-cube prism, subjected to the gravity field, which moves vertically in a vacuum chamber. The IMGC-02 takes into account for both the rise and fall motions of the flying object, while the FG5 instrument measures the acceleration during the free-fall motion only.

Automated systems are employed to centre, launch and receive the object event by event with nominal rates of about (0.02 to 0.1) Hz during data taking sessions of several hours. An interferometric system is implemented to obtain time and distance coordinates of the

trajectory using a visible laser beam. A laser interferometer measures the distance between the free falling corner cube test mass and a second retroreflector mounted on the quasi-inertial mass of a vibration isolation system that is a seismometer and a super-spring system for IMGC-02 and for the FG5, respectively [Niebauer et al., 1995; D'Agostino et al., 2008].

The final measurement value at the observation point is the average value of the measurements collected during a measurement session after removing instrumental and geophysical effects.

As for the FG5, a total of 700 time-position points are recorded over the 20 cm length of each drop. Drops can be produced up to every two seconds but in routine operation, the drops are repeated every 10 s, 100 times per hour. Typically the average of 50 or 100 drops is a "set", which exhibits standard deviations of 4 to 15 μGal under normal conditions [Van Camp et al., 2003]. Measurements usually consist of one set per hour with the average of several sets (usually 12 to 48) providing a "gravity value". The instrumental accuracy of the FG5 is about (1 to 2) μGal as reported by the manufacturer [Niebauer et al., 1995]. However, the contribution to the uncertainty of the environmental effects corrections, affect the gravity value uncertainty in a wide frequency band (from minutes to decades).

As for the IMGC-02, in laboratory environmental conditions, one observation session lasts typically 12 hours and consists of about 1500 launches. It corresponds to an experimental standard deviation of the population of measurement results equal to 35 μGal and to an uncertainty of the mean value lower than 1 μGal. In practice, the observation time depends on the scattering of the collected acceleration values: the larger the scattering, the longer the

observation time. The data scattering is mostly due to the ground vibration at the site (also induced by the recoil effect), which is partially transferred to the inertial mass of the seismometer supporting the reference retro-reflector.
When the instrument is operating in noisy environmental conditions, an experimental standard deviation of the population of measurement results equal to 50 μGal requires about 2500 launches to reach an uncertainty of the mean value equal to 1 μGal. But halve the above reported experimental standard deviation requires four times the number of launches.
Data scattering, together with the sensitivity to the strong temperature fluctuations, are the major cause of uncertainty of measurements performed with both the FG5 and IMGC-02 gravimeters when they are operating outside the laboratory.

2.2 Uncertainty Evaluation

The uncertainty associated to the g measurement, u_{comb}, is evaluated by combining the contributions of the instrumental uncertainties, u_{inst}, to the contribution of uncertainty depending on the observation site, u_{site}, and the scattering of measurements, u_{stat}. With regards to the instrumental uncertainty, most important influence factors which are characteristic of absolute gravimeters are: vacuum level, non-uniform magnetic field, temperature gradient, electrostatic attraction, mass distribution, laser beam verticality and divergence, overall drift, air gap modulation, length and time standards, retro-reflector balancing, radiation pressure and reference height.

Considering all the contributions to the uncertainty, the minimum achievable combined uncertainties, like when they are used in the international comparisons, are 2.6 μGal and 4.3 μGal, respectively for FG5 and IMGC-02 [Jiang et al., 2011]. However, it is interesting to note that the uncertainty of both instruments significantly increases when they are used on-field in sites affected by hard environmental conditions such as those encountered on a volcano [Pistorio et al., 2011; Greco et al., 2012].

Main influence factors that are dependent from the observation site are: Coriolis force, floor recoil, and geophysical effects, such as local barometric pressure, gravity tides, ocean loading, and polar motion; the combined standard uncertainty is estimated to be 1.1 μGal for both absolute gravimeters. Another contribution characteristic of the observation site is the scattering of measurements: this effect is estimated with the experimental standard deviation of the mean g value; it is strongly depended on the ground vibrations and the floor recoil. The analysis of the data acquired with both FG5#238 and the IMGC-02 gravimeters is carried out with different post-processing software that allow to vary data analysis procedures. Outputs of this processing are the value of the free-fall acceleration and its standard deviation due to the scattering. Combining this latter contribution with the instrumental uncertainty and the other contribution due to the site-dependent influence factors, it is possible to calculate the combined standard uncertainty and the expanded uncertainty (at the 95% confidence level) related to the measurements acquired with both gravimeters.

2.3 Free-Air Vertical Gravity Measurements

Measurements of the free-air vertical gravity gradient were carried out at all the absolute stations to refer values collected by the two absolute gravimeters to the same height from the ground. Measurements have been taken with Scintrex CG-3M and CG-5 relative gravimeters.

The free-air vertical gradient γ was estimated by measuring the gravity variation at four different levels from the floor: h_0 = 15 mm, h_1 = 265 mm, h_2 = 515 mm and h_3 = 765 mm. Was adopted the step method, in which adjacent elevations were connected at least three times. After the correction for the earth tide, γ was obtained by fitting the following equation model to the experimental data, i.e. the collected g value and the acquisition time t:

$$g = \gamma \cdot h + \alpha \cdot t + k \qquad (2.1)$$

where the estimate parameter γ, h, α, k are respectively the vertical gradient, the level from the floor, the instrumental drift, and the gravity offset.

The vertical gravity gradients spans from station to station from (–278.6 to –335.1) μGal/m. Uncertainties of 3.9 μGal/m, 4.2 μGal/m and 2.6 μGal/m are evaluated respectively for the vertical gravity gradient at CTA, Turin and SLN stations measured in 2009 and 2011 (Tab. 2.2).

The following equation can be used to refer a measurement result $g(h_m)$ collected at a level h_m from the floor to a level h:

$$g(h) = g(h_m) + \gamma \cdot (h - h_m) \qquad (2.2)$$

Acronym	FAG [µGal/m]	u_{FAG} [µGal/m]
CTA	-278.6	3.9
INRiM	-273.6	4.2
SLN	-335.1	2.6

Table 2.2 – The vertical gravity gradients and uncertainties at CTA, INRiM and SLN stations.

The combined uncertainty at the level h is therefore

$$u_g(h) = \sqrt{u_g(h_m)^2 + (h - h_m)^2 \cdot u_\gamma^2} \qquad (2.3)$$

where $u_g(h_m)$ is the combined uncertainty of the measurement result and u_γ is the uncertainty of the free-air vertical gravity gradient evaluated with the fitting algorithm.

2.4 Absolute Measurements

Were performed absolute free-fall acceleration measurements at the different sites between 2009 and 2011 (Tab. 2.1). Measurements in Catania (CTA) and at Mt Etna volcano (SLN) were carried out in July 2009, while in Metrology Laboratory of INRiM at Turin (Italy), in November 2011.

Due to different designs of the instruments, the measurement values carried out by FG5#238 and IMGC-02 are referred to about 1.2 m and 0.5 m from the ground, respectively. Therefore, were compared the results by referring all the measurement values to the same level to the ground (0.5 m) using the free-air vertical gravity gradients

measured at each station, in the same period of the absolute measurements.

Concerning the FG5#238 gravimeter, each set was acquired with 100 drops and data processing was performed by setting a threshold of three standard deviations.

Concerning the IMGC-02 gravimeter, the measured data are filtered by applying rejecting criteria. The most critical factor is the visibility variation of the interference signal during the trajectory, which highlights an horizontal motion of the test-body. The effect due to the Coriolis force and the beam share are minimized by rejecting those launches with a decrease of visibility bigger than 10%. Outliers are found by applying the Chauvenet criterion to the collected *g* values and other estimating parameters such as the vertical gradient and the friction of residual air.

As results of the latest studies on the Self Attraction Effect (SAE) of the absolute gravimeters, to improve the results of the comparisons, all the data have been reprocessed to apply the correspondent Self Attraction Corrections (SAC) due to the masses of the single parts that compose the different gravimeters. Biolcati et al. (2012), calculated the SAE for the FG5#238 and for the IMGC-02 that are (–1.2 ± 0.2) μGal and (0.6 ± 0.1) μGal, respectively. Although the application of the SAC of 1.2 μGal and 0.6 μGal should not significantly change the *g* values with respect to the combined standard uncertainty of the measurements, according with Biolcati et al. (2012), were applied the SAC and removed 1.2 μGal and add 0.6 μGal to the measurements acquired with the FG5#238 and with the IMGC-02 gravimeters, respectively.

In Table 2.3, for both gravimeters, in addition to the absolute value of the free-fall acceleration acquired at the different sites, it is given the height, h, above the ground where g is referred and the standard uncertainty due to the scattering, u_{stat}. The table shows also the instrumental standard uncertainty, u_{inst}, the site-dependent standard uncertainty, u_{site}, and the combined standard uncertainty, u_{comb}, taking into account all three contributions of uncertainty.

Gravimeter	Acronym	Date	Height [m]	$g(h)$ [μGal]	$g(h)$+SAC [μGal]	u_{inst}	u_{site}	u_{stat}	u_{comb}
FG5#238	CTA	03-05 July 2009	1.2867	980031291.7	980031290.5	2.3	1.1	1.87	3.2
IMGC-02	CTA	08-09 July 2009	0.5009	980031505.9	980031506.5	3.8	1.8	3.0	5.2
FG5#238	INRiM	29-30 October 2011	1.2922	980533990.7	980533989.5	2.3	1.1	1.86	3.2
IMGC-02	INRiM	25-26 October 2011	0.4772	980534203.6	980534204.2	3.8	1.6	2.6	4.9
FG5#238	SLN	11 July 2009	1.2937	979641362.1	979641360.9	2.3	1.1	1.85	3.2
IMGC-02	SLN	09-10 July 2009	0.4982	979641630.8	979641631.4	3.8	1.8	2.2	4.8

Table 2.3 – Measured values of g at the absolute stations using FG5#238 and IMGC-02 gravimeters in Catania, Turin and Serra La Nave. The values of g after the SAC was applied is also presented. Table also shows the height above the ground of the measurements, the instrumental uncertainty, the statistical uncertainty, the site uncertainty, and the combined uncertainty.

2.4.1 Gravity Laboratory at Catania

The absolute gravity station of Catania (CTA; Lat. 37.514° N, Long. 15.083° E, 50 m a.s.l.) is located at the underground Gravity Laboratory of the Istituto Nazionale di Geofisica e Vulcanologia (INGV; Fig. 2.1).

Figure 2.1 – Gravity laboratory at Catania (INGV): on the left the FG5#238 and on the right the IMGC-02.

The instruments can be settle on a suitable concrete pillar, insulated from the building. The laboratory conditions are optimal, with low humidity and stable ambient temperature. During the day the vibrations induced by human noise are significant but still acceptable. The data scattering is relatively low, therefore an observation session lasting 12 hours is enough in order to reach a satisfying uncertainty.

With the FG5#238 the measurements were carried out from 3 to 5 July 2009, during the week-end when the noise is reduced. A total of 40 sets were acquired, in about 39 hours. There was no need to eliminate any set of measurements. The final measurement value at 1.2867 m was 980031291.7 μGal ± 3.2 μGal (combined standard uncertainty).
With the IMGC-02 gravimeter, the measurements were carried on 08-09 July 2009 [D'Agostino et al., 2009]. The instrument processed and stored 1337 trajectories. The final measurement value at 0.5009 m, obtained by averaging 477 trajectories, was 980031505.9 μGal ± 5.2 μGal (combined standard uncertainty).

2.4.2 Gravity Laboratory at Turin

The absolute gravity station of INRiM in Turin (INRiM; Lat. 45.0170° N, Long. 7.6427° E, 236 m a.s.l.) is located at the Metrology Laboratory of the Istituto Nazionale di Ricerca Metrologica (INRIM; Fig. 2.2) [Germak, 2006]. In the laboratory there is a stable concrete basement where the instruments can be installed. The human noise is practically absent and the data scattering is extremely low. The low ambient humidity and the temperature stability didn't significantly affect the measurement uncertainty.
The gravimeter FG5#238 were installed at INRiM from 29 to 30 October 2011. A total of 46 sets of 50 drops each one, in about 36 hours, were recorded. There was no need to eliminate any set of measurements. The final measurement value at 1.2922 m was 980533990.7 μGal ± 3.2 μGal (combined standard uncertainty).

Figure 2.2 – Gravity laboratory at Turin (INRiM): on the left the FG5#238 and on the right the IMGC-02.

The IMGC-02 gravimeter collected gravity data on 25-26 October 2011 (during the night). The instrument processed and stored 1867 trajectories. The final measurement value, at 0.4772 m, obtained by averaging 473 trajectories was 980534203.6 μGal ± 4.9 μGal (combined standard uncertainty).

2.4.3 Mt Etna (Serra La Nave) Absolute Station

The observation station of Mt Etna (SLN; Lat. 37.694° N, Long. 14.973° E, 1730 m a.s.l.) is located at Serra La Nave site in a bunker within the area of the Astrophysical Observatory. Inside the bunker there is a big stable concrete basement where the instruments can be installed (Fig. 2.3).

Figure 2.3 – Gravity station at Serra La Nave (Mt Etna): on the left the FG5#238 and on the right the IMGC-02.

The human noise is practically absent and the data scattering is extremely low. The high ambient humidity and low temperature, even if not controlled, didn't significantly affect the measurement uncertainty.

From 10 to 11 July 2009, a total of 33 sets were acquired with the FG5#238 gravimeter in about 19 hours (most during the night). The first three sets of measurements were rejected. The final measurement value at 1.2937 m was 979641362.1 μGal ± 3.2 μGal (combined standard uncertainty).

The IMGC-02 gravimeter collected gravity data on 09-10 July 2009, during the night. The instrument processed and stored 1462 trajectories. The final measurement value was obtained by averaging 372 trajectories. The final measurement value at 0.4982 m was 979641630.8 μGal ± 4.8 μGal (combined standard uncertainty).

2.4.4 Validation via the International and European Comparisons of Absolute Gravimeters

To validate the absolute measurements performed with the two instruments, was included a link to the International and European Comparisons of Absolute Gravimeters (ICAGs 2005 and 2009 organized by the Bureau International des Poids et Mesures (BIPM) of Sèvres (France) and ECAG 2011 organized by Walferdange Underground Laboratory for Geodynamics (University of Luxemburg).

Specifically, data from the 7^{th} and 8^{th} ICAGs were selected for the IMGC-02 and FG5#238, respectively. Data from the ECAG 2011 are also taken for the IMGC-02. Unfortunately, it was no possible to make a comparison during ICAGs and ECAG between both instruments, because during ICAG-2005 the FG5#238 did not exist yet, during ICAG-2009 the IMGC-02 did not work properly and during the ECAG-2011 the FG5#238 didn't take part to the comparison.

Absolute gravity measurements at the BIPM were performed in a laboratory of the Pavillon du Mail building where the site B (B; Lat. 48.8294° N, Long. 2.2194° E, 56.33 m a.s.l.) comprises 7 stations where the instruments can be installed (Fig. 2.4). The foundation for the site B (composed of the stations B, B1, B2, B3, B4, B5 and B6) is a concrete block with a mass of more than 80 tones with the dimensions 6.0 m in length, 4.0 m in width and 1.5 m in depth. The top surface of the foundation is leveled to the floor to minimize the non homogeneity of the gravity field [Jiang et al., 2011].

Figure 2.4 – International and European Absolute Comparisons: on the left the IMGC-02 during the ICAG 2005; in the middle the FG5#238 during the ICAG 2009; on the right the IMGC-02 during the ECAG 2011.

During the 7th international comparison of absolute gravimeters (ICAG 2005), the IMGC-02 was installed in different sites. The results obtained show that with respect to the reference gravity values calculated for all absolute gravimeters participating in the ICAG 2005, the IMGC-02 obtained a difference less than 1 μGal, with an expanded uncertainty at 95% confidence level of 8.6 μGal [Jiang et al., 2011].

During the ECAG 2011, the IMGC-02 was installed in three sites of measurement in Underground Laboratory for Geodynamics in Walferdange in Luxemburg (Lat. 49.6647° N, Long. 6.1528° E, 295 m a.s.l.). The *g* values obtained by the IMGC-02 during ECAG 2011 are consistent with the Key Comparison Value: a difference of 2.2 μGal with a declared uncertainty of 5.4 μGal was obtained.

During the 8th international comparison of absolute gravimeters (ICAG-2009), the measurements were carried out between

September and October 2009. Each gravimeter measured at three gravity stations (Fig. 2.4).
In the site B, the gravimeter FG5#238 was installed twice: during the first installation, from 29 to 30 September 2009, a total of 26 sets were acquired in about 15 hours. In the second installation, from 2 to 3 October 2009, a total of 46 sets were acquired (in this case of 50 drops each one) in about 22 hours. In the site B6, from 30 September to 1st October 2009, a total of 38 sets of 50 drops each one were acquired in about 18 hours, while in the site B5, from 1st to 2nd October 2009, a total of 38 sets of 50 drops each one were acquired in about 18 hours.
The final measurement values in three different stations displayed that with respect to the reference gravity values, the FG5#238 obtained less than 5 μGal of degrees of equivalence calculated for all absolute gravimeters participating in the ICAG 2009, with an expanded uncertainty at 95% confidence level of 5.8 μGal [Jiang et al., 2012].

2.5 Comparisons between Data

The absolute gravity measurements presented in this study were conducted in different years (between 2005 and 2011) and at different latitude (from about 37° N to about 48° N) where the values of the absolute acceleration *g* are very different. The participation of both gravimeters used for this work to the International and European Comparisons of Absolute Gravimeters, allowed us to validate data normally acquired at any site and to understand the performance of both instruments when they are used in laboratory specially equipped

for gravity measurements. The goal is to verify if using these instruments in laboratories not specially prepared or even in field conditions their performance are still acceptable or comparable to that achieved when they are used in the best conditions. This goal was also useful to test different measurement procedures and instrumental setup, allowing to balance the accuracy and the efficiency of gravity measurements, saving also time and resources.

The results presented highlight the very high performances of both gravimeters even when they are used in sites where the environmental conditions are very hard such as those encountered on Mt Etna, the most high and active volcano in Europe. It is important to note that, using the FG5 even if the number of the set is significantly low (3-5 set), the *g* value and the set scatter are still comparable with those obtained after a long session.

Table 2.4 shows the absolute measurements at the three different sites referred to 0.5 m using the experimental values of the vertical gravity gradient measured at each station. At each measures is also associated the combined uncertainty, evaluated considering also the uncertainty of the vertical gravity gradient.

Concerning the CTA station, the environmental parameters during the measurements session with the FG5#238 were enough stable. The ambient temperature varied from 33.5 °C to 34.5 °C and the local pressure changed from 1008 mbar to 1006 mbar. The dispersion between the drops acquired is of the order of ± 20 μGal while the dispersion between the set is less than ± 10 μGal.

Also during the measurements session performed with the IMGC-02 the environmental parameters were stable with a maximum variation of the temperature between 30.0 °C and 32.0 °C. Concerning the

pressure, it varied between 1008.0 mbar and 1010.4 mbar. The apparatus experienced an oscillation of about ± 15 μGal and averaged trajectory residual within ± $1 \cdot 10^{-9}$ m.

Gravimeter	Acronym	Date	*g*(0.5 m) [μGal]+SAC	u_{comb}
FG5#238	CTA	03-05 July 2009	**980031509.7**	4.4
IMGC-02	CTA	08-09 July 2009	**980031506.8**	5.2
FG5#238	INRiM	29-30 October 2011	**980534206.2**	4.6
IMGC-02	INRiM	25-26 October 2011	**980534204.6**	4.8
FG5#238	SLN	11 July 2009	**979641626.9**	3.8
IMGC-02	SLN	09-10 July 2009	**979641630.8**	4.8

Table 2.4 – The *g* values reported at 0.5 m from the ground and the combined uncertainties of the final *g* values, evaluated considering also the uncertainties of the gradients.

The results of the measurements at CTA station showed a good agreement (Fig. 2.5), within few microgals (2.9 μGal) and within the combined standard uncertainty of the difference (5.2 μGal).
Concerning the Turin station at the INRiM, the environmental parameters during the measurements session with the FG5#238 were enough stable. The mean value of the ambient temperature is 28.1 °C with variations within 0.2 °C and the mean value of the local pressure is 996 mbar with variations of 0.1 mbar. The dispersion between the drops acquired is of the order of ± 20 μGal while the dispersion between the set is less than ± 10 μGal.
During the measurements session performed with the IMGC-02 at the gravity laboratory of Turin, the temperature varied between 26.0 °C and 26.4 °C, while the pressure changed between 984.0 mbar and 990.1 mbar. The apparatus experienced an oscillation of about ± 15

μGal and averaged trajectory residuals within ± $2.5 \cdot 10^{-9}$ m. A difference of 1.4 μGal (Fig. 2.5) was observed between measured collect with the FG5#238 and IMGC-02. The estimated uncertainties of the difference is 4.8 μGal.

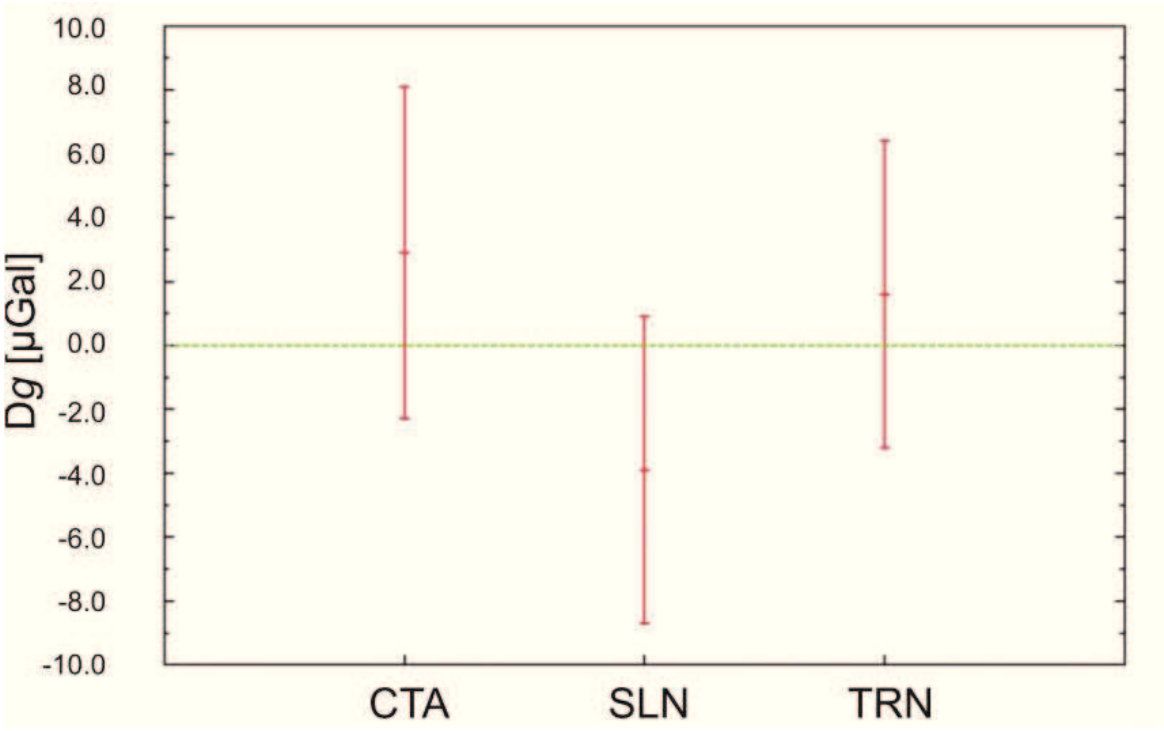

Figure 2.5 – Gravity differences (Δg) between the two absolute gravimeters in the three different stations CTA (2.9 ± 5.2) μGal, SLN (-3.9 ± 4.8) μGal and TRN (1.4 ± 4.8) μGal. The error bars represent the combined standard uncertainties.

Finally, regarding the SLN station, the environmental parameters during the measurements session with the FG5#238 were very stable. The mean value of the ambient temperature is 25.0 °C with variations within 0.5 °C, the mean value of the local pressure is 830 mbar with variations of 0.15 mbar while the humidity is about 60%. The ground vibration due to the volcano activity is not particularly high. The

dispersion between the drops acquired is of the order of ± 20 μGal (some set showed an higher dispersion) while the dispersion between the set is less than ± 10 μGal.
The IMGC-02 measurements performed at SLN showed stable environmental parameters. A maximum variation of the temperature between 38.0 °C and 40.3 °C was measured. The pressure variation between 829.5 mbar and 831.4 mbar was present. An oscillation of about ± 10 μGal was found in the collected data and averaged trajectory residuals within ± $1 \cdot 10^{-9}$ m were estimated.
The comparison of the results displayed a fairly good agreement, the difference between the two measures is 3.9 μGal (Fig. 2.5), within the estimated uncertainties of the difference (4.8 μGal).

2.6 Test Measurements Using FG5#238

Absolute data presented in this thesis refer to stations located at elevations ranging between 1400 and 2800 m a.s.l. Using the FG5#238 gravimeter at elevations higher than 2000 m a.s.l., it was impossible to take measures because the laser beam was not generated. In order to isolate the possible cause of the problem, was carried out various considerations taking into account: the power supply system, humidity, temperature and pressure of the sites where the tests were carried out. On Etna is used the same gasoline generator at all absolute stations without any problems. So, is excluded that the problem was related to the power generator. It was also excluded the humidity because *g* was measured at lower-altitude sites but with wetter conditions. For the ambient temperature, to ensure an operative temperature in the stations, was used a gas heater

which faces the laser. Although the temperature had reached about 20 °C, the instrument didn't work. After these tests were performed, the hypothesis that the problem could be due to the high altitude of the sites (which corresponds to low atmospheric pressure values) where the instrument is used was taken into account.

Gravity measurements are affected by the simultaneous action of various physical parameters acting both on the local gravity field and on the behavior of gravimeter. A scheme of a generalized configuration that brings out the significant input-output relationships present in all measuring apparatus is shown in Figure 2.6 [Doebelin, 1990].

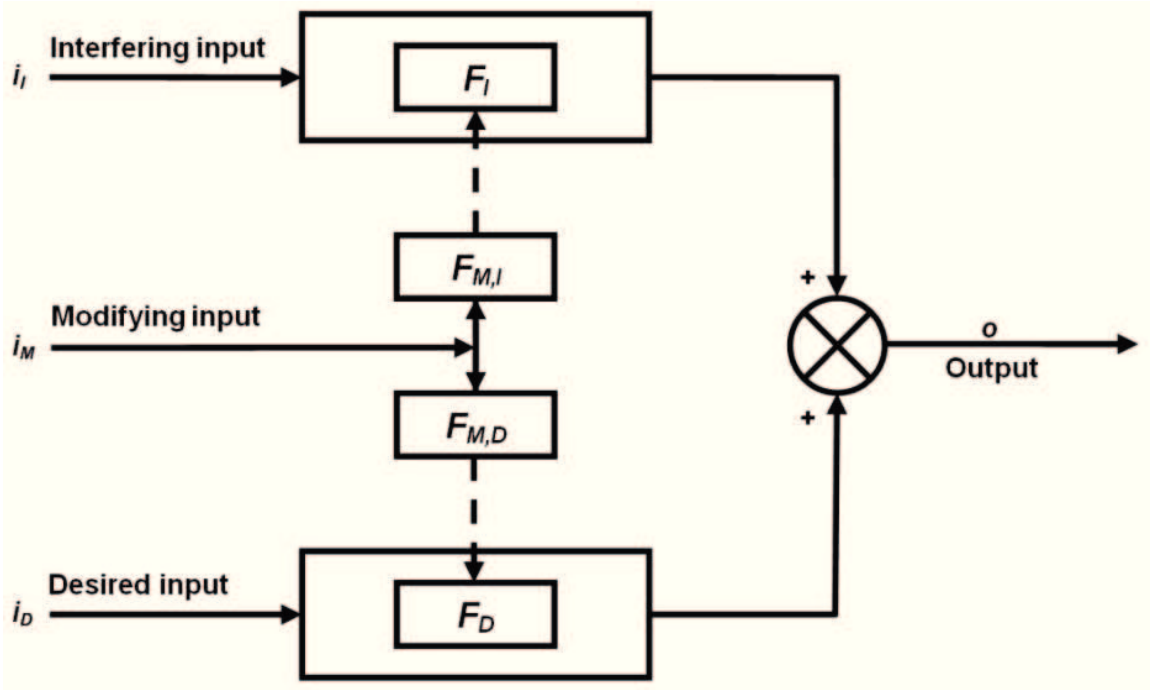

Figure 2.6 – Scheme of a generalized configuration highlighting the significant input-output relationships present in all measuring apparatus [After Doebelin, 1990].

Input quantities are classified in three categories: desired inputs, interfering inputs, and modifying inputs. Desired inputs represent the quantities that the instrument is specifically intended to measure. Interfering inputs represent quantities to which the instrument is unintentionally sensitive. F_D and F_I are the symbolized input-output relations for desired and interfering inputs respectively. Modifying inputs are the quantities that cause a change in the input-output relations for the desired and interfering inputs. The symbols $F_{M,I}$ and $F_{M,D}$ represent the specific manner in which i_M affects F_I and F_D, respectively. Basically, both for relative and absolute gravimeters, the main interfering inputs are temperature and humidity while the pressure is considered as a modifying input (at least with modern gravimeters). Changes in atmospheric pressure affect the gravity measurements in two ways: directly through the gravitational effect and indirectly, but to a lesser extent, with the Earth's surface deformation due to the weight of the atmosphere [Warburton and Goodkind, 1977]. The effects produced in the measuring instrument and therefore not related to a gravity field variation, are considered negligible. However, for the FG5#238 was assumed that the pressure is both a modifying input and an interfering input. In order to demonstrate this hypothesis, was tried to reproduce the same atmospheric pressure conditions at the high elevation sites as in the Catania laboratory (50 m a.s.l.). So, it was developed a hyperbaric chamber where the laser was isolated (see Figure 2.7a and 2.7b). The hyperbaric chamber was obtained from a PVC pipe, sealed at both ends, in which the cavity to allow the passage of the cables and optical fiber was made; all cavities were made watertight. In addition to the laser, inside the chamber were also placed an absolute pressure

sensor (PTX 1400), a temperature sensor (LM 35) and a humidity sensor (HIH 3605). The temperature was also monitored outside the chamber through another temperature sensor similar to the previous one. All signals have been sampled at 1 minute and stored by a datalogger (CR10X). The experiment was performed at the PDN observatory (2800 m a.s.l.).

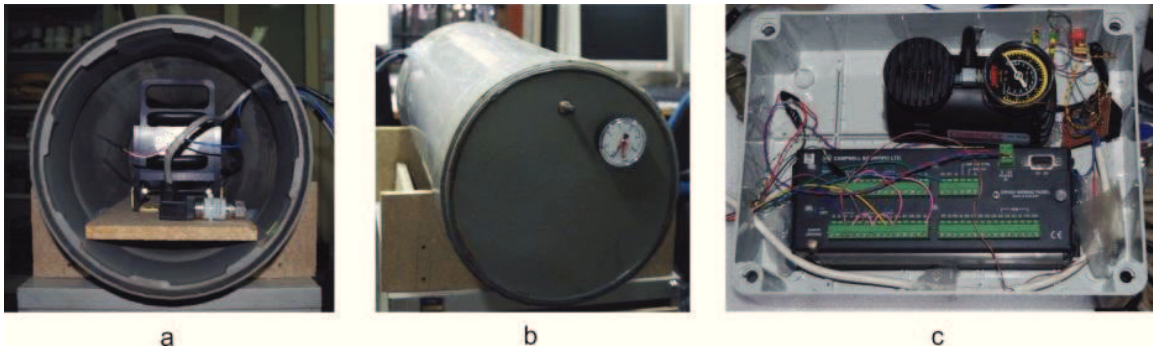

Figure 2.7 – The hyperbaric chamber made from a PVC pipe. The laser, together with pressure (PTX 1400), temperature (LM 35) and humidity sensors (HIH 3605), were placed inside the chamber (see Figure 2.7a-b). All signals have been sampled at 1 minute and stored by a datalogger (CR10X). A 12 V compressor was installed for automatic adjustment around the operative pressure values threshold (see Figure 2.7c).

After compressing within the chamber, the pressure value moved from 707 mbar (corresponding to the pressure value at an altitude of 2800 m) up to 900 mbar. At about 900 mbar the laser suddenly worked (see Figure 2.8). A threshold value for the pressure (just above the 900 mbar) was found and an automatic system using a Schmitt Trigger circuit (with window 65 mbar) to manage a 12 V compressor (see Figure 2.7c) was installed for automatic adjustment around the pressure values threshold. Using this extraordinary

solution, it was possible to take measures also at stations higher than 2000 m altitude.

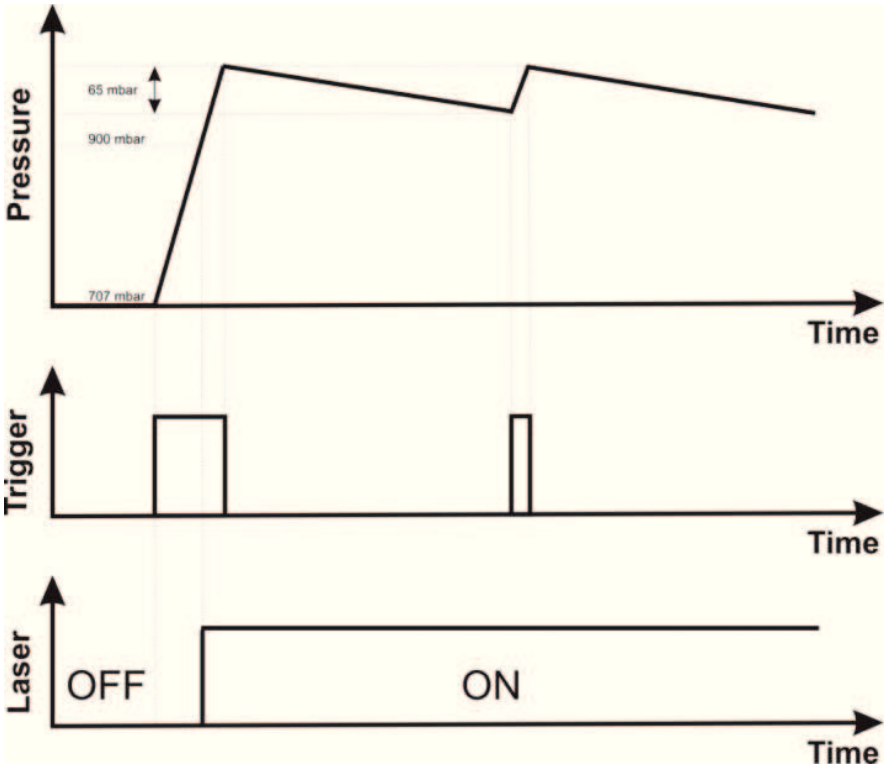

Figure 2.8 – Waveforms of the internal pressure of the chamber, the signal to drive the 12 V compressor and the activation of laser.

This experiment clearly showed a net dependence of the laser equipped the FG5#238 absolute gravimeter from the absolute pressure value. Unfortunately, it is not possible to export this solutions to all sites because it is very difficult reproduce these quasi-laboratory conditions.

Chapter 3

The Hybrid Method

In volcanic areas, discrete gravity measurements are usually carried out using relative spring gravimeters, which highlight spatiotemporal gravity variations with respect to a fixed reference site [Battaglia et al., 2003; Greco et al., 2010]. In a relative gravimeter, the spring-like device that suspends a mass of known quantity is susceptible to many influences, which degrade the precision of the gravity measurements. Changes in the characteristics of the spring-like device naturally occurring over time may become very high when such instruments are subjected to mechanical and thermal shocks typically encountered during handling and transportation. Often, the effects of temperature, pressure, tare or drift can combine, making it impossible to accurately measure small variations in gravity. Recently, field-usable absolute gravimeters (e.g., Micro-g LaCoste Inc. A-10, FG5 and

IMGC-02 prototype - see the Chapter 2 of this thesis) have been developed enabling gravity measurements at active volcanoes [Yoshida et al., 1999; Berrino, 2000; Furuya et al., 2003; Greco et ak., 2012], and such gravimeters are instruments much more technically sophisticated than relative spring gravimeters [Ferguson et al., 2008]. While the uncertainty of the gravity measurements obtained using an absolute gravimeter is theoretically low (less than ±5 μGal) compared to the uncertainty in measurements obtained with a relative spring gravimeter in extreme environmental conditions (±15 μGal), the sensitivity and complexity of the absolute gravimeters have, however, made it very difficult to employ them in other than laboratory conditions. Furthermore, the use of such transportable absolute gravimeters is time consuming and needs well-trained operators. These factors have the effect of limiting the number of points where absolute gravity can be measured within a limited measurement schedule. Under typical conditions encountered on a volcano, absolute gravity measurements can be made at only a few stations per day. For these reasons, repeated large-scale surveys are rarely conducted using absolute gravimeters, even though absolute gravity measurements could have better precision than the equivalent relative gravity measurements. In order to achieve a trade-off between uncertainty and efficiency of gravity measurements, the hybrid method has been developed for volcano monitoring that combines the use of absolute and relative gravimeters [Yoshida et al., 1999; Berrino, 2000; Furuya et al., 2003; Greco et al., 2012]. This approach takes advantage of the low uncertainty of absolute gravity measurements along with the simplicity and speed of relative gravity measurements. The hybrid method enables one to make gravity

measurements using relative spring gravimeters that are comparable in uncertainty to the gravity measurements from an absolute gravimeter, and without the need to loop back to a remote reference station. Furthermore, hybrid gravimetry might be especially useful in volcanic areas where gravity changes over time at the reference site could occur [Furuya et al., 2003]. Since 2007, the hybrid gravity survey has been systematically applied to monitor the Etna volcano. The use of the transportable absolute gravimeters has greatly improved the efficiency and changed the nature of the gravity survey. Combining absolute and relative gravity measurements provides reliable gravity data also in the summit area of the Mt Etna, where environmental conditions may significantly affect the quality of data acquired only with relative gravimeters. Here, are presented the results of three hybrid gravity surveys conducted at Mt Etna in the summers of 2007, 2008, and 2009, and encompassing several episodes of lava fountaining from the South-East Crater as well as the 2008–2009 flank eruption. After an overview of how absolute gravimeters operate in the gravity monitoring network of Etna volcano, will be discussed the outcomes of hybrid gravity observations and will be showed that a very good uncertainty of typically 10 μGal has been achieved. The gravity measurements were sufficiently accurate to detect at some times gravity changes attributed to subsurface mass redistributions driven by magmatic processes, which highlights the value of hybrid surveys for volcano monitoring purposes.

3.1 A New Scheme for Precise Measurements with Absolute and Relative Gravimeters

With the aim of introducing a new scheme for precise in situ measurements that combines absolute and relative gravity measurements, in this thesis was adopted a reproducible field methodology. The absolute acceleration of gravity is established by measuring the value at selected stations (reference points) using a transportable absolute gravimeter. The absolute acceleration of gravity at other stations is then determined on the basis of the difference in gravity measured by using relative gravimeters. Figure 3.1 shows the configuration of the proposed hybrid gravity network with relative and absolute gravimeters combined.

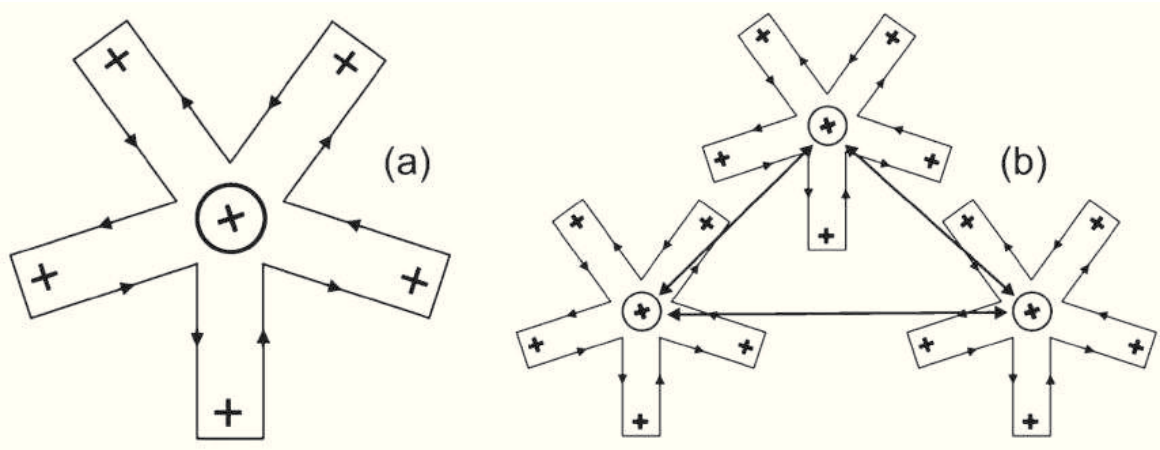

Figure 3.1 – (a) Star loop configuration of the hybrid gravity measurements. The *cross-shape marks* show the gravity benchmarks for relative gravity measurements and the *circled cross-shapes* show the reference stations where the absolute gravity measurements are conducted. (b) Following the arrow's directions, each relative benchmark is connected to the reference station at least three times. The distance between each pairs of points is typically less than 1-2 km. Each loop is connected with the adjacent through one or more points.

Generally, are connected five or six relative gravity benchmarks with each absolute site located a few kilometers away from the next, so that one sequence of relative measurements (connected in a star loop configuration) can be completed within a few hours to minimize the influence of the instrumental drift.

3.2 Uncertainty Estimate in Gravity Data

To demonstrate how the hybrid method improves the quality of data, reducing the value of the uncertainty in the gravity measurements, reference will be on two different gravity surveys accomplished in the western part of the volcano. The first survey was performed in 2005 in 13 stations of the gravity network and only a spring relative gravimeter was employed (Scintrex CG-3M#9310234). The second one was carried out in 2010 and besides the same relative stations, 5 absolute stations were added and measured by FG5#238 gravimeter as reference points for the relative ones (hybrid approach). Even if was considered a restricted number of absolute and relative stations, the results from this case study may be considered representative for the entire network since the Etna gravity network has more or less the same characteristics.

3.2.1 Absolute Gravity Data

Software supplied by the Micro-g LaCoste Company, used for data acquisition and analysis, provides an immediate value for the local gravity; it also includes a full-featured post-processor that allows to vary data analysis procedures and calculates the statistical

uncertainty, u_{stat}, given by the standard deviation of the absolute gravity values obtained for each set, σ_{set}, divided by the square root of the number of sets, N_{set}

$$u_{stat} = \sigma_{set}/\sqrt{N_{set}} \quad (3.1)$$

The total uncertainty, u_{abs}, for the final gravity value is given by

$$u_{abs} = \sqrt{u_{stat}^2 + u_{inst}^2} \quad (3.2)$$

where u_{inst} is the instrumental uncertainty due to different components of the measurement that can be grouped into four separate areas: Modeling, System, Environmental and Set-up, see the Chapter 2 for more details. The instrumental uncertainty of the FG5 is about 2.3 μGal.

The measurements of the absolute gravity with the total uncertainty, u_{abs}, gathered in 2010 in 5 selected stations of the Etna gravity network, are labeled in Table 3.1. Considering the difficulties of running such measurements in non-laboratory conditions in an environment where the observation sites are affected by severe ambient conditions, absolute gravity values (reduced for earth tides, ocean loading, local atmospheric and polar-motion effects) display a total uncertainty ranging between 2.7 μGal and 7.5 μGal (Tab. 3.1). Data scattering due to the strong floor vibrations, together with strong temperature and humidity fluctuations, were the most significant limitation to the uncertainty of the measured absolute gravity values acquired at Etna.

Station	Lat. [deg]	Long. [deg]	Elevation [m]	g_{abs} [µGal]	h [m]	u_{abs} [µGal]	FAG±u_{FAG} [µGal/m]
*SLN	37.694	14.973	1730	979641363.5	1.2927	2.7	336.5±2.8
*GAL	37.732	14.950	1875	979600598.0	1.2937	7.5	279.6±3.3
*MSC	37.770	14.950	1720	979632850.7	1.2897	4.0	282.1±3.0
*MSP	37.823	14.961	1450	979693569.4	1.2917	3.0	297.5±2.2
*GPL	37.827	15.028	1570	979667690.6	1.2962	2.8	310.8±3.5

Table 3.1 – Results of absolute microgravity measurements acquired in 2010 by FG5#238. The first four columns represent respectively the station acronym and the coordinates of the absolute gravity stations (the location of the sites is mapped in Figure 1.2). In the last four columns are reported: the measured microgravity values, g_{abs}, referred to the height h, the total uncertainty, u_{abs}, and the free-air vertical gradient (FAG) with the uncertainty, u_{FAG}, at the different stations.

3.2.2 Relative Gravity Data

To measure the gravity network of Mt Etna with spring gravity meters, the "step method" is mainly used. Following the multiple occupation sequence in the various stations, as required by the method (A-B B-A A-B B-C …), starting from a primary reference point, each station is occupied at least three times. In this way the final Δg values between pairs of adjacent stations can be obtained from the mean of the three Δg calculated and the uncertainty of the link, $u_{\Delta g}$, to assign to this value, will be the square root of the sum of the squares of the individual uncertainties attributed to each Δg. Table 3.2 shows gravity differences Δg with the uncertainty $u_{\Delta g}$ between pairs of adjacent stations, collected in 2005 in 13 selected stations of the relative microgravity network, reduced for tidal effect

using a local tide model, corrected for the instrumental drift and referred to a single reference station (ADR). The distance between adjacent stations ranges between 1 km and 3 km and each station can be reached on unpaved roads.

Station	Link	Δg [mGal]	$u_{\Delta g}$ [μGal]	g_{ADR} [mGal]	u_{rel} [μGal]
IFO	IFO-MDZ	–10.288	8	650.856	6
MDZ	MDZ-MFO	–32.148	10	640.568	7
MFO	MFO-MPA	–22.502	8	608.442	8
MPA	MPA-MNZ	29.085	5	585.940	8
MNZ	MNZ-BCH	32.148	10	615.025	8
BCH	BCH-RLN	33.901	6	647.173	8
RLN	RLN-MSP	12.925	6	681.074	8
MSP	MSP-L81	16.658	6	693.999	9
L81	L81-MSM	–49.171	3	710.657	7
MSM	MSM-GLA	–25.376	7	661.486	7
GLA	GLA-GPA	20.633	3	636.110	6
GPA	GPA-MRO	13.474	3	656.743	9
MRO	MRO-MAR	29.392	5	670.317	6

Table 3.2 – Results of traditional microgravity measurements acquired in 2005 in 13 selected relative gravity stations of the Etna gravity network. The columns indicate respectively: the station acronym, the link between two adjacent relative stations, the gravity differences, Δg, between two adjacent relative stations, the uncertainty, $u_{\Delta g}$, associated to each Δg, the microgravity values, g_{ADR}, at each station obtained with the least squares method as described in the text and referred to ADR station and the associated uncertainty u_{rel}.

Considering all gravity stations as part of a loop, to evaluate the gravity value at each station with the associated total uncertainty, was

applied a strict compensation procedure based on the least squares adjustment method, by solving a linear system consisting by observation equations (method of indirect observations).

Errors in the gravity measurements can occur both in the measuring point and during the transfer from one station to another. Obviously, these errors will have an accidental and a systematic component. Errors that can be accumulated at the measurement point, are errors arising from incorrect reading or imperfect leveling of the instrument, errors induced by external environmental (i.e. mechanical vibrations, microseisms, magnetic effects, etc.). During the transfer from one station to another, particularly critical are the mechanical vibrations that induce changes in behavior or properties of the gravimeters. The most important systematic error originates between two stations; to eliminate this, observations are treated as gravity differences between pairs of stations occupied consecutively. It is considered that the differences between the accidental errors of the two stations have a stochastic distribution.

The systematic components of the error are included in the observation equation which takes the general form:

$$\sqrt{P_n}\left(g_i - g_j - k_m \Delta g_{ij}\right) = \varepsilon_{ij} \qquad (3.3)$$

where P_n is the observation weight, g_i and g_j are the unknown gravity values at the i-th and j-th stations, k_m is the unknown scale factor for the m-th link, Δg_{ij} is the measured gravity difference between the i-th and j-th station and ε_{ij} is the residual. The solution, with the least squares method, of the linear system of observation equations, whose number exactly corresponds to the measured gravity differences, leads to the adjusted of g values. In order to describe the

mathematical procedure, considering the P_n term of the Equation 3.3 equal 1, the equation simplifies to

$$g_i - g_j - k_m \Delta g_{ij} = \varepsilon_{ij} \quad (3.4)$$

starting from the known terms g_i^0, g_j^0 and k_m^0

$$g_i = g_i^0 + x_i \quad (3.5)$$

$$g_j = g_j^0 + x_j \quad (3.6)$$

$$k_m = k_m^0 + x_m \quad (3.7)$$

where x_i, x_j and x_m are the unknown corrections to be made to the known terms g_i^0, g_j^0 and k_m^0, therefore the Equation 3.4 becomes

$$\left(g_i^0 + x_i\right) - \left(g_j^0 + x_j\right) - (k_m^0 + x_m)\Delta g_{ij} = \varepsilon_{ij} \quad (3.8)$$

by known terms g_i^0, $g_j^0$and k_m^0

$$g_i^0 - g_j^0 - k_m^0 \Delta g_{ij} = l_{ij} \quad (3.9)$$

the Equation 3.4 is further simplified in

$$x_i - x_j - x_m \Delta g_{ij} + l_{ij} = \varepsilon_{ij} \quad (3.10)$$

or in matrix notation

$$\boldsymbol{Ax} + \boldsymbol{l} = \boldsymbol{v} \quad (3.11)$$

where $\boldsymbol{A}$ is the $n \times r$ matrix of the r unknowns (x_i, x_j and x_m) due to the n measured gravity difference: the coefficients of the matrix are +1 for x_i, -1 for x_j and $-\Delta g_{ij}$ for x_m; $\boldsymbol{x}$ is the vector of the r unknown corrections, $\boldsymbol{l}$ is the vector of the n errors calculated with the known terms g_i^0, g_j^0 and k_m^0 and $\boldsymbol{v}$ is the vector of the n residuals.
To satisfy the least squares method, such relationship must exist

$$\boldsymbol{v}^{\mathrm{T}}\boldsymbol{v} = min \tag{3.12}$$

by defining the following matrix

$$\boldsymbol{R} = \boldsymbol{A}^{\mathrm{T}}\boldsymbol{A} \tag{3.13}$$

the unknowns x_i,x_j and x_m are obtained by the expression

$$\boldsymbol{x} = \boldsymbol{R}^{-1}\boldsymbol{A}^{\mathrm{T}}\boldsymbol{l} \tag{3.14}$$

and the residuals ε_{ij}

$$\boldsymbol{v} = \boldsymbol{A}\boldsymbol{x} + \boldsymbol{l} \tag{3.15}$$

Therefore, through Equation 3.14 is possible to calculate the corrections to be included in Equations 3.5, 3.6 and 3.7 in order to obtain the values of gravity. The determination of the gravity values at each station (Tab. 3.2) is achieved through iterative methods: after each iteration the new approximate values are calculated and used for the next iteration. All links in which residuals ε_{ij} exceed the limit of $3\sigma_0$, where σ_0 is the standard deviation of the unit weight, are rejected. The value σ_0 is related to the theoretical variance of the unit weight σ_0^2 from the equation

$$\sigma_0 = \sqrt{\sigma_0^2} = \sqrt{\frac{\sum \boldsymbol{v}^{\mathrm{T}}\boldsymbol{v}}{n-r}} \tag{3.16}$$

where n is the number of accepted links and r is the number of unknowns; in this way, a small number of links with major errors are separate from others who have a normal error distribution. To calculate the total uncertainty u_{rel} of each station (Tab. 3.2), use the r_{ii} diagonal elements of $\boldsymbol{R}$ matrix and apply the relationship

$$u_{rel} = \sqrt{\sigma_0^2 \cdot r_{ii}} \tag{3.17}$$

Applying the procedure described above to data acquired in 2005 in the 13 selected gravity stations, the total uncertainty is between 6 and 9 μGal (Tab. 3.2). Although the uncertainty $u_{\Delta g}$ between some pairs of stations is small enough (3 μGal in some cases) at the end of the compensation procedure a larger total uncertainty at each measurement is assigned to all values. Consequently, the final gravity value at each station will depend both on the uncertainty $u_{\Delta g}$ and on the closure error of the loop formed by the stations.

3.2.3 Hybrid Gravity Data

Following the hybrid method, Table 3.3 shows data acquired in 2010 in the western part of the volcano in 13 relative stations (the same used in 2005 to evaluate the uncertainty of the relative data; see paragraph 3.2.2) and at 5 absolute stations located in the same area of the volcano and used as reference for relative measurements. As stated before, each relative station was linked with the closest absolute one, labeled with the symbol "*" in Table 3.3. Following this hybrid approach, and considering that at each absolute station the free-air vertical gravity gradients is measured (Table 3.2), the total uncertainty was estimate at each station according to the equation

$$u_{\mathrm{hyb}} = \sqrt{u_{\Delta g}^2 + u_{\mathrm{FAG}}^2 + u_{\mathrm{abs}}^2} \qquad (3.18)$$

where $u_{\Delta g}$ is the uncertainty calculated to all differences, Δg, necessary to connect a relative gravity station to an absolute site, u_{FAG} is the uncertainty of the vertical gravity gradient and u_{abs} is the total uncertainty for each absolute measurement calculated as described in

the previous paragraph 3.2.1. The uncertainties attributed to each Δg, $u_{\Delta g}$, is calculated as described in the section 3.2.2.

Station	Link	Δg [mGal]	$u_{\Delta g}$ [µGal]	g_{abs} [mGal]	u_{hyb} [µGal]
IFO	*SLN-IFO	9.158	3	650.837	5
MDZ	*GAL-MDZ	39.736	4	640.626	9
MFO	*GAL-MFO	7.570	2	608.460	8
MPA	*GAL-MPA	14.894	3	585.996	9
MNZ	*MSC-MNZ	–18.120	5	615.024	7
BCH	*MSC-BCH	14.009	7	647.153	9
RLN	*MSP-RLN	–12.868	5	681.011	6
MSP	*MSP-MSP	0.062	4	693.942	5
L81	*MSP-L81	16.550	6	710.430	7
MSM	*GPL-MSM	25.362	4	661.430	6
GLA	*GPL-GLA	–31.949	2	636.067	5
GPA	*GPL-GPA	–11.231	5	656.785	7
MRO	*GPL-MRO	2.281	6	670.296	8

Table 3.3 – Results of hybrid microgravity measurements acquired in 2010 in 13 selected relative gravity stations and 5 absolute gravity reference points of the Etna gravity network. The columns indicate respectively: relative stations acronym, link between a relative station and an absolute reference point, gravity difference, Δg, between a relative station and an absolute reference point and associated uncertainty, $u_{\Delta g}$, absolute gravity values acquired at the reference point by FG5#238 absolute gravimeter and the associated uncertainties. Each relative station was linked with the closest absolute reference point indicated with the symbol "*".

Results highlight that the hybrid method applied to collect data in the western part of the volcano includes 13 relative and 5 absolute stations, allowing to obtain microgravity data with a total uncertainty, calculated by Equation 3.18, between 5 and 9 µGal (Tab. 3.3).

Results indicated that the final total uncertainty strongly depends on the $u_{\Delta g}$ uncertainty calculated between each single couple of stations and propagation errors are not included.

3.3 Hybrid Gravity Measurements

Between 2007 and 2009, were conducted three surveys at Mt Etna, in June 2007, July 2008, and July 2009. According to the above considerations, is applied a combined method of precise in situ gravity measurements and differential GPS measurements to provide effective volcano monitoring. At each reference point, i.e., circled cross-shape in Figure 3.1, absolute gravity measurements, vertical gravity gradient, and GPS measurements were conducted. Gravity and GPS measurements were generally occupied at the same marks to ensure the uncertainty of a few centimeters in height and 10 μGal of gravity (each measurement session takes approximately 6 h). Using a commercial GPS receiver (e.g., Leica GX1230), the precision of vertical measurement is 10 mm + 0.5 ppm. Therefore, it is not so difficult to attain 1 cm uncertainty in the GPS height measurements. Nonetheless GPS measurements could not be conducted at some absolute sites for logistical reasons (e.g., the dense vegetation on some areas of Etna masks the GPS satellite signal). However, since are integrated the GPS data with those acquired at the GPS periodic network managed by the INGV team [i.e., Bonforte et al., 2007a], the spatial resolution of elevation data is sufficient for estimating the vertical uplift in the gravity stations [Bonaccorso et al., 2011a].

Absolute gravity data acquired with both IMGC-02 (stations at elevation more than 1800 m a.s.l.) and FG5 (stations at elevation less

than 1800 m a.s.l.) gravimeters were all reduced to 0.25 m from the ground through the vertical gravity gradient acquired at each absolute station. Table 3.4 shows all the measured values at the absolute stations using FG5 and IMGC-02 gravimeters in 2007, 2008, and 2009. The absolute stations located on Etna volcano were used as references for relative measurements acquired in different benchmarks of the relative gravity network, so that the high precision absolute values for all relative benchmarks were obtained by adding the differences (Δg) between each absolute station with the relative ones to the absolute value measured at each reference point. The relative data reduction included the removal of solid Earth tides and daily gravimeter drift.

The uncertainty affecting absolute gravity data is shown in Table 3.4, while the error affecting a single Δg measured with the relative gravimeter Scintrex CG-3M between an absolute station and a relative benchmark generally ranges between 3 μGal and 7 μGal. Higher errors, sometimes up to 15 μGal, are observed in some stations located on the summit area of the volcano due to the harsh environment and the greater distances (up to 5 km) between absolute and relative sites. Thus, the uncertainties on temporal gravity changes observed by combining absolute and relative gravity measurements, at the 95% confidence interval, are mostly less than 10 μGal, although uncertainties more than 10 μGal were obtained in a few sites with extremely unfavorable environmental conditions.

In order to check if absolute gravimeters show any working anomalies, are conducted repeated measurements at the CTA station at the beginning and at the end of each survey at Etna, where the FG5 is usually maintained. Generally, is obtained a good reproducibility

of the absolute measurements at this station (the gravity values are always comparable within 6 μGal). Only the gravity data collected at the CTA station in 2007 by IMGC-02 gravimeter are probably biased due to some problems in the vacuum system and the seismometer.

Date	Gravimeter	Station	Lat. [km]	Long. [km]	Elevation [m]	h [mm]	g(h) [μGal]	Ug [μGal]	$\gamma \pm U_\gamma$ [μGal/m]
30 June 2007	IMGC-02	CTA	4151.897	507.335	50	499.9	980031500.8[a]	12.4	-
1 July 2007	IMGC-02	SLN	4171.864	497.619	1730	492.2	979641610.2	10.1	-
2 July 2007	IMGC-02	MNT	4174.638	500.264	2550	487.1	979468483.7	17.3	-
4 July 2007	IMGC-02	PDN	4179.852	501.585	2820	480.4	979379856.3	21.5	-
3 July 2008	IMGC-02	CTA	-	-	-	517.7	980031537.4	10.6	305±13.6
5 July 2008	IMGC-02	MNT	-	-	-	515.6	979468458.5	21.7	275.2±15.1
6 July 2008	IMGC-02	SLN	-	-	-	514.2	979641609.3	10.6	361.2±6.5
8 July 2008	IMGC-02	PDN	-	-	-	515.3	979379797.8	30.1	293.5±16.5
10 July 2008	IMGC-02	DNV	4193.618	511.430	1250	514.2	979741042.9	10.2	315.6±16.9
11 July 2008	IMGC-02	CTA	-	-	-	518.9	980031537.8	16.1	-
9 July 2009	IMGC-02	CTA	-	-	-	500.9	980031505.9	10.4	-
10 July 2009	IMGC-02	SLN	-	-	-	498.2	979641630.8	9.6	-
11 July 2009	IMGC-02	MNT	-	-	-	498.1	979468506.4	10	-
12 July 2009	IMGC-02	PPR	4183.403	503.081	1825	497.5	979618347.9	10.4	258.7±8.3
14 July 2009	IMGC-02	PDN	-	-	-	489.7	979379869.1	25.1	378.8±9.6
30 June 2009	FG5#238	GVL	4176.081	495.594	1875	1291.7	979600585.1	8.8	285.0±4.3
1 July 2009	FG5#238	MSC	4180.297	495.596	1720	1288.7	979632850.2	7.4	274.2±5.7
2 July 2009	FG5#238	MSP	4186.177	496.567	1450	1289.7	979693562.5	9.7	297.2±4.9
3 July 2009	FG5#238	CTA	-	-	-	1286.7	980031291.7	6.4	278.6±7.8
7 July 2009	FG5#238	GPA	4186.620	502.464	1570	1298.7	979667698.9	6.3	312.2±6.6
11 July 2009	FG5#238	SLN	-	-	-	1293.7	979641362.1	6.3	335.1±5.3
17 July 2009	FG5#238	CPC	4177.748	507.664	1150	1298.7	979767827.4	12.5	291.7±6.1
21 July 2009	FG5#238	SES	4180.519	504.491	1735	1293.7	979637857.4	11.9	288.5±8.6
22 July 2009	FG5#238	CVE	4172.197	502.203	1680	1291.2	979669188.5	9	306.6±6.3
23 July 2009	FG5#238	CTA	-	-	-	1290.7	980031297.6	6.3	-

Table 3.4 – The first six columns represent: (1) date; (2) absolute gravimeter employed; (3) acronym and (4-6) coordinates of the absolute gravity stations. Coordinates are in UTM projection, WGS84 ellipsoid. The locations of the sites are mapped in Fig. 1.2. The last four columns represent: (7) reference height h; (8) measured gravity values g referred to the height h; (9) expanded uncertainty U (p=95 %) of g; (10) free-air vertical gradient γ with the expanded uncertainty U (p=95 %).

[a] Biased g value (see text for details).

3.3.1 Gravity Changes During 2007-2008 Period

The gravity variations observed between June 2007 and July 2008 are plotted in Fig. 3.2. Using GPS data, gravity measures were corrected for the free-air effect through the value of the free-air gravity gradient measured at absolute stations in 2008 (Table 3.4). GPS measurements at absolute stations and geodetic surveys [Bonaccorso et al., 2011c] showed negative vertical variations up to −2.7 cm in the benchmarks along the North-East Rift. The residual gravity field calculated for the 2007-2008 period is mainly characterized by a negative variation in the upper north-east sector of the volcano, with wavelength of about 5 km (defined by stations along the North-East Rift) and a maximum variation of about −60 μGal (at stations DP, MC, and UM; Fig. 1.2). Moving eastward, the amplitude of the gravity change decreases rapidly, being almost within error at benchmark MAR. Largely because of extensive snow cover, could not obtain enough gravity data on the summit craters area in June 2007.

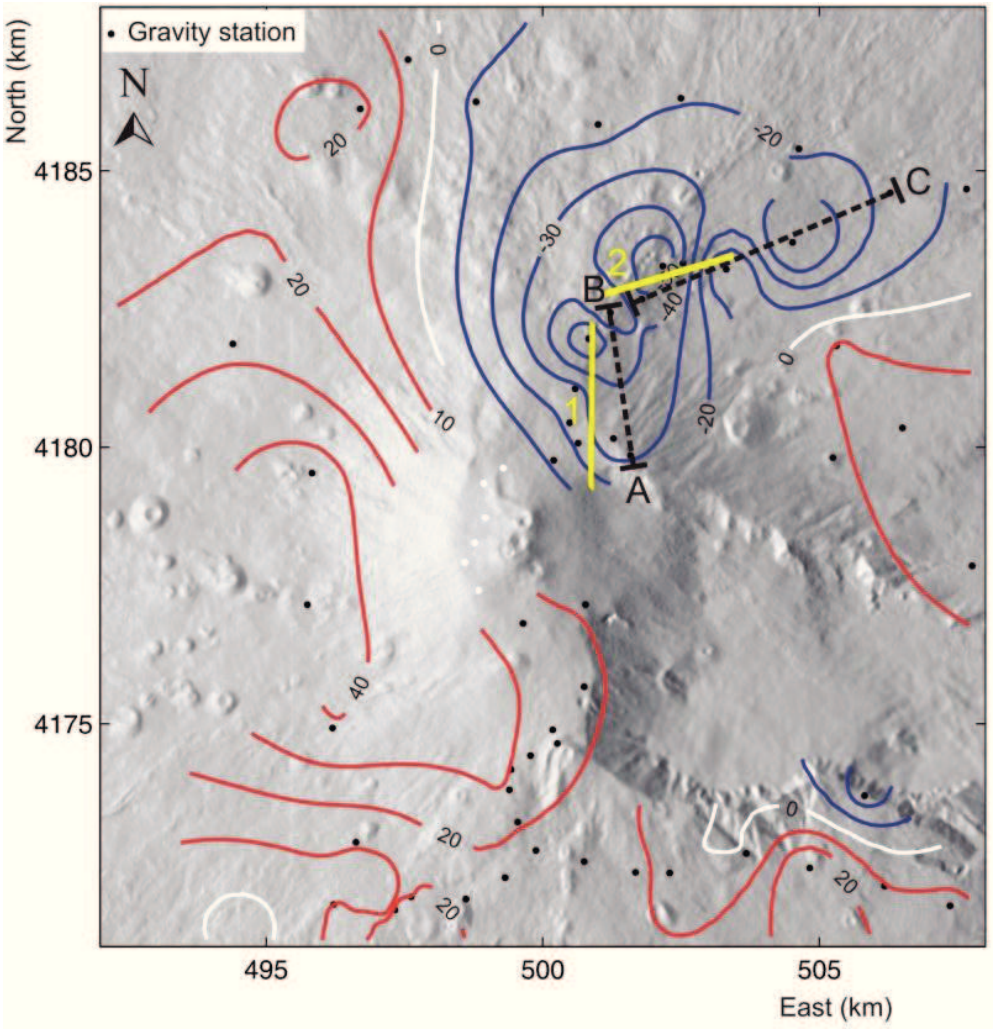

Figure 3.2 – Hybrid gravity contour maps at 10 μGal intervals showing the June 2007-July 2008 gravity change. In June 2007, the gravity stations in the summit craters area were not occupied because of snow coverage (white circles). The trace of the A-B-C profile (black dashed lines) and the projection on the surface of the modeled sources (yellow lines) are also drawn. Geographical coordinates are expressed in UTM projection, zone 33 N (WGS84 ellipsoid).

3.3.2 Gravity Changes During 2008-2009 Period

The gravity variations observed between July 2008 and July 2009 are plotted in Figure 3.3. It was calculated the residual gravity changes using the measured values of the free-air gravity gradient at each absolute station (Tab. 3.4). The results show a free-air gradient close to the theoretical value (−308.6 μGal/m) for some reference stations (GPA and MSP). Across the North-East Rift, the free-air gradient differs considerably, with values of −347.7±33 μGal/m in the PDN station and −258.7±16 μGal/m in the PPR station (Tab. 3.4). In the South flank, the free-air gradient ranges between −281.4±30 μGal/m in the MNT station and −358.2±13 μGal/m in the SLN station. These differences are generally caused by topographic effect and the local Bouguer anomalies [i.e., Rymer, 1994]. However, no significant vertical ground movements (less than 1-2 cm), able to produce significant gravity changes, are evidenced by GPS measurements at absolute stations and geodetic surveys [Bonforte et al., 2011] in the considered period. The residual gravity field shows positive variations up to 80 μGal with a wavelength of about 10–12 km, affecting mainly the central and eastern zones of the volcano. The annual contour map shows also a negative gravity variation exceeding the measure error (uncertainty) in some stations located in the peripheral part of the volcano (Fig. 3.3).

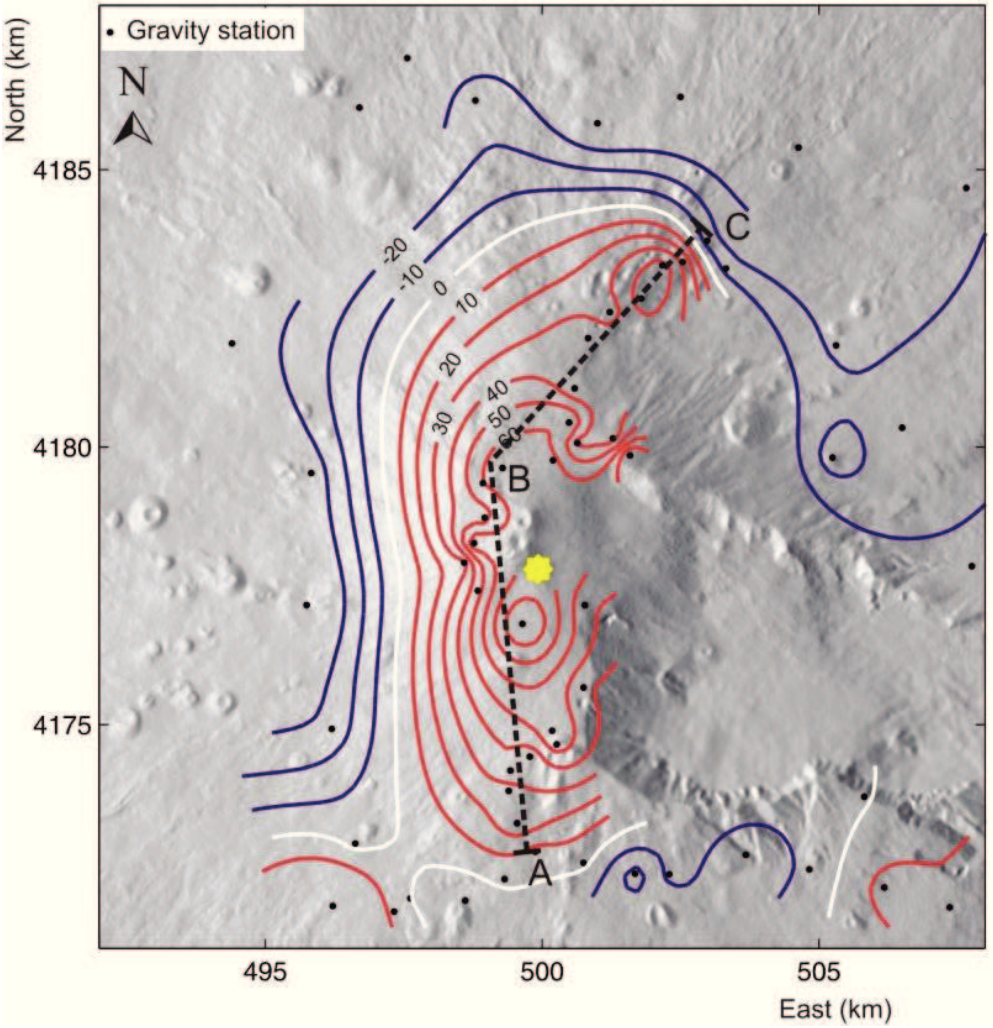

Figure 3.3 – Hybrid gravity contour maps at 10 μGal intervals showing the July 2008–July 2009 gravity change. The trace of the A-B-C profile (black dashed lines) and the projection on the surface of the modeled source (yellow star) are also drawn. Geographical coordinates are expressed in UTM projection, zone 33 N (WGS84 ellipsoid).

3.4 Case Study: Eruptive Activity From 2007 to 2009

During 2007-2008, eruptive activity of Etna was confined to the volcano's summit area and characterized by seven short episodes of lava fountaining from the South East Crater. The main paroxysmal episode occurred on 4-5 September 2007 and lasted for more than 10 h [Andronico et al., 2008]. All the paroxysmal events were also accompanied by lava flow emission from fissures opened at the base of the South-East Crater. On 10 May 2008, a new vent opened at the eastern base of the South-East Crater. This vent produced intense lava fountaining, anticipating by only 3 days the onset of a new effusive flank eruption from a system of eruptive fissures propagating SE from summit craters toward the western border of the Valle del Bove. After the initial phase of the eruption, when the lavas emerged, North-South dry fractures formed in the upper portion of the North-East Rift. No eruptive activity was involved with these fractures. After about 14 months of continuous lava effusion, the eruption ended on 6 July 2009 (http://www.ct.ingv.it).

The source location of volcanic tremor suggests that the eruptive episodes in 2007-2008 were fed by magmas stored in the central conduit region at depths of 1 to 2.8 km a.s.l. Magma was systematically transferred from the central upper plumbing system toward South-East Crater prior to each paroxysmal event [Bonaccorso et al., 2011b]. The intrusion associated with the 2008-2009 eruption was characterized by a near-vertical intrusion starting from the central conduit system at a depth of 1.6 km below the summit area and propagating towards the east [Napoli et al., 2008;

Aloisi et al., 2009; Currenti et al., 2011b]. The departure from the upper conduit of the propagating dike could be triggered by the rapid rise of significant volume of rich-gas magma erupted through the powerful lava fountain on May 10, 2008, 3 days before the beginning of 2008-2009 flank eruption [Bonaccorso et al., 2011b].

3.4.1 Interpreting the 2007-2008 Gravity Observations

The period 2007-2008 is marked by a negative gravity variation in the upper northeastern sector of the volcano (Fig. 3.2). This area is one of the main intrusion zones of Etna and it is affected by active extensional tectonics [Borgia et al., 1992; Lo Giudice and Rasà, 1992; Froger et al., 2001] and a movement toward ESE [Bonforte and Puglisi, 2003, 2006; Puglisi and Bonforte, 2004]. Geodetic measurements provided insights on three possible dislocation sources positioned as shallow vertical planes bordering the sliding sector of the North-East Rift and beneath the summit craters [Bonforte et al., 2007a, b]. The movements of these dislocation structures produce a general eastward motion of the northeastern sector of Mt Etna. The moving sector is bounded westward by the Provenzana fault-North-East Rift system, which behaves mainly as a normal fault, and northward by the left-lateral transcurrent Pernicana fault (Fig. 1.2). Southwestward, it is bounded by a tensile structure. The general eastward motion is also accompanied by a westward tilt of the sliding block and a lowering of the North-East Rift. Furthermore, as consequences of this complex eastward movement of the eastern flank, significant extensions of the North-East Rift area and the

uppermost part of the Pernicana fault are normally observed [Bonforte et al., 2007b].
Unfortunately, don't have gravity information on the summit craters area, owing to extensive snow cover in June 2007. Therefore, lack sufficient information to interpret the 2007-2008 residual gravity field. Considering the structural context within which the 2007-2008 gravity changes took place, there is the possibility that, rather than being directly associated to magma withdrawal, the observed gravity change could reflect an increase in the rate of micro-fracturing affecting this unstable area of the volcano, implying a decrease in the local rock density (gravity decrease). This hypothesis is also fairly consistent with negative height changes observed in the same area during the investigated period [Bonaccorso et al., 2011c].
Accordingly, the residual gravity changes (Fig. 3.2) are interpreted assuming an underground mass deficiency (as a consequence of a rarefaction process of the medium related to the opening of new voids). It is adopted the same geometry already used to interpret gravity variations due to mass changes below the North-East Rift zone encompassing the 2002-2003 eruption [Bonforte et al., 2007a]. To assess the geometrical characteristic of the source and the amount of mass involved in the redistribution process occurring between June 2007 and July 2008, a 3D model was derived using a forward method. Were used the analytical solutions for a prismatic body [Blakely, 1995] and included the topography, taking into account the altitude difference between the gravity stations and the source. For more details on the analytical forward models and on the geophysical inverse problem, see the Appendix A.

The June 2007-July 2008 gravity changes were matched (Fig. 3.4) using two prismatic-shaped bodies (for their characteristics see Table 3.5) along the Provenzana fault-North-East Rift system, roughly coincident with ground deformation sources inferred by geodetic data inversion to explain ground deformation patterns in this sector of the volcano [Bonforte et al., 2007a, b].

In keeping with the good fit obtained (Fig. 3.4), the RMSE calculated between observed and calculated data is lower than 10 μGal. A density contrast of −110 kg/m^{3}and −150 kg/m^3 has been determined by the modeling procedure for the sources 1 and 2, respectively. The total mass deficiency inferred is about -10×10^9 kg for source 1 and about -13×10^9 kg for source 2 (Tab. 3.5). Assuming an average value of 2500 kg/m^3 as density of the volcanic rocks, was estimate also the degree of mediumrarefaction. The computed negative density variations of about −110 kg/m^3 for source 1 and about −150 kg/m^3 for source 2 point to a rarefaction of the medium of the order of 4% and 6% for the sources 1 and 2, respectively.

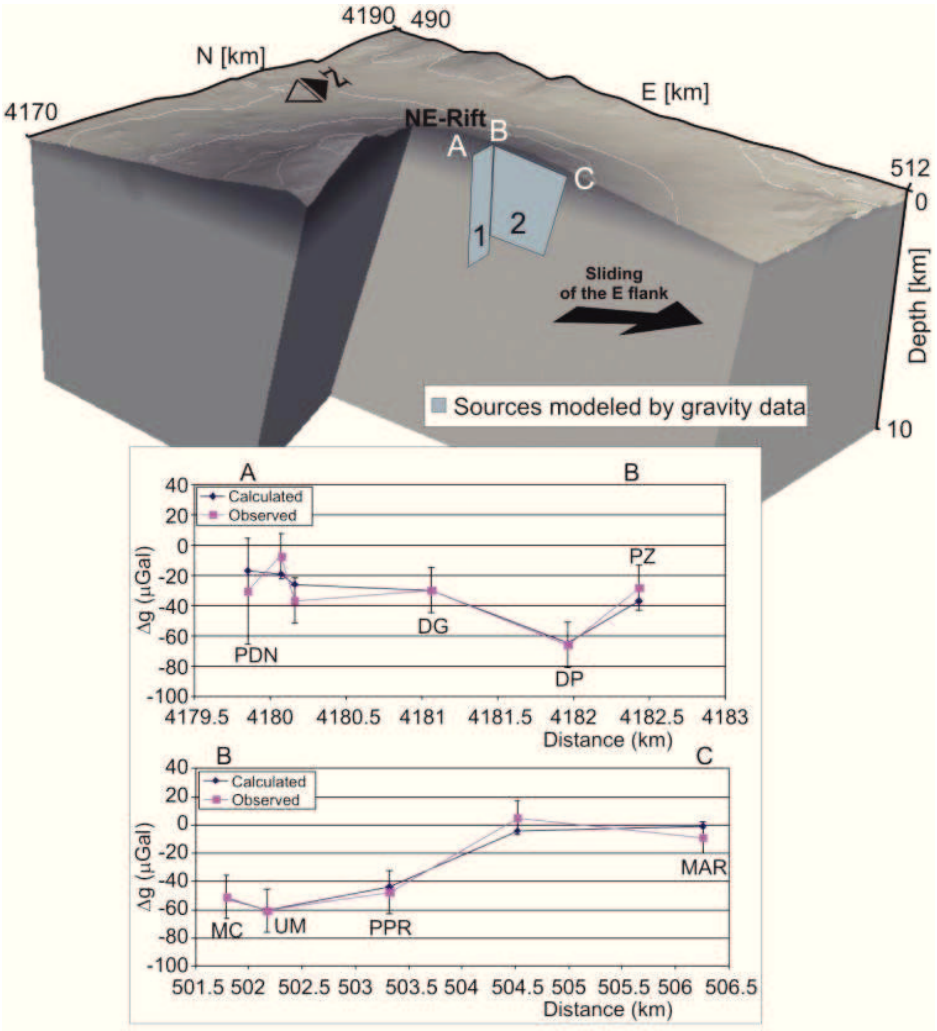

Figure 3.4 – 3D perspective block diagram showing the sources modeled through 2007-2008 gravity variations observed on the upper north-east sector of the volcano (see Table 3.5 for the parameters of the sources). The comparison between gravity changes observed in 11 stations located on the upper north-east sector of the volcano (A-B-C profile) and the effect of the best-fitting model sources is also shown.

Parameter	Gravity source 1	Gravity source 2
Longitude	500.910 km	502.250 km
Latitude	4180.490 km	4183.120 km
Azimuth	N0°E	N73°E
Depth	3000 m a.s.l.	2550 m a.s.l.
Length	3050 m	2600 m
Dip	90°	90°
Thickness	10 m	14 m
$\Delta\rho$ density contrast	–110 kg/m^3	–150 kg/m^3
ΔM	$-10\cdot10^9$ kg	$-13\cdot10^9$ kg
ΔV	$91\cdot10^6$ m^3	$92\cdot10^6$ m^3

Table 3.5 – The best models parameters found through gravity data observed during 2007-2008 period. Coordinates are in UTM projection, WGS84 ellipsoid.

3.4.2 Interpreting the 2008-2009 Gravity Observations

The period 2008-2009 was characterized by a significant positive gravity variation involving almost all the volcano edifice (Fig. 3.3). Gravity, ground deformation, and geochemical data [Bonaccorso et al., 2005; 2011a; Spilliaert et al., 2006; Greco et al., 2010] allowed to identify a shallow-intermediate magma plumbing system at intermediate depth of 2-6 km b.s.l. It is made up of a vertically elongated storage volume that bounds the western side of the high-density body detected by gravity prospecting [Schiavone and Loddo 2007] and represents the preferential pathway for magma ascent, even for recent volcanic activity. This intermediate elongated

pressurizing storage provokes a wide ground deformation pattern as revealed by geodetic measurements [Bonforte et al., 2008; Bonaccorso et al. 2011a]. Most of the magma mass accumulates at the shallower interface at the upper limit of the high-density body and is normally detected by the gravity changes [Bonaccorso et al., 2011a].

Also, the position and the wavelength of the 2008-2009 gravity anomaly points towards a source located at intermediate depth in the South-East flank of the volcano. The gravity change was computed using the analytical solutions for an ellipsoidal mass source [Clark et al., 1986; Fig. 3.5]. The effects associated with coupling between gravity and elastic deformation are disregarded because they are negligible when deep sources are considered [Currenti et al., 2007]. The real topography of Etna is taken into account considering the effective distance between the source center and the observation points at surface. The source parameters are retrieved by minimizing the misfit between the observed and computed gravity changes.

The observed gravity change is best explained with a prolate ellipsoid located at a depth of 2 km b.s.l., with the major semi-axis of 1100 m and the other two semi-axes $b = c = 350$ m (for the characteristic of the model, see Table 3.6). A density contrast of about 400 kg/m^3 is necessary to account for the measured gravity variation, yielding a mass increase of about 200×10^9 kg. The comparison between the calculated and observed gravity variations along a North-South profile shows that this simplified model fits well the amplitude and the wavelength of the gravity variations observed in the summit area of the volcano (Fig. 3.5). Gravity changes highlighted that during the 2008-2009 eruption, a new episode of magma accumulation started

just 2 km below the sea level in the shallow-intermediate magma storage zone already affected by recharging processes [Carbone et al., 2003; Greco et al., 2010; Bonaccorso et al., 2011a].

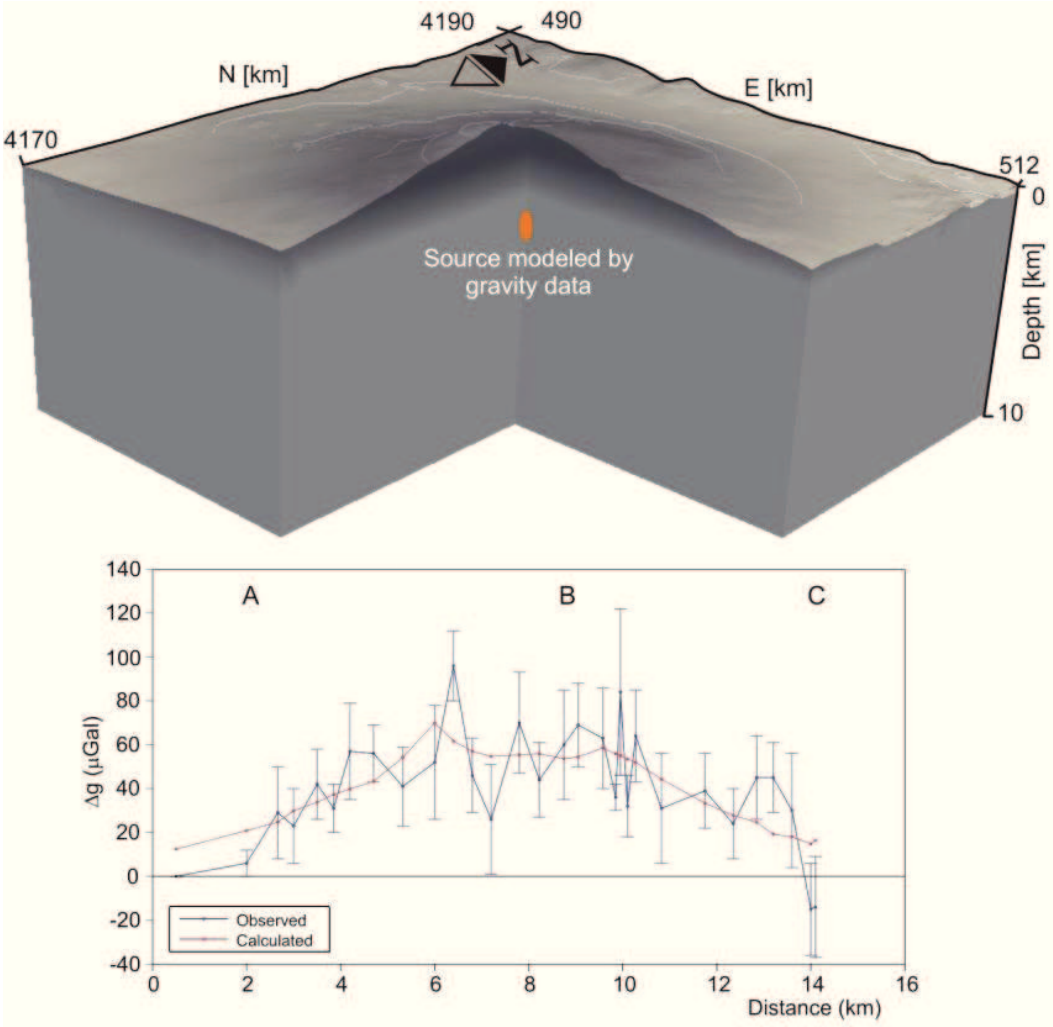

Figure 3.5 – 3D perspective block diagram showing the source position modeled through 2008-2009 gravity variations observed at the scale of the volcano (see Table 3.6 for the source parameters). The comparison between gravity changes observed at the stations located in the summit area along a North-South profile (A-B-C profile) and the effect of the best-fitting model source are also shown.

Parameter	Gravity source
Longitude Xc	500.000 km
Latitude Yc	4178.100 km
Depth (Zc)	–1.8 km b.s.l.
Length (*A* axis)	1100 m
Length (*B* axis)	350 m
Length (*C* axis)	350 m
$\Delta\rho$ density contrast	400 kg/m^3
ΔM	$200 \cdot 10^9$ kg
ΔV	$500 \cdot 10^6$ m^3

Table 3.6 – The best models parameters found through gravity data observed during 2008-2009 period (coordinates are in UTM projection, WGS84 ellipsoid).

Chapter 4

Relative Gravimeters Characterization Using a Vibrating Platform

As stated in the introduction, gravity time sequences collected at Etna volcano with spring relative gravimeters in coincidence of lava fountains have shown significant variations in close temporal relationship with both, the phases of the paroxysmal events and the intensity of the high frequency seismicity, recorded by the seismic stations. Since these observed gravity variations can be only partially related to the subsurface mass redistributions phenomena, was hypothesized that these variations could be also attributed to a conversion of high amplitude and high frequency signals, both in the vertical and in the horizontal component, into gravity signals at low frequency. To evaluate this hypothesis, laboratory tests were performed for the characterization of the degree of coupling between the high frequency signals Out-of-band response and the In-band response of two relative spring gravimeters used for monitoring the

Etna volcano: a Scintrex CG-3M and a LaCoste & Romberg model D. The characterization was performed using a vibrating platform, specially implemented, for accelerating the instruments with an appropriate sinusoidal high-frequency in both the vertical and horizontal directions. Analysis performed on the seismic signals recorded at Etna volcano during the lava fountains allowed to retrieve the amplitudes and the frequencies of the accelerations used as input to the vibration platform. The signals has been generated by means of linear actuators and opportunely measured using a laser interferometer. These tests permitted to determinate the frequency and amplitude dependency between the high frequency seismic signals and the gravity output, due to the non-linear behavior of the mechanical structure of the instruments. A close connection with the previous experimental activity was observed in the seismic and gravity time series, recorded in the 2011 and 2012, during the lava fountains events at Etna volcano.

4.1 Data Presentation and Analysis

The gravity stations installed on the southern flank of the volcano (SLN and BVD, at 1740 m and 2920 m a.s.l., respectively), are equipped with LaCoste & Romberg spring gravimeters, acquire at one data per minute sampling rate (resolution better than 1 μGal), gravity and tilt along two perpendicular axes and several meteorological parameters (pressure, humidity and temperature), which are used to reduce the gravity signal in order to acquire the volcano-related signal [Del Negro et al., 2008].

Figure 4.1 shows the raw gravity sequences recorded between 06:00 and 16:00 UT during the April 2011 lava fountain, after removing the effects of Earth tide and instrumental drift. Starting from about 08:48, the mean value of the reduced gravity signal acquired at SLN station slowly increased up to reach a maximum positive variation of about 50 μGal in coincidence with the most intense phases of lava fountaining. At BVD station, from about 09:22, a more rapid and marked changes is displayed and the maximum negative gravity variations reached a value of about 200 μGal. The above gravity changes were accompanied with an increase of about one order of magnitude of the background signal noise, that is usually within ±1 μGal. Subsequently, at the end of the paroxysmal event, the mean value of the gravity sequences changes of about -15 μGal and +30 μGal at SLN and BVD stations, respectively, with reference to their original levels.

To extract the parameters with which to excite the vibration platform, were considered two seismic sequences acquired in two stations close to the continuously recording gravity stations (SLN and BVD), that were operative during the 10 April 2011 lava fountain. In the Fig. 4.2 is shown the seismic data recorded during this event and used to perform the mentioned characterization.

In order to get correlations between the seismic and gravity signals, the experimental laboratory activity consisted to impose to the gravimeter a seismic acceleration as occurs during the Etna volcano lava fountain. Specifically, the seismic signals (velocity; Fig. 4.2), recorded at SLN and BVD stations during the aforementioned lava fountain, were converted to retrieve the accelerations used to perform the characterization. Figure 4.3 and 4.4 shows, respectively, the *x*, *y*

and *z* components of the inertial acceleration (obtained by the first derivative of the seismic data) and their spectrograms.

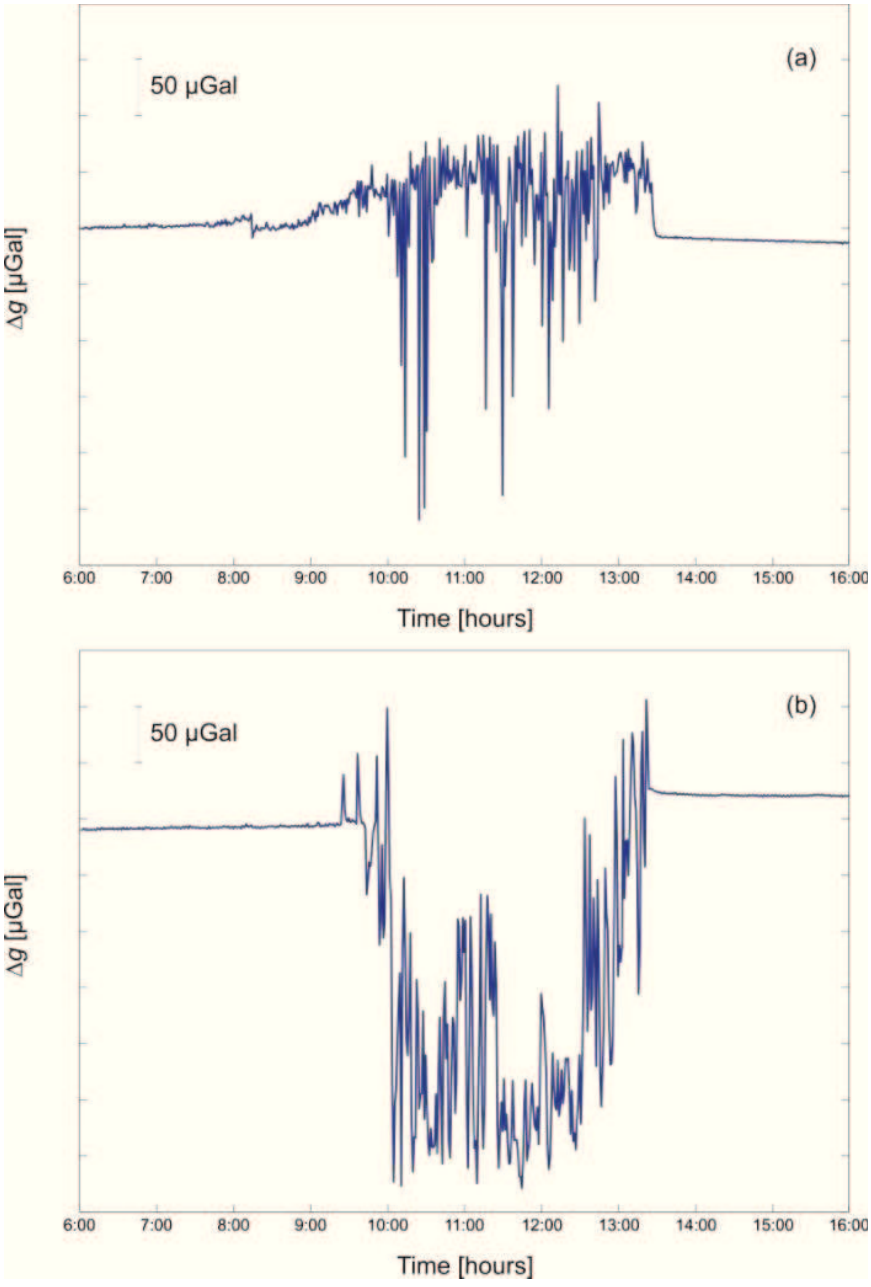

Figure 4.1 – Gravity sequences observed at (a) SLN and (b) BVD stations between 06:00 and 16:00 UT during the 10 April 2011 lava fountain, after removing the effect of Earth tide and instrumental drift.

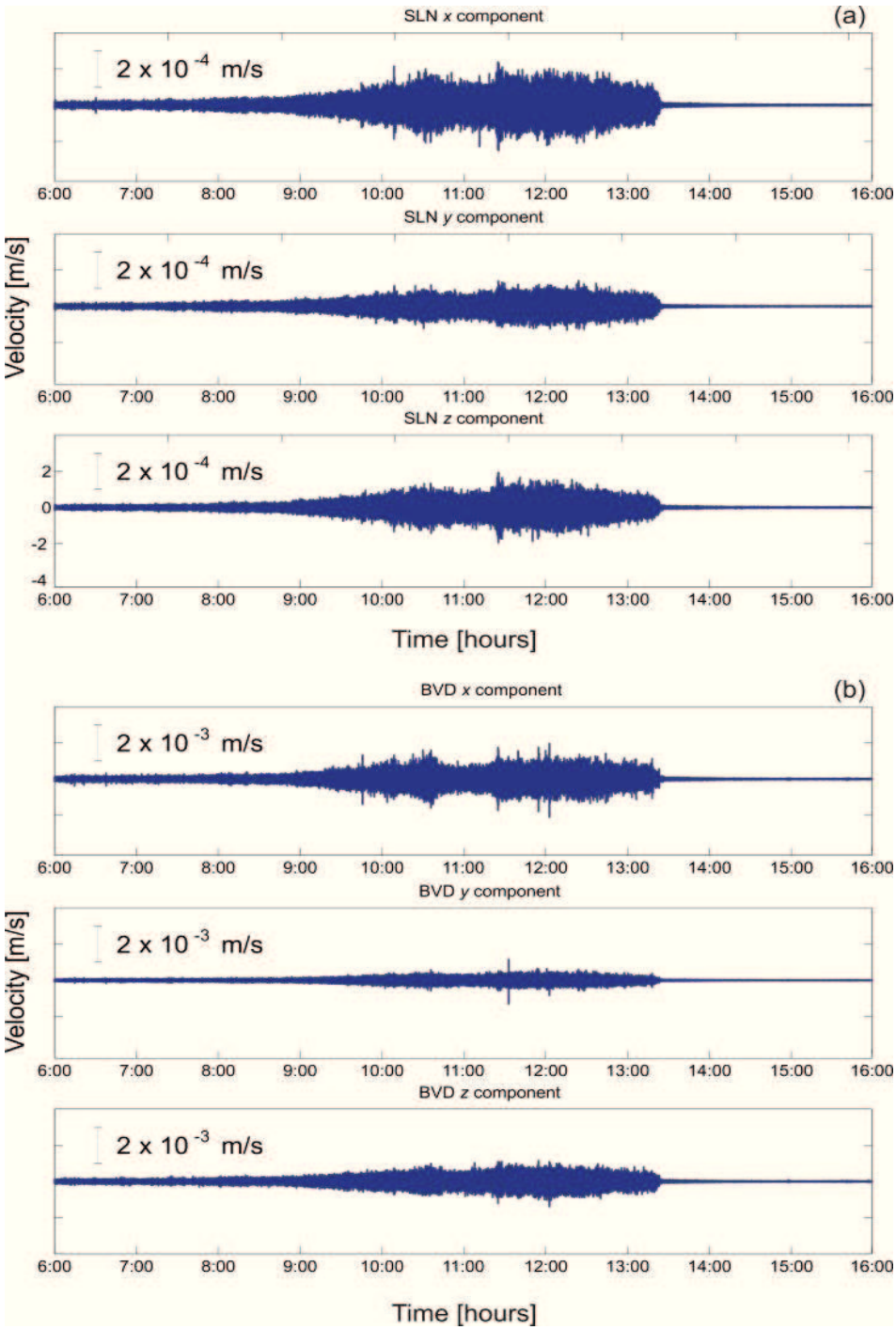

Figure 4.2 – Seismic signal components observed at (a) SLN and (b) BVD stations between 06:00 and 16:00 UT during the 10 April 2011 lava fountain.

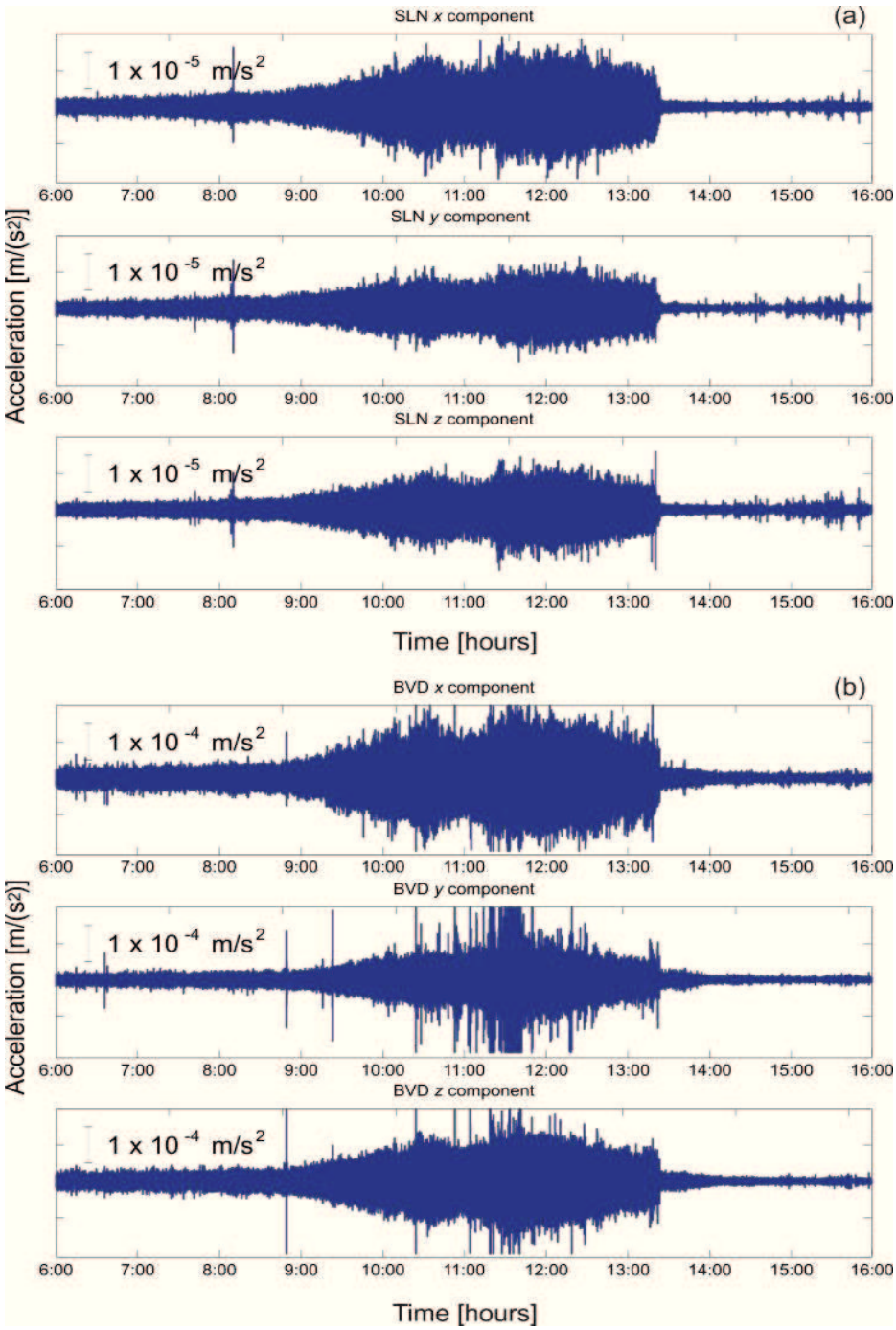

Figure 4.3 – *x*, *y* and *z* components of the inertial acceleration at (a) SLN and (b) BVD stations, obtained by the first derivative of the seismic data (Fig. 4.2).

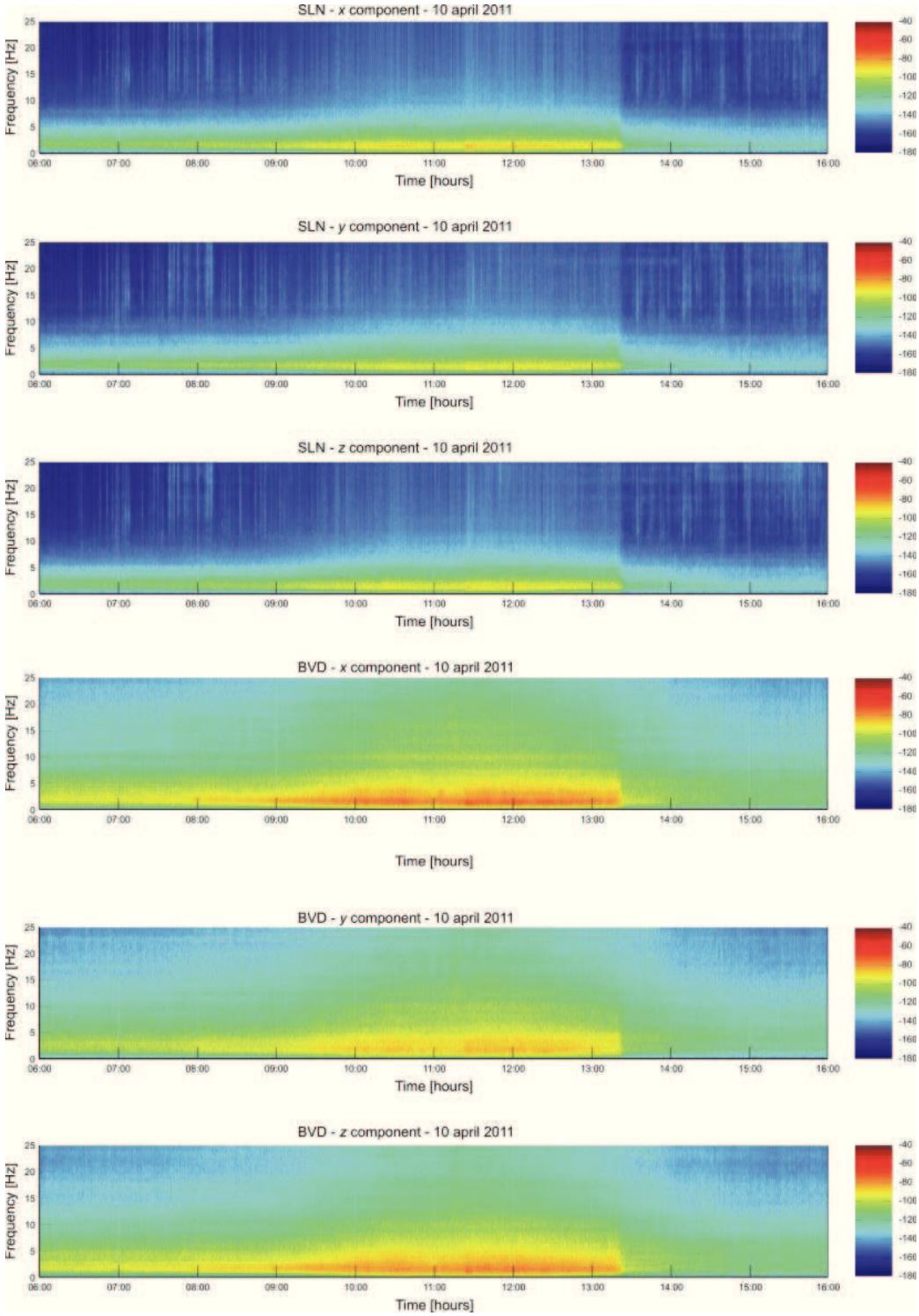

Figure 4.4 – Spectrograms of the x, y and z components of the inertial acceleration at SLN and BVD stations.

The maximum peak-to-peak values for the *x*, *y* and *z* acceleration components at SLN and BVD stations (Fig. 4.3a and 4.3b), reported in Table 4.1, were used as input to the vibration platform during the characterization of the gravimeters. Then, the amplitude and frequency values, both for horizontal and vertical inertial accelerations to which excite the gravimeters are almost comparable with those recorded during paroxysmal events at Etna. Amplitude values ranging between 0.2 mg and 4 mg are produced by imposing platform movements around a few tens of μm, in the frequency range between 2 Hz and 17 Hz.

Component	SLN	BVD
$a_{x,\text{p-p}}$	0.418 mg	3.172 mg
$a_{y,\text{p-p}}$	0.285 mg	4.699 mg
$a_{z,\text{p-p}}$	0.316 mg	3.629 mg

Table 4.1 – The maximum peak-to-peak values for the *x*, *y* and *z* acceleration components at SLN and BVD stations.

Results of the seismic analysis shows that the amplitude values at BVD station are about one order of magnitude greater than at SLN (Tab. 4.1; most probable because this station its very close, less than 1 km, to the eruptive event). Moreover, the Figure 4.4 shows that the most frequency content of the signals is within 10 Hz: this spectral content is in agreement with the seismic activity generally observed on active volcanoes [Chouet, 2003; Del Pezzo, 2008].

4.2 Description of the Facility Used for the Gravimeters Characterization

In the following is described the implemented vibrating platform used to perform the gravimeters characterization, and able to reproduce some specific frequencies of the dynamic noise present during Etna paroxysmal events.

The mains components of the vibrating platform used to perform the tests are: the shaker (consisting of an aluminium movable platform actuated using piezoelectric actuators); the power amplifier; the function generator; the displacement detectors and the vibrations controller. Details of this vibrating platform for test along x, y and z directions are shown in Figure 4.5. It may be noted that the aluminum platform is placed on thicknesses yielding so to allow horizontal displacements under the action of the piezoelectric actuators, but it represents a "quasi-stable" support in absence of solicitations. The function generator provides signals of appropriate shape to the calibration, which are suitably amplified by the power amplifier and then sent to drive the piezoelectric actuators. The displacement measurements are made by a pair of high precision laser interferometric Keyence, which measure the platform displacements along the horizontal (Laser#1) and vertical (Laser#2) directions. The vibrations controller, formed by an acquisition system and a PC, allows the evaluation of the accelerations, both in time and frequency domain, to which is subjected the platform and the instrument placed on it. All the structure is accommodated on an optical bench.

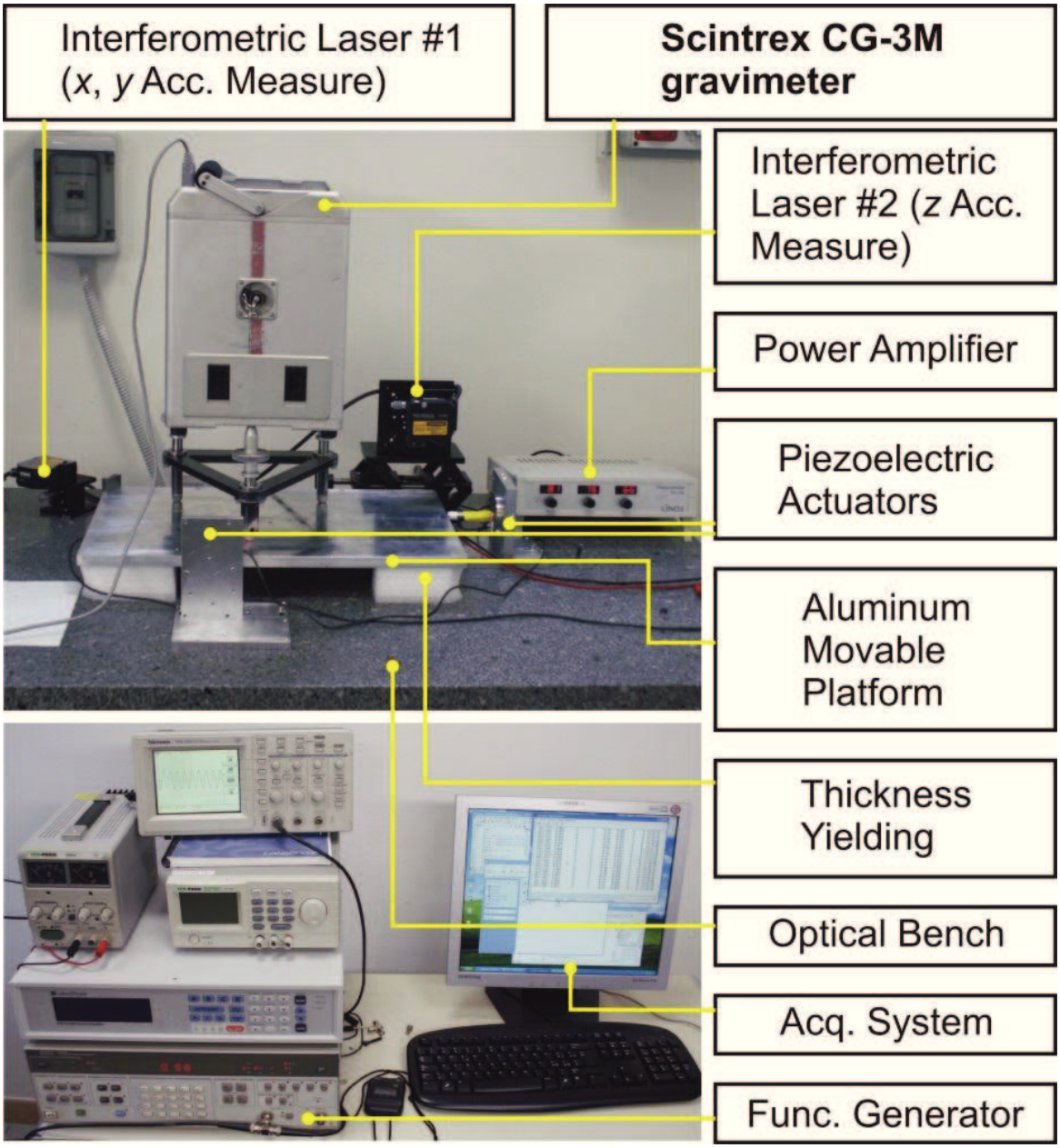

Figure 4.5 – Vibrating platform for test along *x*, *y* and *z* directions.

4.3 Experimental Determination of the Coupling Factor between Horizontal (x, y) and Vertical (z) Excitation at High Frequency and In-band Response in the z Component of the Gravimeters

In this section is reported the experimental activities performed to obtain the decoupling factor between "high" frequencies forcing acceleration in the *x*, *y* and *z* direction and the low frequencies response of the Scintrex CG-3M and LaCoste & Romberg model D spring relative gravimeters in the *z* direction. The decoupling factor *K* is defined by means of the following formula:

$$K_{(i)z} = a_{(i)}/a_z \qquad (4.1)$$

where $a_{(i)}$ is the amplitude of the *i*-th excitation signals (in mg) and a_z is the variation of the output signals of the gravimeter (in μGal); *i* stay for the components *x*, *y* and *z*. Low values of decoupling factor indicate the frequencies to which there is the maximum transfer of spurious signals in the gravity component at low frequency.

The characterization was performed by using the facility described in the previous paragraph. Referring to the Figure 4.5, to determine the decoupling factor $K_{(x,y)z}$, the vibration platform was actuated using the horizontal actuators and the appropriate Laser#1 to measure the respective displacement; in this case, the Laser#2 is used to monitor possible undesired movements in the vertical component of the platform. For the determination of the decoupling factor $K_{(z)z}$, the experimental set-up, opportunely modified by moving the piezoelectric actuators below the aluminum platform, permits to force the vibration platform in the *z* direction and to perform the

measurements of the relative displacements using the Laser#2 (see Figure 4.6 for the Scintrex CG-3M).

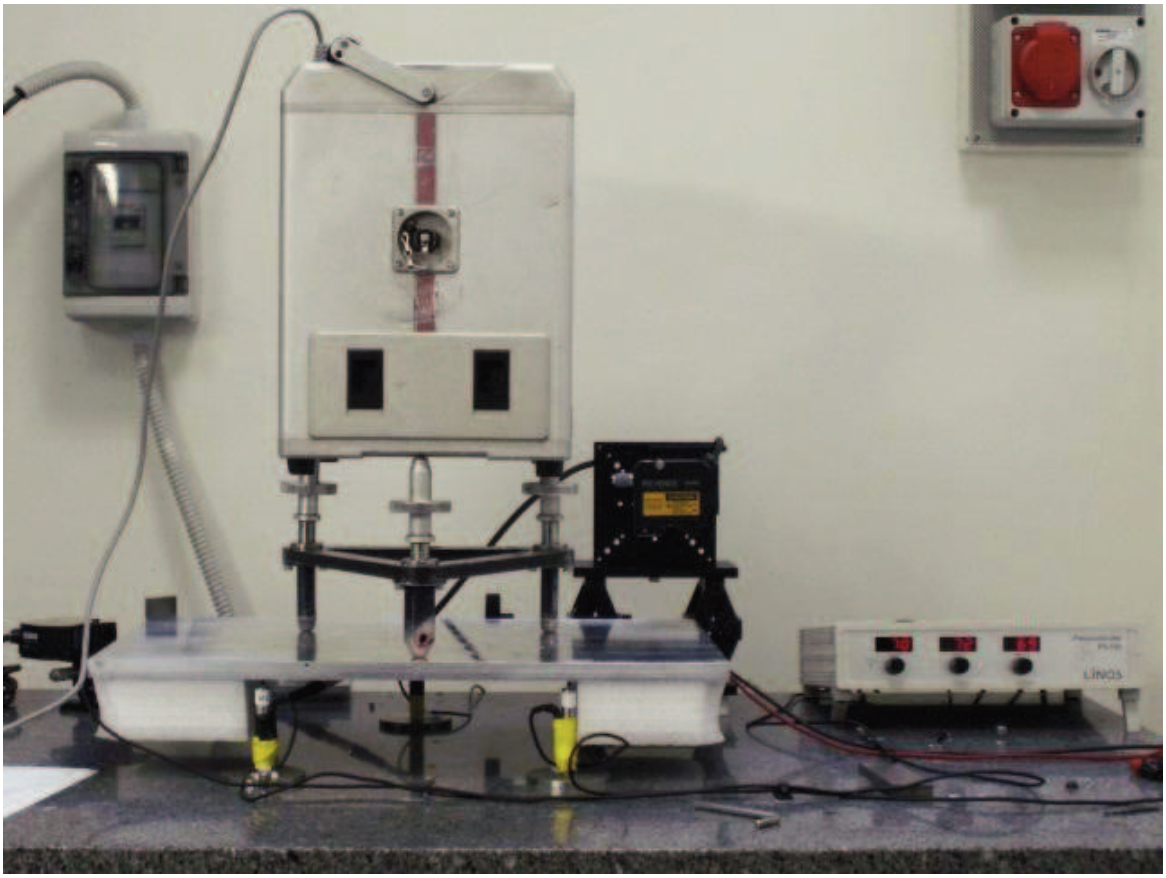

Figure 4.6 – Experimental set-up used for the determination of the coupling degree between high-frequency vertical accelerations and the In-band response of the Scintrex CG-3M. The figure shows the piezoelectric actuators placed below the movable platform.

4.3.1 Characterization Test of the Scintrex CG-3M

During the characterization, the output digital data from the Scintrex CG-3M gravimeter was recorded at a frequency of 0.1 Hz as result of the mean of 4 samples. Data are corrected for the tidal effect by

means of a software installed on the instrument. In addition, the tilt sensors equipped the gravimeter provide the measurement of the vertical variations of its base; this information permits to determine the contribute due to the inclination on the gravity measure allowing to exclude its effect on the response of the gravimeter.

Horizontal Excitation

In Figure 4.7 is shown the results concerning the characterization of the Scintrex CG-3M for the coupling between the horizontal excitation at high frequency and its In-band response.

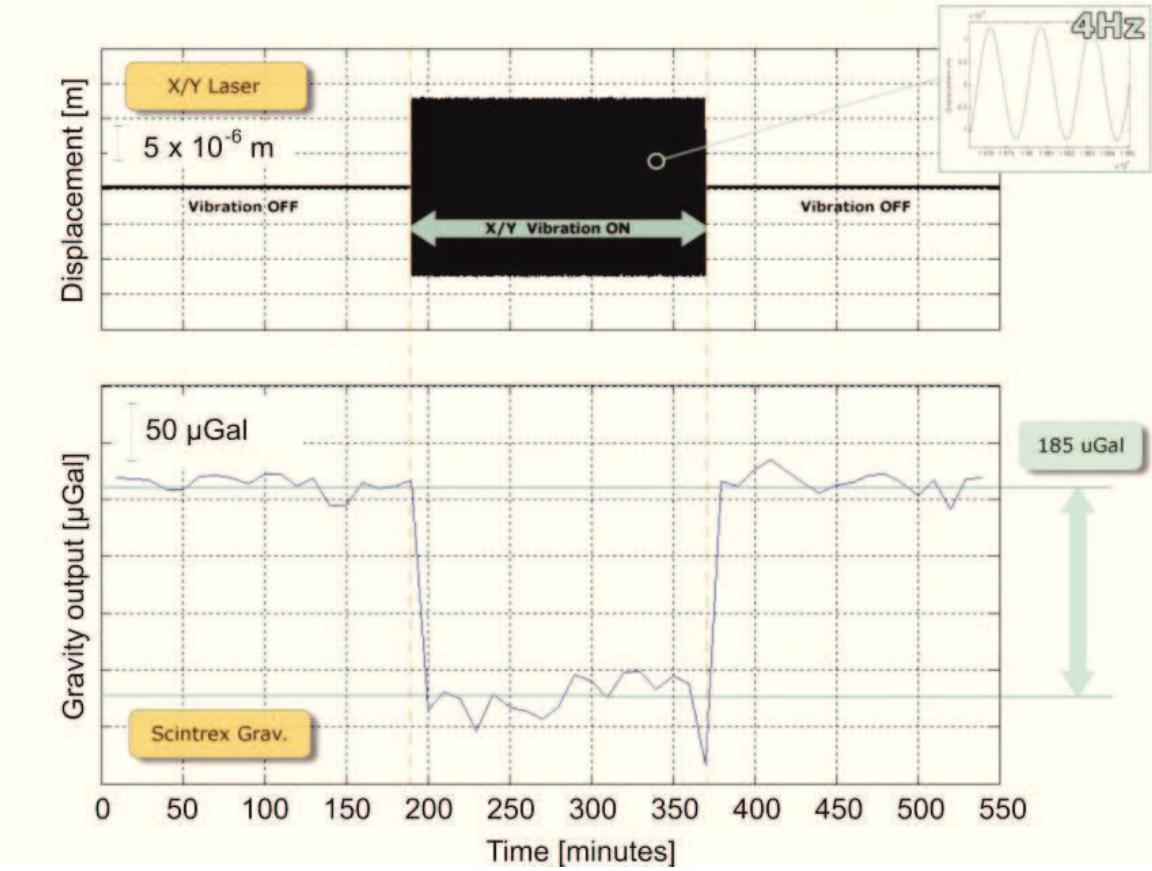

Figure 4.7 – Results of the characterization of the coupling between horizontal excitation at high frequency and the gravimeter In-band response.

Figure 4.7 on the top, shows the horizontal displacement of the platform, given by the piezoelectric actuators, while in the bottom is shown the output signal, simultaneously acquired with the gravimeter. For the first 200 s, the horizontal force was switched off, then the platform was forced so to obtain an horizontal displacement of 25 μm with a frequency of 4 Hz (equivalent to about 1 mg) for approximately 200 s, finally the excitation was switched off again for other 200 s.

It is possible to observe that during the excitation phase in the horizontal direction, the gravimeter exhibits a negative variation in the DC level with amplitude of about 185 μGal.

In the Figure 4.8 is shown the spectral analysis of the platform displacement which shows the main peak at 4 Hz with amplitude of about 12.5 μm. This displacement, at 4 Hz corresponds to an acceleration of $7.8 \cdot 10^{-3}$ m/s^2 = 0.8 mg. The spectral analysis evidences also a second harmonics at 8 Hz and the absence of other significant components.

In the Figure 4.9 is shown the output of the two Scintrex CG-3M tilt sensors, acquired during the characterization; is evident that, during the test, the instrument has not undergone to any significant inclination.

This characterization reveals that at a frequency of 4 Hz horizontally imposed, the decoupling factor $K_{(x,y)z}$ for the gravimeter (given by the ratio between the amplitude of horizontal acceleration at 4 Hz and In-band response - see Equation 4.1), is equal to:

$$K_{(x,y)z}(4\ \text{Hz}) = \frac{0.8 \cdot 10^{-3}}{185 \cdot 10^{-9}} = 4324 \qquad (4.2)$$

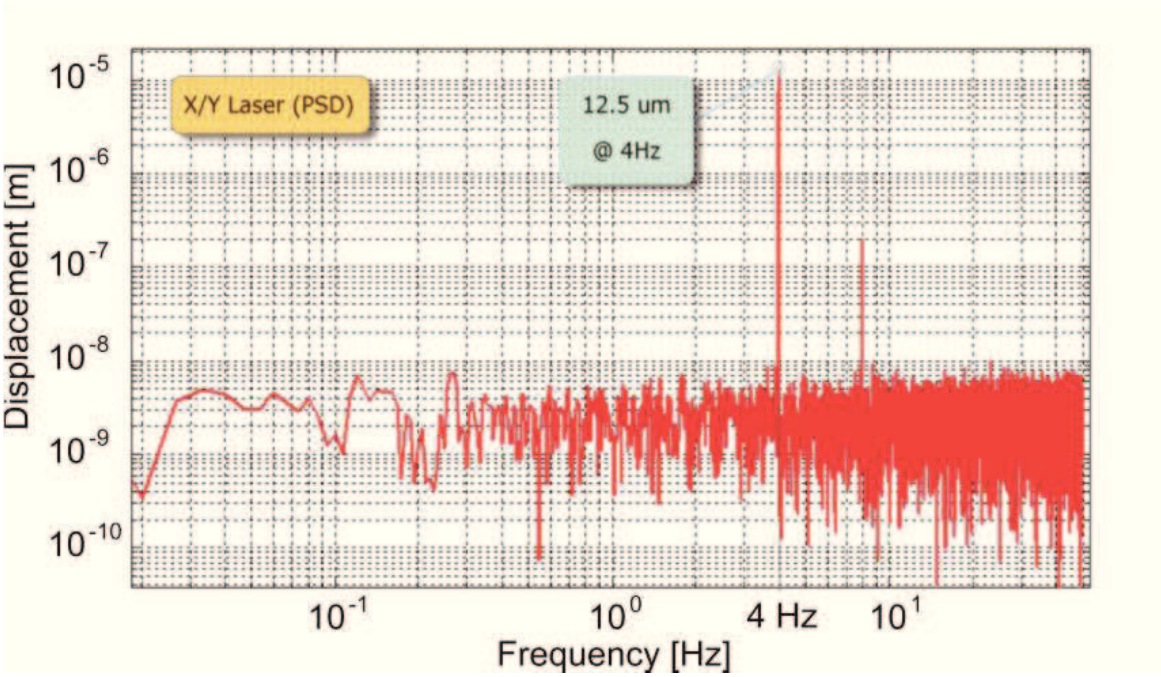

Figure 4.8 – Spectral analysis of the platform displacement in the horizontal direction.

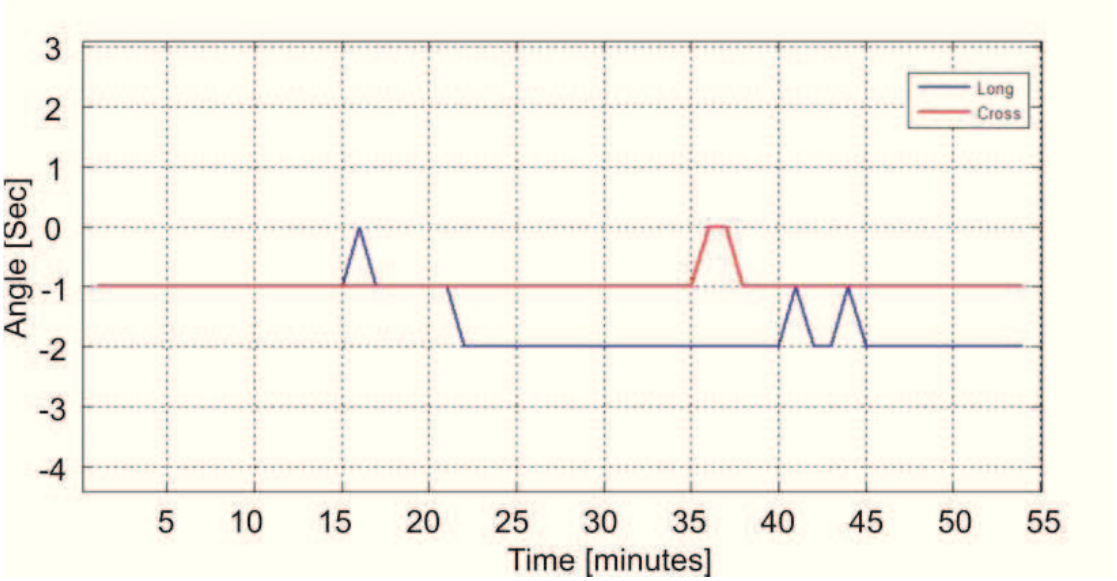

Figure 4.9 – Outputs of the two tilt sensors of the Scintrex CG-3M, acquired simultaneously to the characterization at 4 Hz, from which it is evident that during the test the instrument has not undergone inclinations.

In a second step, the characterization of the decoupling factor was made by varying the excitation frequency in the range between 4 Hz and 25 Hz. The Figure 4.10 shows the decoupling factor values obtained in function of the horizontal excitation frequency. It is worth to note that there are three frequencies in which there is a maximum peak of coupling (resonance frequencies); for frequencies above 14 Hz, the coupling is not significant.

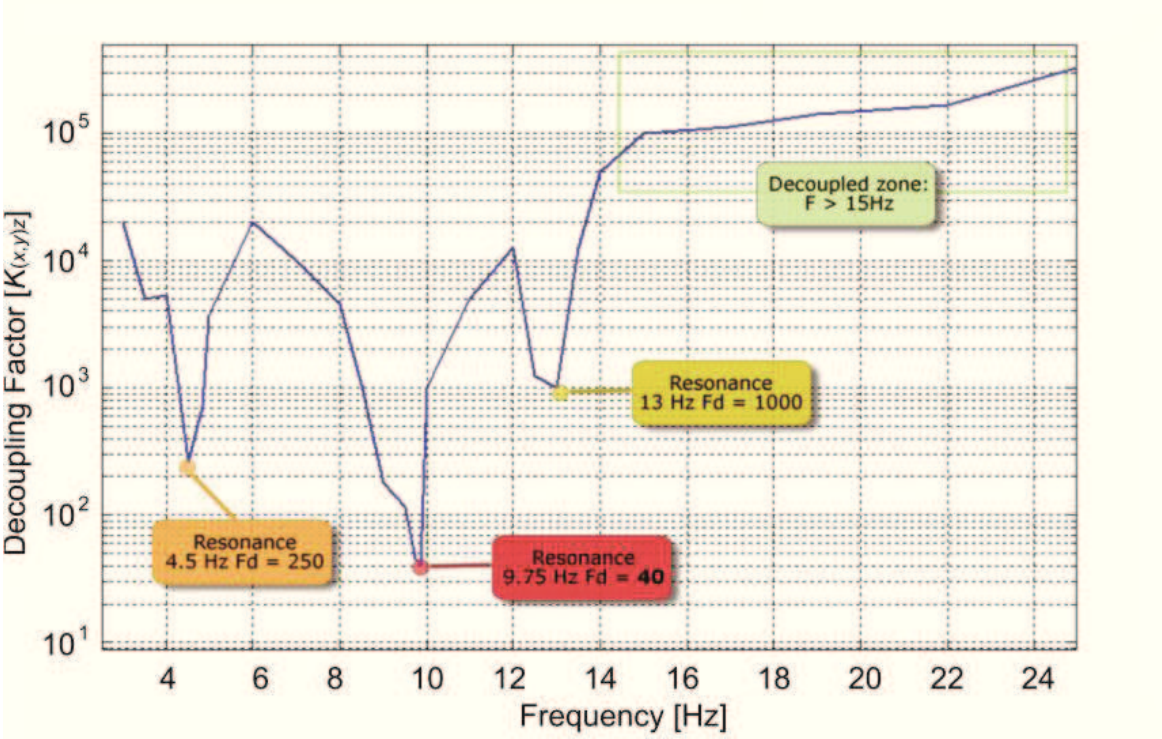

Figure 4.10 – Decoupling factor $K_{(x,y)z}$ as function of the horizontal excitation frequency.

In Table 4.2 are reported the values of the resonance frequencies, together with the obtained decoupling factors. In particular, at a frequency of 9.75 Hz, the decoupling factor is extremely low, which

means that any signal present at this frequency will be reported at low frequencies attenuated only by a factor of 40.

Frequency [Hz]	Decoupling factor, $K_{(x,y)z}$
4.50	250
9.75	40
13.00	1000

Table 4.2 – Frequency values corresponding to the minimum decoupling between excitation and response in band in the vertical component.

With the present apparatus (vibrating platform horizontally excited) it was not possible to perform the characterization for frequencies below 4 Hz, since the piezoelectric actuators are not able to produce large displacements so to determine accelerations of the order of 1 mg.

In Figure 4.11 is shown the Scintrex CG-3M gravimeter gravity output, as function of the amplitude value of the horizontal excitation at the fixed frequency of 9.75 Hz. In Figure 4.12 is shown the similar curve for a fixed frequency of 13 Hz. In both cases it is evident a a non-linearity relationship. The figures show the “best fit” of the quadratic function.

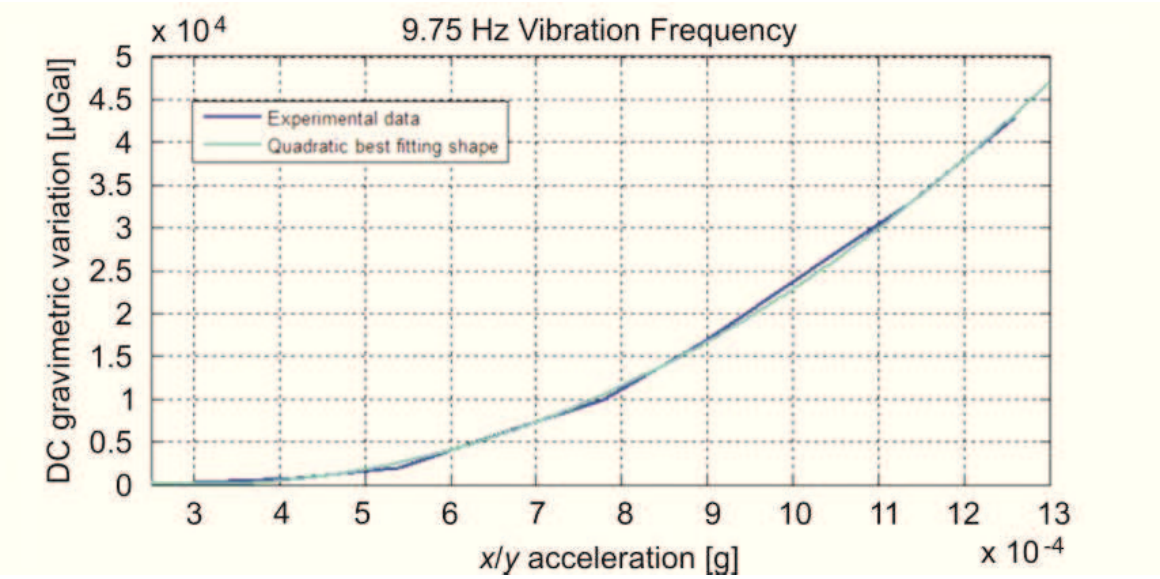

Figure 4.11 – Gravity output for the Scintrex CG-3M as function of the excitation amplitude at frequency of 9.75 Hz.

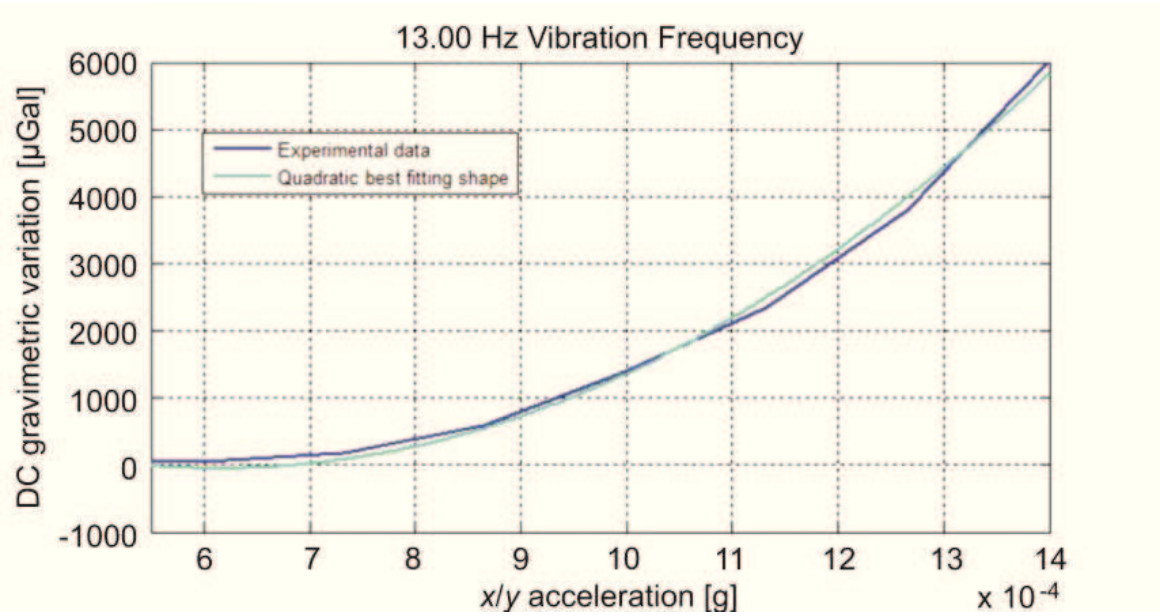

Figure 4.12 – Gravity output for the Scintrex CG-3M as function of the excitation amplitude at frequency of 13 Hz.

Vertical Excitation

In Figure 4.13 is shown the decoupling factor $K_{(z)z}$ calculated for the Scintrex CG-3M as a function of the vertical excitation frequency. Results show that the decoupling factor is very high for higher frequencies but rapidly decreases at frequencies below 6 Hz.

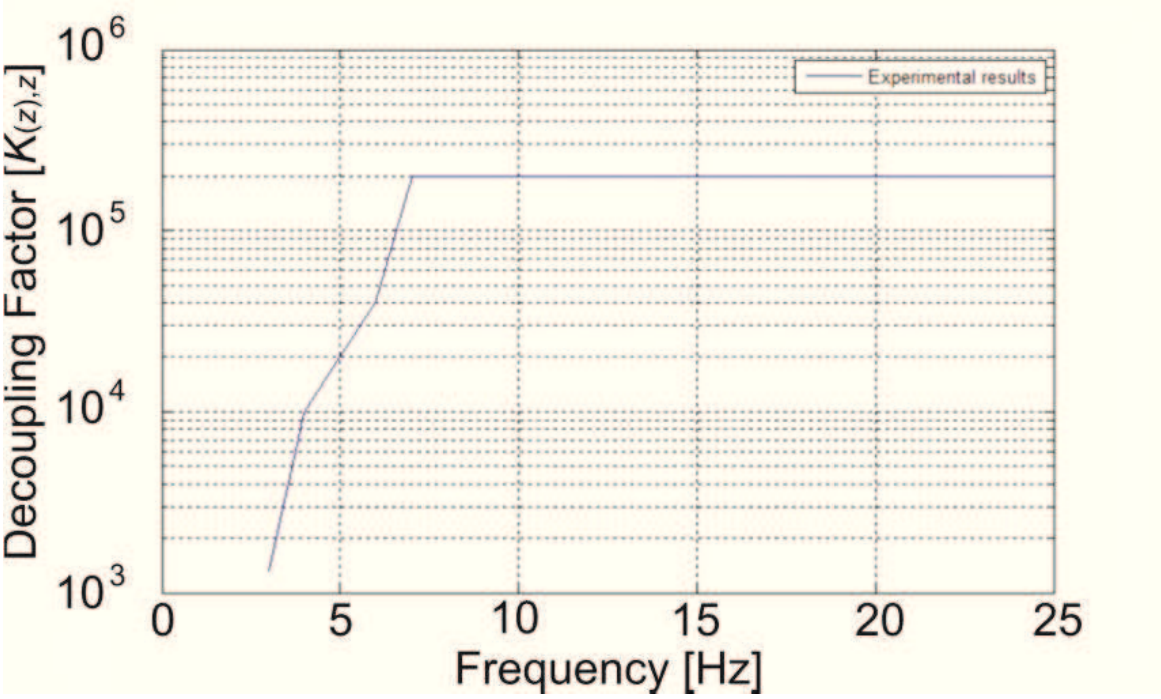

Figure 4.13 – Decoupling factor $K_{(z)z}$ between vertical excitation at high frequency and response In-band of the gravimeter.

4.3.2 Test on LaCoste & Romberg D-185

For the LaCoste & Romberg D-185 gravimeter characterization, the data are recorded acquiring its analog output at 1 datum/min sampling rate through a CR10X Campbell Scientific datalogger. Each stored datum is the average value between 60 samples acquired

at 1 Hz. The tidal effect correction is performed a posteriori with an additional software. Also in this case, the gravimeter provides the measurement of the variations of the tilt angles of its base. This gravimeter was operative at BVD station during the 10 April 2011 Etna volcano lava fountain.

Horizontal Excitation

The experimental set-up used for the measurement of the coupling degree between horizontal excitations and the response of the LaCoste & Romberg D-185 gravimeter is shown in Figure 4.14 (see the previous paragraph for the description).

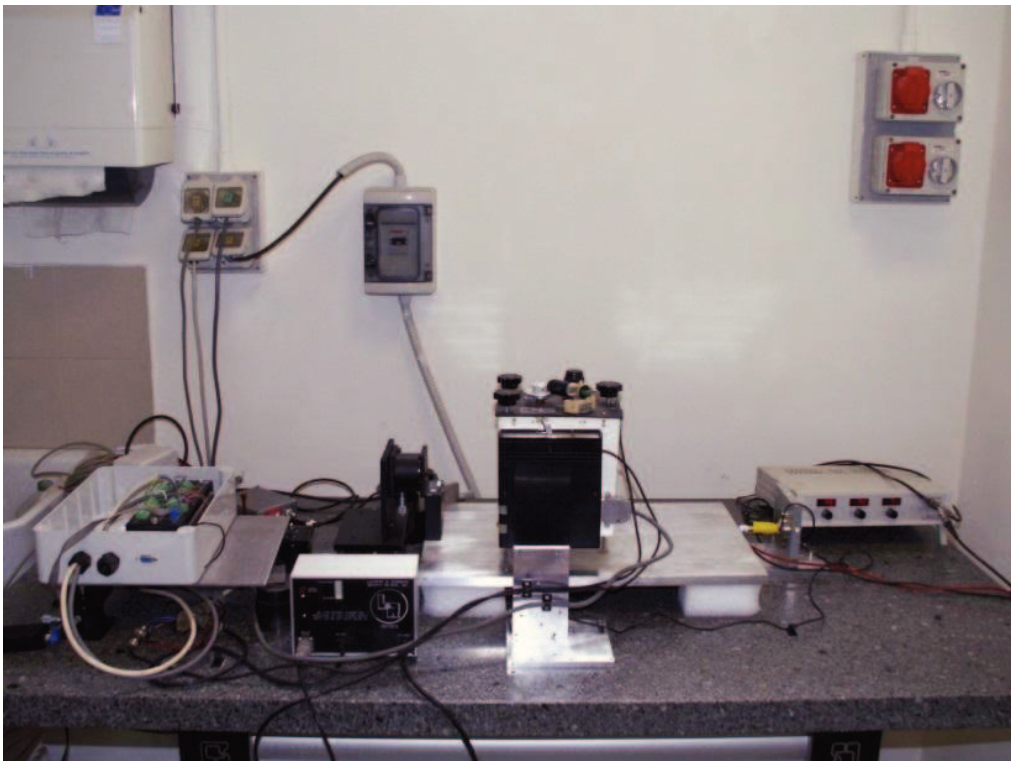

Figure 4.14 – Experimental set-up used for the measurement of the coupling degree between horizontal excitations and the In-band response of the LaCoste & Romberg gravimeter.

In the Figure 4.15 is shown the response of the gravimeter excited along the horizontal axes with a signal of amplitude equal to 2 mg (typical amplitude value recorded at BVD Etna station during paroxysmal events) and frequency ranging between 2 Hz and 20 Hz. The maximum coupling is obtained at a frequency of 4.2 Hz. The gravimeter output in these cases shows a phase shift of 180°.

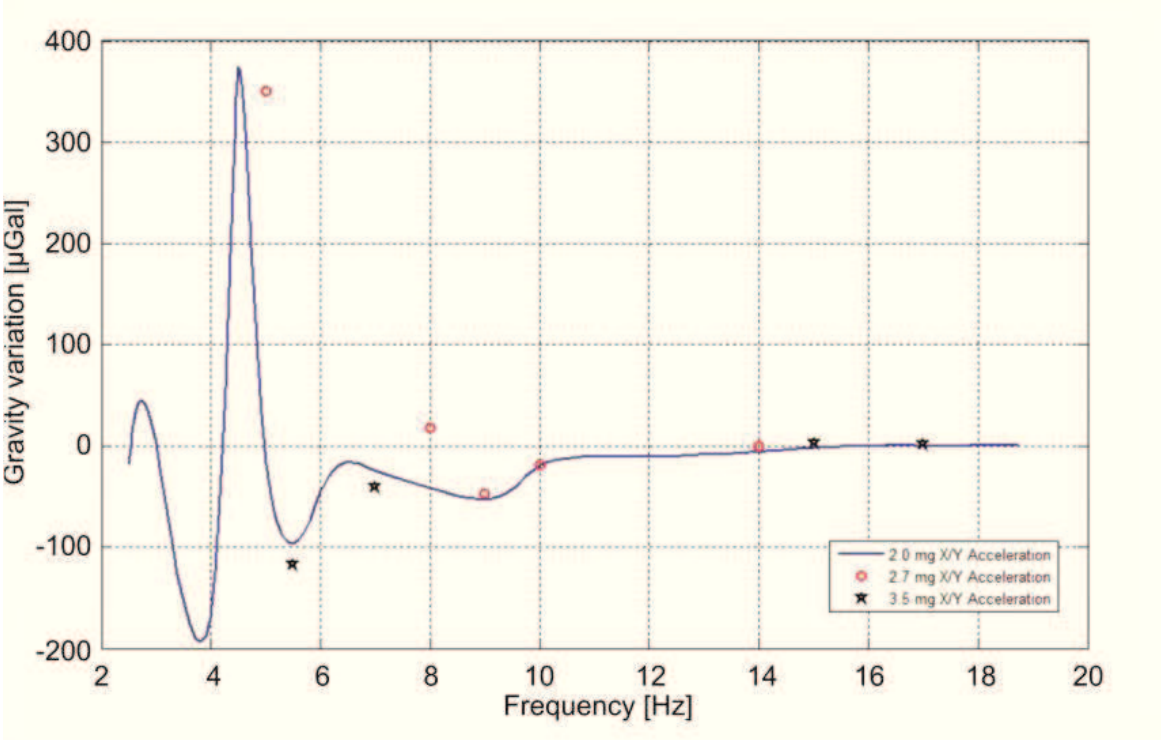

Figure 4.15 – Response of the LaCoste & Romberg D-185 gravimeter horizontally excited with a signal of amplitude of 2 mg (typical amplitude value recorded at BVD station during paroxysmal events) varying in frequency between 2 Hz and 20 Hz.

The analysis regarding the output of the gravimeter versus the amplitude of the horizontal applied solicitations (black stars for amplitude values of 2.7 mg and red circles for amplitude equal to 3.5 mg in the Figure 4.15), do not show a strong dependence from the

excitation amplitude. By considering the Figure 4.15, it is possible to obtain the decoupling factor by mean the equation 4.1. The decoupling factor values obtained in function of the horizontal excitation frequency is significantly variable in the frequency range between 2 Hz and 6 Hz and rapidly increases at frequencies over about 6 Hz.

Vertical Excitation

In the Figure 4.16 is shown the low frequency gravity output with respect to the high excitation frequencies along the vertical axis. The blue line is obtained by determining the DC response of the instrument when it is excited in the vertical direction with a signal of frequency ranging between 1 Hz and 18 Hz and a fixed amplitude of 1 mg. In the same figure is shown the DC response resulting from different excitation frequencies and amplitude of 0.18 mg (black stars) and 0.5 mg (red circles).

Figure 4.16 shows also that the decoupling factor is directly related with the excitation frequency, and there are no variable peaks of maximum coupling, as observed during the previous horizontal excitations. In this case there is a linear relationship between the gravity output and the amplitude of excitation signal.

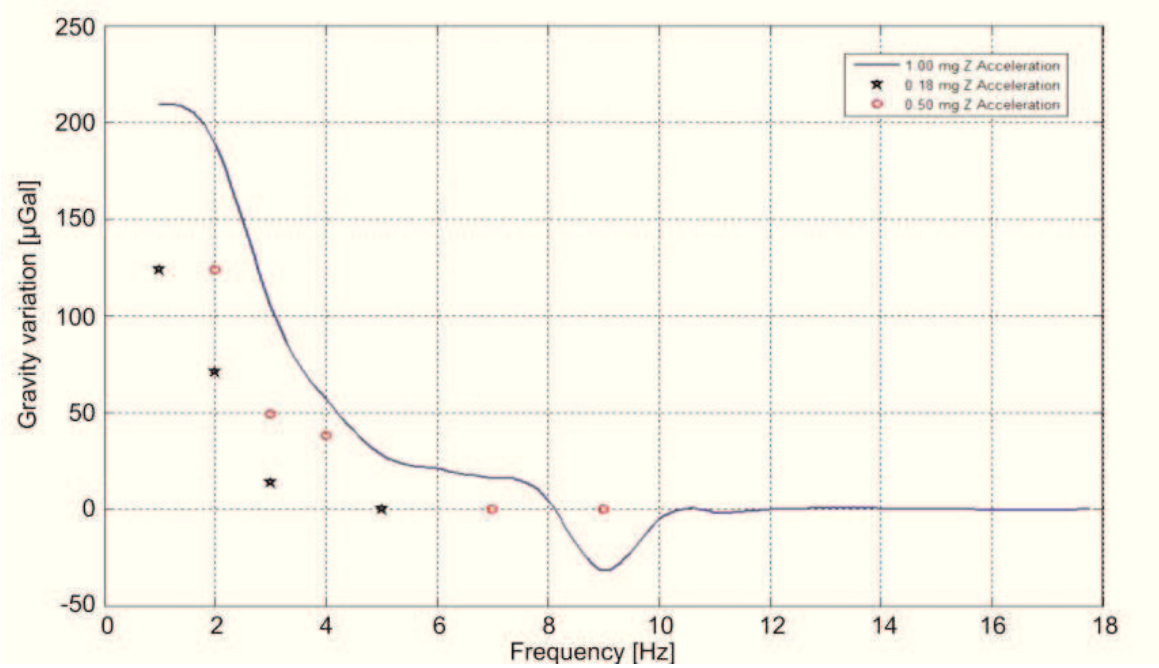

Figure 4.16 – Characterization of the coupling degree between high-frequency vertical excitations and the DC response of the gravimeter. The blue curve is obtained by determining the DC response of the instrument when it is excited in the vertical direction with frequencies between 1 Hz and18 Hz and amplitude of 1 mg.

4.4 Comparison between Seismic and Gravity Signals Recorded during the Etna Paroxysmal Event

In the previous sections have been reported the experimental results concerning the laboratory characterization of the decoupling factors for the horizontal and vertical excitations for the In-band response of the used gravimeters and determined specific frequencies at which this coupling is significant. Results highlight that this effect is

connected to some instruments non linearity. These effects produce an “apparent” signal in the vertical component recorded by gravimeters whose can not only make the detection of volcanic source effects more difficult but also may lead to misinterpret data.
According to the laboratory results, the low frequencies signal of the gravimeters, recorded at Etna during paroxysmal activity, can be due to reconversion of the high level seismic noise acting on it at high frequencies. In order to analytically evaluate this quadratic reconversion phenomena, has been performed the analysis of the seismic signals recorded with a seismometer, operating in coincidence with the gravimeter, in a near site. In the Figure 4.17 is reported a comparison between the gravity signal recorded at SLN station during the 10 April 2011 lava fountain and the square root of the sum of the squares of the three seismic components recorded by the seismometer, opportunely rescaled to permit the qualitative comparison. The comparison of these signals shows the strong correlation between them.
The quadratic relationship between the gravity and seismic signals can be observed also between the gravity and seismic signals registered at BVD station as shown in Figure 4.18. In this case, in addition, there is a delay between the increase of the seismic signals with respect to the gravity one. This delay, of the order of 100 minutes, may be due to a threshold of the seismic intensity under which the gravimeter is not sensible; from the Figure 4.3b, this threshold can be estimated to about 10 μg.

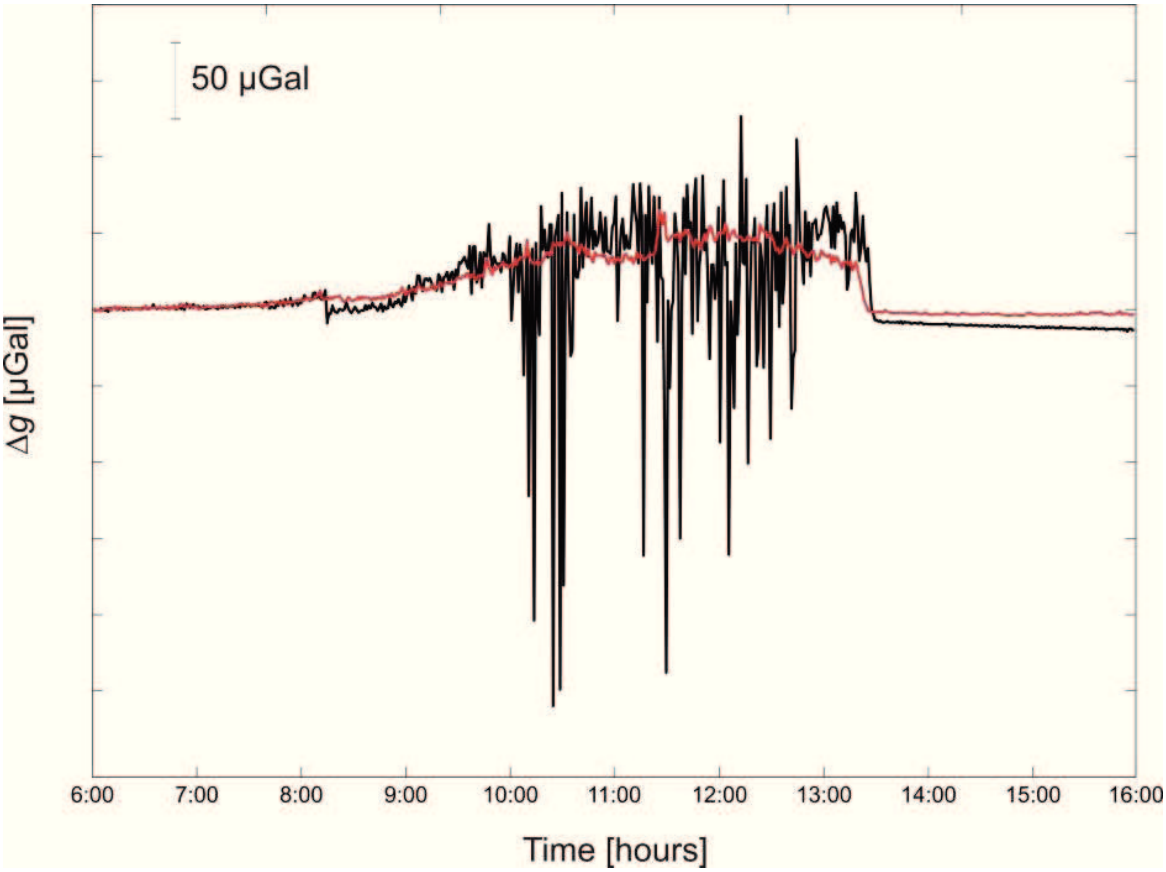

Figure 4.17 – Comparison between the gravity data and the vector sum of the three seismic components, at SLN station during the 10 April 2011 lava fountain, appropriately filtered and scaled to allow the comparison over time of the signals.

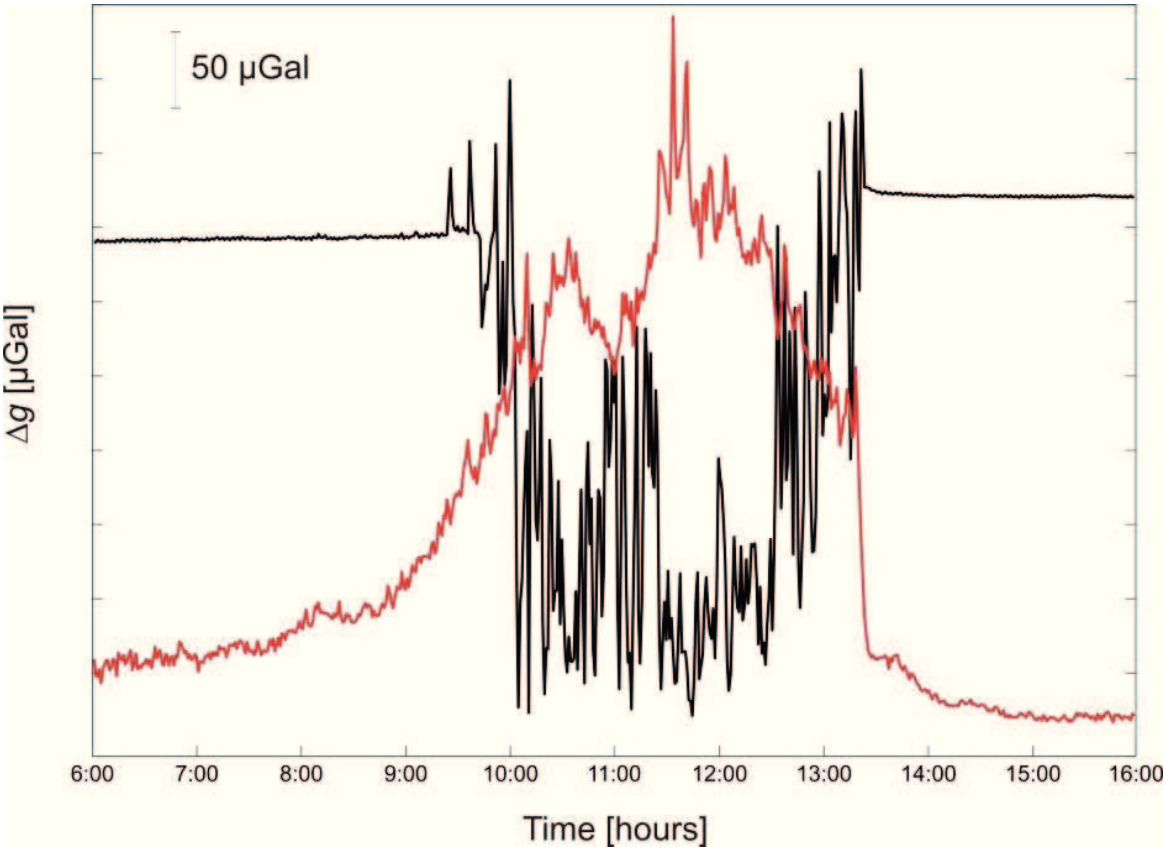

Figure 4.18 – Comparison between the gravity data and the vector sum of the three seismic components, at BVD station during the 10 April 2011 lava fountain, appropriately filtered and scaled to allow the comparison over time of the signals.

From this last observation, can be derived that in coincidence of paroxysmal activity of Etna, after the activity exceeds a minimum threshold, the output signal of a gravimeter can be influenced by the seismic activity. To mitigate these reconversion effects on the gravimeters, and to evaluate correctly the subsurface mass redistribution phenomena due to volcano activity, several strategies can be adopted. Among the different strategies, a posteriori

correction through an approach based on neural networks was applied.

4.4.1 A Neural Network to find the Dependence of the Gravity Signal from the Inertial Acceleration

The seismic waves could affect the measuring system of spring gravimeters normally used to monitor and study active volcanoes. As a consequence, the signal will be the combination of the gravity field component due to the subsurface mass or density variations and the inertial acceleration component due to the ground oscillation. Then, the inertial acceleration must be separated from the gravity signal to assess the amount of mass redistributed during the studied process.

Considering the correlation between the inertial components and the gravity signal, to extract the volcano-related gravity contribute from the data sequences acquired during the lava fountains, a neural network approach was developed.

The main characteristics of the neural networks are summarized in the follow.

Designed on basis of the connections inside the human brain, the neural networks are tools used as function approximators [Sifaoui et al., 2008]. They consist of n elementary units (called Artificial Neurons or Processing Elements) interconnected each other. These elementary units are organized in layers, each neural network will then have a variable number of neurons based on the variable number of layers. Each neuron is characterized by a threshold value and a transfer function. The threshold value is the minimum value that must be present in the input of the neuron for its activation. The

transfer function, take the input values to provide the output value [Zurada, 1992]. The most used transfer functions are the *Hard Limit*, the *Linear*, the *Log Sigmoid* the *Tansig* and *Purelin* [Dorofki et al., 2012]. Considering a neural network as a function approximator, presenting at the input one or more independent variables, is possible to reproduce at the output the values of the dependent variable. To allow the network to best approximate the function under test, it is necessary to subject it to a training process [Zurada, 1992]. This process consists to check the response of the network when input values are independent variables for which is known the exact value of the dependent variable (Training Set). In this way, by changing the weights of the connections, it is possible to minimize the difference between the desired output (the function value for certain input values) and the effective output (the output value of the neural network for the same input values). This procedure is called Supervised Learning Method [Tang et al., 2003]. In practice, after that the network architecture is determined, the weights values are initially assigned in a random manner and the network is trained by subjecting it to the training phase. After the training phase, the effectiveness of the network is tested on a new data set, the Test Set. This data set must be constituted by input and output values never seen by the network. If the results offered by the network are close to those effective, then is possible to consider it valid.

The network architecture developed to reduce the gravity signal consists in an intermediate layer, formed by 50 neurons, and by an output layer with only 1 neuron corresponding to the dependent variable. The chosen transfer functions for the intermediate layer and the output layer are the *Tansig* and *Purelin*, respectively. These

transfer functions and the number of neurons selected are those that have allowed to obtain the best fit between data.

For the training process of the neural network, as values of the independent variables (input data), were taken into account the amplitude and frequency values used as input during the laboratory test to excite the vibrating platform; as value of the dependent variable (target data), was considered the gravity output of the LaCoste & Romberg model D instrument with respect its original level, i.e. in the absence of mechanical solicitations. It is worth noting that, with this choice of the Training Set, the observed gravity variations are free from geophysical effects.

After the training phase, the test phase was performed with the inertial data calculated from the seismic data acquired at BVD station during the lava fountain of 10 April 2011 (see paragraph 4.1). Several tests were carried out varying the structure of the Test Set. The final choice of the Test Set was made as follow: first of all, through the calculation of the Fourier transform on the inertial data at high frequency (100 Hz), were searched the highest frequency components by using a one-minute long window to the data and progressively shifted by one minute without overlapping. Then, as input data, were provided the instantaneous values of the inertial acceleration (at 100 Hz) and the highest frequencies found in the aforementioned time intervals (within the same time interval the frequency value has been assumed constant). Finally, to make the output signal produced by the neural network comparable with the gravity signal, the output data were averaged to one minute.

Simulating the neural network previously trained with the results of laboratory tests performed with the LaCoste & Romberg D-185

gravimeter, the same gravimeter that recorded the 10 April 2011 lava fountain at BVD station, have been observed some problems of convergence. More precisely, repeating the Training and Test phases, without changing the network architecture implemented, the output obtained from the simulation has given different results. This is most likely due to the small number of data obtained experimentally and with which the network, subsequently, was trained. The best results obtained with the simulation that had the highest correlation with the gravity signal is shown in Figure 4.19.

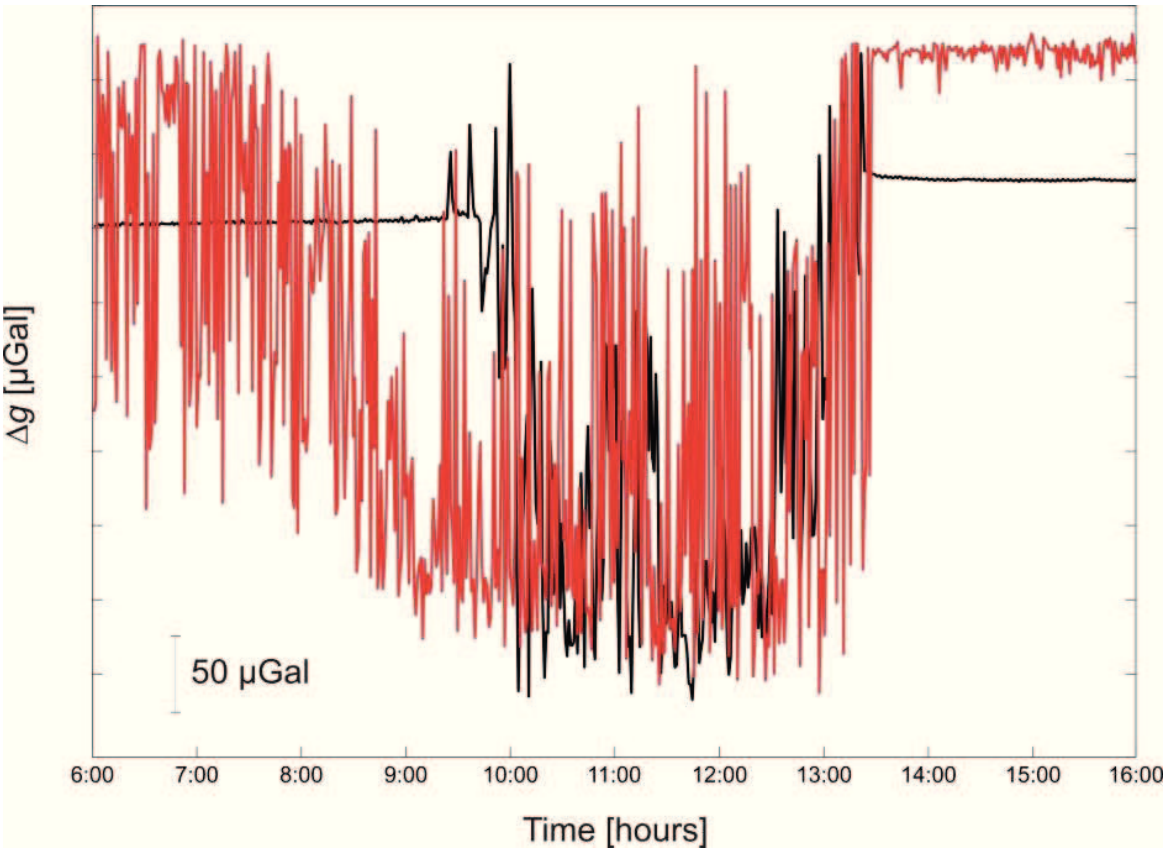

Figure 4.19 – Result of the simulation (red signal) that had the highest correlation with the gravity signal (black signal).

The objective of this latter application has been to propose a possible mathematical approach, able to split the signal from the gravimeter into gravity field and inertial acceleration components.
Despite the results are encouraging, the neural network implemented is not applicable for all gravimeter used. Furthermore, each instrument acts in different manner during the same seismic activity as widely explained in the previous paragraphs. For this reason, the mathematical approach should be applied for each gravimeter used for volcano monitoring.

Conclusions

This thesis aims to improve the gravimetric monitoring of volcanic areas through innovative experimental and computational approaches. The combined use of relative and absolute gravity observations at Etna volcano provided quality control for observing gravity changes and the possibility to examine gravity variations that are caused by volcano unrest in more detail. The use of absolute gravimeters in field surveys of the summit craters area of Mt Etna is unprecedented.

Firstly, the measurements techniques used on active volcanoes with spring relative and absolute gravimeters, are presented. The complexity of the gravity signals was widely discussed and the different gravity contributions in volcanic areas were quantified. The existing gravity monitoring network of Mt Etna was also shown.

In order to highlight the advantages of the hybrid gravity method, which combine relative and absolute gravimeters, the results of a comparison carried out between two transportable absolute

gravimeters in three different sites at different latitude are presented. By operating the transportable absolute gravimeters at different stations characterized by different logistics and environmental conditions, it has been found that in all the sites the two instruments did not present dependences on the external conditions and the obtained measurements of the local acceleration of gravity are always consistent. In fact, results highlight that the high accuracy in the determination of the absolute value of g is not significantly influenced by the environmental conditions found out of the dedicated laboratories in which the instruments guarantee the best performances. The repeated comparison was also very useful to test the behaviour of the instruments when they are used within dedicated laboratories and on the "field". Different measurement procedures were also experimented, allowing to balance the accuracy and the efficiency of gravity measurements, saving also time and resources. This latter aspect is very important because the use of such transportable absolute gravimeters is time consuming and needs well-trained operators. These factors have the effect of limiting the number of points where absolute gravity can be measured within a limited measurement schedule. For these reasons, it is important to find a good trade-off in using these instruments, and according to the study objectives and field conditions, repeated large scale high accuracy surveys may be conduct using absolute transportable gravimeters.

The results of experimental tests performed on the FG5#238 absolute gravimeter inside an hyperbaric chamber, that allowed to take gravity measures over a certain altitude, was also presented. Nowadays it is no longer necessary to use the hyperbaric chamber since, thanks to

the efforts made during these experiments, it was determined the optimal configuration of the instrument to perform absolute measurements also at high altitude with the FG5#238 gravimeter.

The hybrid gravity method has allowed to optimize traditional techniques of gravity measurements on Etna's gravity stations, ensuring an improvement in the quality of the data. The principal benefit of this combined method of absolute and relative gravity measurements is that it allows inexpensive relative gravimeters to achieve the precision of expensive absolute gravimeters when conducting a gravity survey. On large volcanoes such as Mt Etna, operators using an absolute gravimeter are not obliged to reach stable reference stations that are far (about 20 km) from the area of interest (summit craters), at the cost of propagating measurement errors and greatly increasing measurement time. Thus, the time required to accomplish discrete surveys drastically decreases and the reliability of discrete data improves. In this way, it was possible to minimize the uncertainty due to instrumental drift, which increases significantly when spring-relative instruments are subjected to mechanical and thermal shocks during long vehicle transportation. Moreover, the availability of absolute points, which are very close to areas experiencing volcanic unrest episodes, gives more specific information about the gravity field where significant time gravity changes are expected.

The results of high-precision gravity data collected at Mt Etna volcano highlighted that the uncertainty in the gravity surveys achieved by the hybrid method is less than the uncertainty affecting the gravity data when a single relative gravimeter is used. This surely improves the interpretation of gravity data. Obviously, this result

depends greatly on the ability of the operators to perform gravity measurements with both of these gravimeters in hostile environments. Moreover, when a single gravimeter is used, the gravity values and the final total uncertainty at each station depend heavily on compensation procedures. This means that if several wrong data are included in the analysis procedure, the final gravity values are adjusted and high uncertainty values are equally assigned to each gravity value. This provides ambiguous results and prevents an unequivocal interpretation of the anomalies observed. In addition, must be considered that the errors of the measurements increase with the number n of the consecutive differences, and after the n-th difference, the measurement error is multiplied by $\sqrt{n}$. The final result also depends on the total number of stations included in the loop. Conversely, the hybrid approach allows the obtaining of the gravity value at each relative station through a direct link between the absolute station and the relative one. In this case, the final total uncertainty strongly depends on the $u_{\Delta g}$ uncertainty that is calculated between each single pair of stations, in addition the propagation errors, in the final gravity values, are not included.

The overall reliability and quality of the data, together with the frequent measurements, makes the hybrid gravity survey an important tool to provide insights into volcano unrest months to years before the beginning of eruptive activity. Specifically, this method provided a significant step toward better understanding the Etna activity during the 2007-2009 period, when several episodes of lava fountaining affected the South-East Crater, and overall processes led to the passage from summit to lateral activity, up to the onset of the 2008-2009 flank eruption. There is an important difference between

the 2007-2008 and 2008-2009 annual gravity changes. Residual gravity data unequivocally provide evidence that during the 2007-2009 period, two main phenomena of mass redistribution occurred in different sectors of the volcano, accompanying different eruptive episodes. It is speculated that the structural instability of the upper northeastern sector of the volcano has played a key role on magma migration from the central conduits toward the east and could have set off or facilitated the lava fountaining in 2007 and consequently the eruption begun on 13 May 2008. This structural instability may also have facilitated the dry fracture field propagation in the upper portion of the North-East Rift after the initial phase of the 2008-2009 eruption. Results are also consistent with a new episode of recharge, started when the 2008-2009 eruption was still ongoing, in a 2-5 km deep reservoir below the summit craters.

These results, obtained by combining relative and absolute gravity measurements, highlight how the hybrid method improves the understanding of volcanic processes and the ability to identify renewed volcanic activity, forecast eruptions, and assess hazards. Therefore, it expected that absolute gravimeters will be extensively used for various purposes in future field gravity surveys.

Finally, was explained the activity that was aimed to reproduce in laboratory the coupling effects between vertical and horizontal solicitations at high frequency (ranging between 1 Hz to 25 Hz), which acts on spring-relative gravimeters in continuous recording during paroxysmal activity at Etna, and the response of the gravimeters in the vertical component at low frequency. A technological limit of this facility is represented by the impossibility to go towards low frequencies values: this is due to the electrical and

mechanical characteristics of the piezoelectric actuators that are not able to reproduce displacements with low frequency and high magnitude. These tests were performed on two gravimeters: the Scintrex CG-3M#9310234 and the LaCoste and Romberg D-185. In laboratory has been verified the hypothesis that high frequency excitations, both in the horizontal and vertical components, due to non-linear effects, determine a response in the measurement band of the gravimeters. The phenomenon is mainly determined by the amplitude modulation of the high frequency signal. Just this modulating signal is transferred in the band measurement of the instruments. It is clear that in the real case the envelope of the seismic signal plays this role, although in this case is not the modulation of a specific and fixed carrier, but rather of a frequencies packet that are modulated. The most important limitations of this sinusoidal test is related to the inability to properly simulate the real conditions, since they have frequencies with a random spectrum. To separate the gravity signal into inertial acceleration and volcano-related components, several strategies can be adopted. Among the different solutions, the acquisitions of seismic signals with instrumentation located at the same site of the gravimeters, and the analysis of data with neural networks are proposed. Although the implemented neural network has shown some convergence problems, the overall results suggest a good efficiency of the proposed approach since it is capable of finding and effectively representing the effect of the inertial acceleration, and allow local features of the signal to be detected. Furthermore, seems that to achieve a good result, the tests on vibrating platforms are indispensable for each different instrument, since it has a different behaviour to mechanical stress.

Appendices and Bibliography

Appendix A

Modeling in Volcano Geophysics

Field measurements are the starting point for the volcano understanding. However, field data alone are not enough for making any quantitative interpretation, but in addition theoretical responses (model responses) are needed and for realistic volcano models they are obtained by modeling techniques. And finally, by examining together field data and model data, the quantitative statement of the structure and dynamics of the volcanoes can be made.

The main goal of volcano modeling is to deduce information about the subsurface distribution of physical properties taking advantage from physical measurements: this represents the *Geophysical Inverse*

Problem. The most promising method to address this issue should be a joint inversion of precursory signals from seismic, deformation, gravity and magnetic signals and ideally from geochemical monitoring as well.
A crucial point in the geophysical inverse problem is to derive a mathematical relationship that relates observations and model (*forward model*). We deal with two main classes of *forward model*: the *analytical* and the *numerical models*.
Elaborated inverse methods typically combine forward models with appropriate algorithms to find the best parameter set that minimizes the misfit between the model values and the observations by means of an objective function. This turns the inversion problem in an optimization problem. Since considered models are highly non-linear and characterized by several parameters, the geophysical inverse problem requires sophisticated identification techniques to be solved.
In this thesis are used analytical forward models: for the low computational cost, they are well suitable for identifications techniques allowing the simultaneous inversion of combined models hence the joint interpretation of multimethod geophysical data. The drawbacks of the analytical formulations for modeling volcanic activities are the assumption of simple geometries for the sources embedded in homogeneous elastic half-space.

A.1.1 Modeling Issues

Physical theories are designed to explain and possibly predict natural phenomena. The explanation by a theory is also a form of prediction

as it states certain consequences for certain causes. Both, the explanation and prediction typically include quantitative representation of the natural system state.

Quantitative assessment of the actual, true, state is fundamentally achievable only by measurements. The Geophysical theories are consequently designed to explain and predict the measurements. The theories are most often expressed in a form mathematical relationships which define a model. *The model in general represents governing physical laws and includes a set of quantities which entirely define the state by the model.* The defining quantities are called control parameters. The control parameters are initial and boundary conditions, external forces and other physical quantities which define medium or environment for a process that is modeled.

The quantification of the system state by application of an assumed set of control parameters by the governing laws is called forward model of the system state or simulation of the measurements. Obviously, under conditions of well known governing laws and accurate quantification of the control parameters the forward model would produce accurate simulation of the measurements and would have ability to predict future states. It is common, however, that the governing physical laws are known but the control parameters values are not. This condition occurs in variety of models which are based on application of fundamental laws for macro scale phenomena such as conservation of energy and mass, propagation of energy through media and bulk energy and mass transformations.

Because the model simulates the measurements, it is natural to ask whether there is a formal and objective way to use the measurements to infer the correct control parameter values for the model? In

volcano geophysics this problem is called geophysical inverse problem.

A.1.2 The Geophysical Inverse Problem

The task of the geophysical inverse problem is equivalent to the task of deducing information about the subsurface distribution of physical properties taking advantage from physical measurements. The expression "physical measurements" has to be meant as involving measurements which are made at the Earth's surface, but also measurements made within the Earth's subsurface [Parker RL, 1977; Tarantola, 1987; Sambridge, 1998]. It's possible to see into the deduction process just described two parts: [Scales and Snieder, 2000]: the first part is given by estimating inverse models starting from a set of given data, while the second part is given by appraising the inverse models with respect to the true earth model, which is obviously unknown.

On this set of inverse models, estimation is performed in order to locate which one of these models has to be considered better. This estimation can be performed following two methods: the first method is a statistical method (in this case the method lays on the Bayesian approach), the second is the deterministic method.

In the deterministic approach the search is focused towards those inverse models that minimize data misfit; at the same time these models are required to fit constraints taking into account a priori information or assumptions of other kind. The goal of modeling is to determine the volcanic source parameters from available

observations, where the words “available observations” are to be meant in its wider interpretation context, that is to say involving Seismicity, Ground Deformation, InSAR, Potential Fields and Geochemistry observations. For this reason, elaborated inverse methods typically combine forward models with appropriate algorithms to find the best parameter set that minimizes the misfit between the model values and the observations by means of a objective function. This turns the inversion problem in an optimization problem. One of the most stressing features in solving this kind of problem is that usually a certain degree of non-uniqueness in the solution must be dealt with, that is to say that the solving procedure leads to more than a solution, all of them solving with a good approximation the problem. Moreover, not all the found solutions make sense under a geophysical point of view, so an a-posteriori analysis has to be performed by a specialist/researcher.

A.1.3 Analytical Methods: Forward Modeling

Analytical models are mathematical models that have a closed form solution, i.e. the solution to the equations used to describe changes in a system can be expressed as a mathematical analytic function.

Over the last decades, straightforward analytical solutions for simplified geometric sources have been devised under the assumption of homogeneous elastic half-space medium. There are mainly three reasons for this: (1) the calculations are simple and rapid, (2) observations were in some cases sufficiently explained by the models, and (3) the quality and quantity of acquired data were not enough to consider more complex models.

A.1.3.1 Joint Modeling of Geophysical Data

In the domain of geophysical modeling, analytical solutions have frequently been used to provide a mathematical formulation that relates magnetic anomalies, gravity, displacements and stress/strain fields associated with a particular volcanic source.

During ascent, magma interacts with surroundings rocks and fluids, and almost inevitably crustal deformation and potential field changes are produced. If the volcanic edifice can be assumed to be elastic, contributions to geophysical signal variations depend on surface and subsurface mass redistribution driven by dilation/contraction of the volcanic source. Indeed ground deformation studies provide insight about volume changes in the magma reservoir and the dynamics of dike intrusion processes [Voight et al., 1998; Battaglia et al., 2003 Murase et al., 2006]. However, deformation data alone are not able to properly constrain the mass of the intrusions. Geodetic studies need to be supported also by gravity observations in order to infer the density of the intrusive body and better define the volcanic source [Carbone et al., 2007b].

Moreover, in volcanic areas, significant correlations were observed between volcanic activity and changes in the local magnetic field, up to ten nanoteslas [Del Negro and Currenti, 2003]. These observations were compared with those calculated from volcanomagnetic models, in which the magnetic changes are generated by stress redistribution due to magmatic intrusions at different depth and by the thermal demagnetization at a rather shallow depth. The magnetic data not only allowed the timing of the intrusive event to be described in greater detail but also, together with other volcanological and

geophysical evidences, permitted some constraints to be set on the characteristics of propagation of shallow dikes [Del Negro et al., 2004].

When the cause of their variations can be ascribed to the same volcanic source, a joint inversion of ground deformation, gravity and magnetic data would be advisable in order to identify the source parameters with a greater degree of accuracy. Indeed, the integrated approach involving geophysical data of different kinds ensures a more accurate solution than when single data types are considered [Nunnari et al., 2001] and leads to the best possible understanding of the physical process adding further constraints to the interpretation.

For an integrated inversion modeling, complex methods are needed to combine forward models with appropriate optimization algorithms and automatically find the best set of source parameters that well matches the available observations.

A.1.3.2 Analytical Forward Models

Volcanic processes are complex geophysical system and it is difficult to derive a forward model, unless important simplifications and approximations are taken into account [McTigue, 1987]. Surface displacements in a homogeneous elastic half-space have been described by Mogi [1958] for a spherical source and by Okada [1985; 1992] for a rectangular fault.

Analytical solution to model gravity changes which are expected to accompany crustal deformation due to volcanic sources have been devised and widely used in literature [Jousset et al., 2003; Okubo 1992]. These models take into account the interaction between the intrusive mass and the effect caused by volcanic pressure sources.

Appendix A

Most of the analytical formulations for modeling inflation and deflation episodes describe the effects caused by sources with a specific shape such as spheres [Hagiwara, 1977], ellipsoids [Battaglia and Segall, 2004] or rectangular prisms [Okubo and Watanabe, 1989].

Bibliography

Aloisi M., Bonaccorso A., Cannavò F., Gambino S., Mattia M., Puglisi G., Boschi E. (2009). A new dyke intrusion style for the Mount Etna May 2008 eruption modelled through continuous tilt and GPS data. *Terra Nova*, **21(4)**, 316-321.

Andronico D., Cristaldi A., Scollo A. (2008). The 4-5 September 2007 lava fountain at South–East Crater of Mt Etna. Italy. *J. Volcanol. Geotherm. Res.*, **173**, 325-328, doi: 10.1016/j.jvolgeores.2008.02.004.

Battaglia M., Segall P., Roberts C. (2003). The mechanics of unrest at Long Valley Caldera, California: 2. Constraining the nature of the source using geodetic and micro-gravity data. *J. Volcanol. Geotherm. Res.*, **127**, 219-245.

Battaglia M., Segall P., (2004). The Interpretation of gravity changes and crustal deformation in active volcanic areas. *Pure Appl. Geophys.*, **161**, 1453-1467.

Battaglia M., Troise C., Obrizzo F., Pingue F., De Natale G. (2006). Evidence for fluid migration as the cause of unrest at Campi Flegrei caldera (Italy). *Geoph. Res. Lett.*, **33**, doi: 10.1029/2005GL024904.

Berrino G. (2000). Combined gravimetry in the observation of volcanic processes in Southern Italy. *J. Geodynam.*, **30**, 371-388.

Biolcati E., Svitlov S., Germak A. (2012). Self-attraction effect and correction on three absolute gravimeters. *Metrologia*, **49(4)**, doi: 10.1088/0026-1394/49/4/560.

Blakely R. J. (1995). Potential theory in gravity and magnetic applications. *Cambridge University Press*, New York, 1995.

Bonaccorso A., Cianetti S., Giunchi C., Trasatti E., Bonafede M., Boschi E. (2005). Analytical and 3-D numerical modelling of Mt. Etna (Italy) volcano inflation. *Geophys. J. Int.*, **163**, 852-862, doi: 10.1111/j.1365-246X.2005.02777.x.

Bonaccorso A., Bonforte A., Currenti G., Del Negro C., Di Stefano A., Greco F. (2011a). Magma storage, eruptive activity and flank instability: inferences from ground deformation and gravity changes during the 1993-2000 recharging of Mt. Etna volcano. *J. Volcanol. Geotherm. Res.*, **200**, 245-254.

Bonaccorso A., Cannata A., Corsaro R. A., Di Grazia G., Gambino S., Greco F., Miraglia L., Pistorio A. (2011b). Multidisciplinary investigation on a lava fountain preceding a flank eruption: the 10 May 2008 Etna case. *Geochem. Geophys. Geosyst.*, **12**, Q07009. doi: 10.1029/2010GC003480.

Bonaccorso A., Bonforte A., Calvari S., Del Negro C., Di Grazia G., Ganci G., Neri M., Vicari A., Boschi E. (2011c). The initial

phases of the 2008-2009 Mount Etna eruption: a multidisciplinary approach for hazard assessment. *J. Geophys. Res.*, **116**, B03203, doi: 10.1029/2010JB007906.

Bonafede M., Mazzanti M. (1998). Modelling gravity variations consistent with ground deformation in the Campi Flegrei Caldera (Italy). *J. Volcan. Geotherm. Res.*, **81**, 137-157.

Bonforte A., Puglisi G. (2003). Magma uprising and flank dynamics on Mount Etna volcano, studied using GPS data (1994-1995). *J. Geophys. Res.*, **108(B3):2153**, doi: 10.1029/2002JB001845.

Bonforte A., Puglisi G. (2006). Dynamics of the eastern flank of Mt. Etna volcano (Italy) investigated by a dense GPS network. *J. Volcanol. Geotherm. Res.*, **153**, 357-369, doi: 10.1016/j.jvolgeores.2005.12.005.

Bonforte A., Carbone D., Greco F., Palano M. (2007a). Intrusive mechanism of the 2002 NE-rift eruption at Mt Etna (Italy) modelled using GPS and gravity data. *Geophys J. Int.*, **169**, 339-347.

Bonforte A., Gambino S., Guglielmino F., Obrizzo F., Palano M., Puglisi G. (2007b). Ground deformation modeling of the flank dynamics prior to the 2002 eruption of Mt. Etna. *Bull. Volcanol.*, **69**, 757-768, doi: 10.1007/s00445-006-0106-1.

Bonforte A., Bonaccorso A., Guglielmino F., Palano M., Puglisi G. (2008). Feeding system and magma storage beneath Mt. Etna as revealed by recent inflation/deflation cycles. *J. Geophys. Res.*, **113**, B05406, doi: 10.1029/2007JB005334.

Bonforte A., Guglielmino F., Puglisi G. (2011). 3D temporal evolution of displacements recorded on Mt. Etna from the 2007 to

2010 through the SISTEM method. *Fringe 2011 Workshop*, Frascati, 19-23 September 2011.

Borgia A., Ferrari L., Pasquarè G. (1992). Importance of gravitational spreading in the tectonic and volcanic evolution of Mount Etna. Nature, **357**, 231-235.

Budetta G., Grimaldi M., Luongo G. (1989). Variazioni di gravità nell'area etnea (1986–1989). *Boll GNV*, **5**, 137-146.

Budetta G., Carbone D. (1998). Temporal variations in gravity at Mt Etna (Italy) associated with the 1989 and 1991 eruptions. *Bull. Volcanol.*, **59**, 311–326.

Cai Y., Wang C. Y. (2005). Fast finite-element calculation of gravity anomaly in complex geological regions. *Geophys. J. Int.*, **162**, 696-708.

Carbone D., Budetta G., Greco F. (2003). Bulk processes some months before the start of the 2001 Mt Etna eruption, evidenced through microgravity studies. *J. Geophys. Res.*, 108(B12):2556.

Carbone D., Currenti G., Del Negro C. (2007). Elastic model for the gravity and elevation changes prior to the 2001 eruption of Etna volcano. *Bull. Volcanol.*, **69(5)**, 553-562.

Carbone D., Greco F. (2007b). Review of microgravity observations at Mt. Etna: a powerful tool to monitor and study active volcanoes. *Pure Appl. Geophys.*, **164**, 1-22.

Charco M., Fernandez J., Luz´on F., Rundle J. B. (2006). On the relative importance of self-gravitation and elasticity in modeling volcanic ground deformation and gravity changes. *J. Geophys. Res.*, **111**, B03404, doi:10.1029/2005JB003754.

Chouet B. (2003). Volcano Seismology. *Pure Appl. Geophys.*, **160**, 739-788.

Clark D. A., Saul S. J., Emerson D. W. (1986). Magnetic and gravity anomaly of a triaxial ellipsoid. *Expl. Geophys.*, **17**, 189-200.

Currenti G., Del Negro C., Ganci G. (2007). Modelling of ground deformation and gravity fields using finite element method: an application to Etna volcano. *Geophys J. Int.*, doi:10.1111/j.1365-246X.2007.03380.x.

Currenti G., Napoli R., Del Negro C. (2011a). Toward a realistic deformation model of the 2008 magmatic intrusion at Etna from combined DInSAR and GPS observations. *Earth Planet. Sci. Lett.*, **312**, 22-27, doi:10.1016/j.epsl.2011.09.058.

Currenti G., Napoli R., Di Stefano A., Greco F., Del Negro C. (2011b). 3D integrated geophysical modeling for the 2008 magma intrusion at Etna: constraints on rheology and dike overpressure. *Phys. Earth. Planet. Int.*, **185**, 44-52.

D'Agostino G., Desogus S., Germak A., Origlia C., Quagliotti D., Berrino G., Corrado G., Ricciardi G. (2008). The new IMGC-02 transportable absolute gravimeter: measurement apparatus and applications in geophysics and volcanology. *Annals of Geophysics*, **51**, 1, 39-49.

D'Agostino G., Germak A., Origlia C., Greco F., Sicali A., Dorizon S. (2009). Absolute measurements of the free-fall acceleration *g* in Catania and Etna volcano. *TORINO:INRIM - Istituto Nazionale di Ricerca Metrologica*, **17**.

Del Negro C., Currenti G. (2003). Volcanomagnetic signals associated with the 2001 flank eruption of Mt. Etna (Italy). *Geophys. Res. Lett.*, **30**(7), 1357, doi: 10.1029/2002GL015481.

Del Negro C., Currenti G., Napoli R., Vicari A. (2004). Volcanomagnetic changes accompanying the onset of the 2002–2003 eruption of Mt. Etna (Italy). *Earth and Planetary Science Letters*, **229**, 1-14.

Del Negro C., Greco F., Napoli R., Nunnari G. (2008). Denoising gravity and geomagnetic signals from Etna volcano (Italy) using multivariate methods. *Nonlin. Processes Geophys.*, **15**, 735-749.

Del Pezzo E. (2008). Seismic wave scattering in volcanoes. *Advances in Geophysics*, **50**, 353-371.

Doebelin E. O. (1990). Measurement System: Application and Design. *McGraw-Hill*, 4th ed., ISBN: 0-07-017338-9.

Dorofki M., Elshafie A. H., Jaafar O., Karim O. A., Mastura S. (2012). Comparison of artificial neural network transfer functions abilities to simulate extreme runoff data. *International Conference on Environment, Energy and Biotechnology*, IPCBEE, **33**, Singapore.

Elawadi E., Salem A., Ushijima K. (2001). Detection of cavities and tunnels from gravity data using a neural network. *Exploration Geophysics*, **32(4)**, 204-208.

Ferguson J. F., Klopping F. J., Chen T., Seibert J. E., Hare J. L., Brady J. L. (2008). The 4D microgravity method for waterflood surveillance: Part III 4D absolute microgravity surveys at Prudhoe Bay, Alaska. *Geophysics*, **73(6)**, WA163-WA171.

Froger J. L., Merle O., Briole P. (2001). Active spreading and regional extension at Mount Etna imaged by SAR interferometry. *Earth. Planet. Sci. Lett.*, **187**, 245-258.

Furuya M., Okubo S., Sun W., Tanaka Y., Oikawa J., Watanabe H., Maekawa T. (2003). Spatiotemporal gravity changes at Miyakejima volcano: Japan: Caldera collapse, explosive eruptions and magma movement. *J. Geophys. Res.*, **108**, doi: 10.1029/2002JB001989.

Genevès G., Villar F., Bielsa F., Gilbert O., Eichenberger A., Baumann H., D'Agostino G., Merlet S., Pereira Dos Santos F., Pinot P., Juncar P. (2010). The e-Mass Euramet Joint Research Project: the watt balance route towards a new definition of the kilogram. *CPEM Digest - Proceeding of 2010 Conference on Precision Electromagnetic Measurements*, Korea.

Germak A. (2006). Description of the IMGC Gravity Laboratory in Turin, Italy. *OLIVIER FRANCIS. CAHIERS DU CENTRE EUROPÉEN DE GÉODYNAMIQUE ET DE SÉISMOLOGIE*, **26**, 37-42, LUXEMBOURG:ECGS, ISBN: 2959980441.

Greco F., Budetta G., Carbone D., Panepinto S., Luzio D. (2007). The application of a denoising method aimed at reducing continuous gravity data. *Communications to SIMAI Congress*, **2**, doi: 10.1685/CSC06091, ISSN 1827-9015.

Greco F., Currenti G., Del Negro C., Napoli R., Budetta G., Fedi M., Boschi E. (2010). Spatiotemporal gravity variations to look deep into the southern flank of Etna volcano. *J. Geophys. Res.*, 115:B11411, doi: 10.1029/2009JB006835.

Greco F., Pistorio A., Currenti G. M., Del Negro C., Napoli R. D., Scandura D. (2011). 4D Hybrid Microgravity Measurements: Two Case Studies of Monitoring at the Mt. Etna Volcano and at a Gas Storage Reservoir in Northern Italy. *Miscellanea INGV*, **12**, 47-50, ISSN: 2039-6651.

Greco F., Currenti G., D'Agostino G., Germak A., Napoli R., Pistorio A., Del Negro C. (2012). Combining relative and absolute gravity measurements to enhance volcano monitoring. *Bull. Volcanol.*, **74**, 1745-1756, doi: 10.1007/s00445-012-0630-0.

Hagiwara Y. (1977). The Mogi model as a possible cause of the crustal uplift in the eastern part of Izu Peninsula and related gravity change. *Bull. Earthq. Res. Inst.*, Univ. Tokyo, **52**, 301-309.

Jiang Z., Francis O., Vitushkin L., Palinkas V., Germak A., Becker M., D'Agostino G., Amalvict M., Bayer R., Bilker-Koivula M., Desogus S., Faller J., Falk R., Hinderer J., Gagnon C., Jakob T., Kalish E., Kostelecky J., Chiungwu L., Liard J., Lokshyn Y., Luck B., Makinen J., Mizushima S., Le Moigne N., Origlia C., Pujo E. R., Richard P., Robertsson L., Ruess D., Schmerge D., Stus Y., Svitlov S., Thies S., Ullrich C., Van Camp M., Vitushkin A., Ji W., Wilmes H. (2011). Final report on the Seventh International Comparison of Absolute Gravimeters (ICAG 2005). *Metrologia*, **48(5)**, 246-260, doi:10.1088/0026-1394/48/5/003.

Jousset P., Dwipa S., Beauducel F., Duquesnoy T., Diament M. (2000). Temporal gravity at Merapi during the 1993–1995 crisis: an insight into the dynamical behaviour of volcanoes. *J. Volcanol. Geotherm. Res.*, **100**, 289-320.

Jousset P., Mori H., Okada H. (2003). Elastic models for the magma intrusion associated with the 2000 eruption of Usu Volcano, Hokkaido, Japan. *J. Volcan. Geotherm. Res.*, **2607**, 1-26.

Kuo J. T., Ottaviani M., Singh S. K. (1969). Variations of vertical gravity gradient in New York City and Alpine, New Jersey. *Geophysics*, **34**, 235-248.

Lo Giudice E., Rasà R. (1992). Very shallow earthquakes and brittle deformation in active volcanic areas: the Etnean region as an example. *Tectonophysics*, **202**, 257-268.

McTigue D. F. (1987). Elastic stress and deformation near a finite spherical magma body: resolution of the point source paradox. *J. Geophys. Res.*, **92**, 12931-12940.

Merlet S., D'Agostino G., Germak A., Baumann H., Bodart Q., Louchet A., Landragin A., Pereira Dos Santos F. (2010). Comparison of 3 absolute gravimeters based on different methods for the e-MASS project. *CPEM Digest - Proceeding of 2010 Conference on Precision Electromagnetic Measurements*. Daejeon, Korea, 13-18 June, 68-69, doi: 10.1109/CPEM.2010.5543307, ISBN: 978-1-4244-6795-2.

Mishra D. C. (2011). Gravity and Magnetic Methods for Geological Studies: Principles, Integrated Exploration and Plate Tectonics. *CRC Press*.

Mochales T., Casas A. M., Pueyo E. L., Pueyo O., Román M. T., Pocoví A., Soriano M. A., Ansón D. (2008). Detection of underground cavities by combining gravity, magnetic and ground penetrating radar surveys: a case study from the Zaragoza area, NE Spain. *Environ. Geol.*, **53**, 1067-1077.

Mogi K. (1958). Relations between the eruptions of various volcanos and the deformations of the ground surfaces around them. *Bull. Earthq. Res. Inst.*, Univ. Tokyo, **36**, 99-134.

Murase M., Irwan M., Kariya S., Tabei T., Okuda T., Miyajima R., Oikawa J., Watanabe H., Kato T., Nakao S., Ukawa M., Fujita E., Okayama M., Kimata F., Fujii N. (2006). Time dependent model of magma intrusion in and around Miyake and Kozu Islands, Central Japan in June–August, 2000. *Volcanol. Geotherm. Res.*, **150**, 213-231.

Nabighian M. N., Ander M. E., Grauch V. J. S., Hansen R. O., LaFehr T. R., Li Y., Pearson W. C., Peirce J. W., Phillips J. D., Ruder M. E. (2005). Historical Development of the Gravity Method in Exploration. *Geophysics*, **70(6)**, p. 63ND-89ND.

Napoli R., Currenti G., Del Negro C., Greco F., Scandura D. (2008). Volcanomagnetic evidence of the magmatic intrusion on 13th May 2008 Etna eruption. *Geophys. Res. Lett.*, **35**, L22301. doi: 10.1029/2008GL035350.

Niebauer T. M., Sasegawa G. S., Faller J. E., Hilt R., Klopping F. (1995). A new generation of absolute gravimeters. *Metrologia*, **32**, 159-180.

Nunnari G., Bertucco L., Ferrucci F. (2001). A Neural Approach to the Integrated Inversion of Geophisical Data Types. *IEEE Transaction on Geosciences and Remote Sensing*, **39(4)**, 736-748.

Okada Y. (1985). Surface deformation due to shear and tensile faults in a half-space. *Bull. Seism. Soc. Am.*, **75**, 1135-1154.

Okubo S., Watanabe H. (1989). Gravity change caused by a fissure eruption. *Geophys. Res. Lett.*, **16**, 445-448.

Okubo S. (1992). Gravity and Potential Changes due to Shear and Tensile Faults in a Half-Space. *J. Geoph. Res.*, **97(B5)**, 7137-7144.

Parker RL. (1977). Understanding inverse theory. *Ann. Rev. Earth Planet. Sci.*, **5**, 35-64.

Pistorio A., Greco F., Currenti G., Napoli R., Sicali A., Del Negro C., Fortuna L. (2011). High precision gravity measurements using absolute and relative gravimeters at Mount Etna (Sicily, Italy). *Annals Geophys*, **54(5)**, doi:10.4401/ag-5348.

Pool D., Eychaner J. (1995). Measurements of aquifer-storage change and specific yield using gravity surveys. *Ground Water*, **33(3)**, 425-432.

Pool D. (2008). The utility of gravity and water-level monitoring at alluvial aquifer wells in southern Arizona. *Geophysics*, **73**, 49-59.

Puglisi G., Bonforte A. (2004). Dynamics of Mt Etna volcano inferred from static and kinematic GPS measurements. *J. Geophys. Res.*, **109(B11)**, B11404, doi: 10.1029/2003JB002878.

Quinn T. J. (1991). The kilogram: the present state of our knowledge. *Transactions on Instrumentation and Measurement, IEEE*, **40(2)**, 81-85, doi: 10.1109/TIM.1990.1032888, ISSN: 0018-9456.

Rymer H. (1994). Microgravity changes as a precursor to volcanic activity. *J. Volcanol. Geotherm. Res.*, **61**, 311-328.

Rymer H., Ferrucci F., Locke C. A. (1998). Mount Etna: monitoring in the past, present and future. *Geological Society, London, Special Publications*, **143**, 335-347, doi: 10.1144/GSL.SP.1998.143.01.22.

Sambridge M. (1998). Exploring multidimensional landscapes without a map. *Inverse problems*, **14**, 427-440.

Scales J. A., Snieder R. (2000). The anatomy of inverse problems. *Geophysics*, **65(6)**, 1708-1710.

Schiavone D., Loddo M. (2007). 3-D density model of Mt. Etna Volcano (Southern Italy). *J. Volcanol. Geotherm. Res.*, **164**, 161-175.

Sifaoui A., Abdelkrim A., Benrejeb M. (2008). On the use of neural network as a universal approximator. *International Journal of Sciences and Techniques of Automatic control & computer engineering*, **2(1)**, 336-399.

Spilliaert N., Allard P., Metrich N., Sobolev A. V. (2006). Melt inclusion record of the conditions of ascent, degassing, and extrusion of volatile-rich alkali basalt during the powerful 2002 flank eruption of Mount Etna (Italy). *J. Geophys. Res.*, **111**, B04203, doi: 10.1029/2005JB003934.

Tarantola A. (1987). Inverse problem theory. *Elsevier,* Amsterdam, New York.

Tang Z., Wang X. G., Tamura H., Ishii M. (2003). An algorithm of supervised learning for multilayer neural networks. *Neural Computation*, **15(5)**, 1125-1142, doi: 10.1162/089976603765202686.

Torge W. (1989). Gravimetry. *Walter de Gruyter, Berlin-New York*.

Van Camp M., Camelbeeck T., Richard P. (2003). The FG5 absolute gravimeter: metrology and geophysics. *Physicalia Magazine, Journal of the Belgian Society*, **25(3)**, 161-174.

Vitushkin L., Jiang Z., Robertsson L., Becker M., Francis O., Germak A., D'Agostino G., Palinkas V., Amalvict M., Bayer R. (2010). Results of the Seventh International Comparison of Absolute Gravimeters ICAG-2005 at the Bureau International des Poids et Mesures, Sèvres. *Springer Heidelberg Dordrecht London*

New York. Gravity, Geoid and Earth Observation. International Association of Geodesy Symposia (GGEO), **135(1)**, 47-53, CRETE: Stelios P. P. Mertikas, ISBN/ISSN: 978-3-642-10633-0/0939-9585, doi: 10.1007/978-3-642-10634-7_7.

Voight B., Hoblitt R., Clarke A., Lockhart A., Miller A., Lynch L., McMahon J. (1998). Remarkable cyclic ground defomation monitored in real-time on Montserrat, and its use in eruption forcastin. *Geophys. Res. Lett.*, **24**, 3405-3408.

Walsh J. B., Rice J. R. (1979). Local changes in gravity resulting from deformation. *J. Geoph. Res.*, **84**, 165-170.

Warburton R., Goodkind J. (1977). The influence of barometric pressure variations on gravity. *Geophys. J. Roy. Astr. S.*, **48(3)**, 281-292.

Williams-Jones G., Rymer H. (2002). Detecting volcanic eruption precursors: a new method using gravity and deformation measurements. *J. Volcanol. Geotherm. Res.*, **113**, 379-389.

Yoshida S., Seta G., Okubo S., Kobayashi S. (1999). Absolute gravity change associated with the March 1997 earthquake swarm in the Izu Peninsula, Japan. *Earth Planets Space*, **51**, 3-12.

Zurada J. M. (1992). Introduction to Artificial Neural Systems. Brooks/Cole, ISBN-10: 053495460X.